

Aus der Fachrichtung Physiologie – Prof. Dr. Dr. Frank Zufall
Theoretische Medizin und Biowissenschaften
der Medizinischen Fakultät
der Universität des Saarlandes, Homburg

Comparative Analyses of Murine and Human Formyl Peptide Receptor 3

*Dissertation zur Erlangung des Grades eines Doktors der Naturwissenschaften
der Medizinischen Fakultät
der UNIVERSITÄT DES SAARLANDES*

2017

vorgelegt von: Hendrik Stempel
geb. am: 22.12.1985 in Homburg

*Es gibt Stunden,
in denen der Mensch von aller
Unzulänglichkeit befreit ist.
Man steht dann auf einem
kleinen Flecken eines kleinen Planeten,
schaut erstaunt die Schönheit des Ewigen,
des in der Tiefe Unergründlichen.
Man fühlt, es gibt nicht mehr Werden und Vergehen,
es gibt nicht mehr Tod und Leben,
sondern nur das Sein.*

Albert Einstein

The following manuscripts emerged from this thesis:

Stempel H, Jung M, Pérez-Gómez A, Leinders-Zufall T, Zufall F, Bufe B (2016) Strain-specific loss of formyl peptide receptor 3 in the murine vomeronasal and immune systems. J Biol Chem 291: 9762-9775

Stempel H, Zufall F, Bufe B. Evidence for an Orthologous Function of Mouse and Human Formyl Peptide Receptor 3. In preparation

Table of Contents

List of Figures.....	IV
List of Tables.....	VI
Abstract.....	VII
Zusammenfassung.....	VIII
Abbreviations.....	X
1 INTRODUCTION.....	1
1.1 Social Recognition and Olfactory Pathogen Recognition	1
1.2 The Vomeronasal Organ.....	3
1.2.1 General Function of the Vomeronasal Organ	3
1.2.2 Anatomy of the Vomeronasal Organ.....	4
1.2.3 Detection Mechanisms in the Vomeronasal Organ	6
1.2.3.1 <i>Vmn1r</i> Expressing Vomeronasal Sensory Neurons	6
1.2.3.2 <i>Vmn2r</i> Expressing Vomeronasal Sensory Neurons	7
1.2.3.3 <i>Formyl Peptide Receptor</i> Expressing Vomeronasal Sensory Neurons	8
1.3 Formyl Peptide Receptors	9
1.3.1 General Function of Formyl Peptide Receptors	9
1.3.2 Genetics of Formyl Peptide Receptors	11
1.3.3 Tissue Distribution of Formyl Peptide Receptors	12
1.3.4 Relationship between Murine and Human Formyl Peptide Receptors	13
1.4 Aims of this Work	14
2 EXPERIMENTAL PROCEDURES.....	15
2.1 Ligands	15
2.1.1 Synthetic Ligands	15
2.1.2 Natural Ligands	16
2.2 Mouse Strains	17
2.3 Molecular Biology	17
2.3.1 Oligonucleotides.....	17
2.3.1.1 <i>Sequencing Primers</i>	18
2.3.1.2 <i>PCR Primers</i>	18
2.3.2 Polymerase Chain Reaction	19
2.3.3 PCR Templates.....	19
2.3.4 RNA Isolation	20
2.3.5 cDNA Synthesis	21
2.3.6 Extraction of Genomic DNA.....	21
2.3.7 Purification of PCR Products	21
2.3.8 Gel Electrophoresis	22
2.3.9 RNA Quantification	22
2.3.10 Enzymatic DNA Digestion.....	22
2.3.11 Expression Vectors.....	22
2.3.12 DNA Ligation.....	24
2.3.13 Transformation of Competent <i>Escherichia coli</i>	24
2.3.14 Isolation of Plasmid DNA from Bacterial Cultures	24
2.3.15 Determining DNA and RNA Concentration	25
2.3.16 DNA Sequencing.....	25
2.3.17 Generation of Bacterial Glycerol Stocks.....	25
2.3.18 Formyl Peptide Receptor Genes.....	25
2.4 HEK293T Cell Culture	26

2.4.1	HEK293T Cells	26
2.4.2	Cell Culture Media	26
2.4.3	Cultivating Culture Cells.....	26
2.4.4	Transient Transfection of Culture Cells	27
2.4.5	Thawing of Cryopreserved Culture Cells.....	27
2.4.6	Storage of Culture Cells	27
2.5	High-Throughput Calcium Imaging	28
2.5.1	Cell Population Calcium Imaging	28
2.5.1.1	<i>Dye Loading of HEK293T Cells for Cell Population Calcium Imaging</i>	28
2.5.1.2	<i>Data Acquisition for Cell Population Calcium Imaging with the FLIPR</i>	28
2.5.1.3	<i>Analysis of FLIPR Experiments</i>	28
2.5.2	Single Cell Calcium Imaging	29
2.5.2.1	<i>Dye Loading of HEK293T Cells for Single Cell Calcium Imaging</i>	29
2.5.2.2	<i>Data Acquisition for Single Cell Calcium Imaging with the Bioimager</i>	30
2.5.2.3	<i>Analysis of Bioimager Experiments</i>	30
2.6	Immunocytochemistry	31
2.6.1	Preparation of Samples for Immunocytochemistry	31
2.6.1.1	<i>Dissociation of Vomeronasal Tissue</i>	31
2.6.1.2	<i>Preparation of Blood Cells</i>	31
2.6.1.3	<i>Preparation of Bone Marrow Cells</i>	31
2.6.2	Immunostaining Protocol	32
2.6.2.1	<i>Image Acquisition and Data Analysis for General Immunostainings</i>	32
2.6.3	Antibodies	32
2.6.3.1	<i>Used Antibodies</i>	32
2.6.3.2	<i>Generation of Fpr3 Antibodies</i>	33
2.6.3.3	<i>Peptide-Spot Array Analysis for Antibody Characterization</i>	34
2.6.3.4	<i>Blocking Peptides</i>	34
2.7	<i>In Situ</i> Hybridization	35
2.7.1	Coronal Slices of the Vomeronasal Organ for <i>In Situ</i> Hybridization	35
2.7.2	Design and Generation of RNA Probes	35
2.7.3	Hybridization.....	36
2.7.4	Washing.....	36
2.7.5	Detection with Alkaline Phosphatase.....	36
2.8	Software and Web Tools	37
2.8.1	Software	37
2.8.1.1	<i>Adobe Photoshop CS5</i>	37
2.8.1.2	<i>Adobe Illustrator CS6</i>	37
2.8.1.3	<i>Microsoft Office 2010</i>	37
2.8.1.4	<i>VectorNTI Suite 9</i>	37
2.8.1.5	<i>FLIPR system software v2.1.2</i>	37
2.8.1.6	<i>BD AttoVision™ software v1.6</i>	37
2.8.1.7	<i>Graph Pad Prism</i>	38
2.8.1.8	<i>Cell^P</i>	38
2.8.2	Web Tools	38
2.8.2.1	<i>Gene Information Gathering</i>	38
2.8.2.2	<i>Prediction of Gene Orthology</i>	38
2.8.2.3	<i>Prediction of Transmembrane Domains (TMHMM)</i>	39
2.8.2.4	<i>Calculation of Primer Melting Temperatures</i>	39
2.8.2.5	<i>Mouse Haplotype Analyses</i>	39
2.9	Statistics and Mathematics	39
2.9.1	Average and Standard Deviation.....	39

2.9.2	Concentration-Response Curves	40
3	RESULTS.....	41
3.1	Generation and Characterization of Two Novel Fpr3 Antibodies.....	41
3.1.1	Characterization of Commercially Available Fpr3 Antibodies.....	41
3.1.2	Generation of Fpr3 Antibodies.....	42
3.1.2.1	<i>Generation of Polyclonal Rabbit Fpr3 Antibodies</i>	43
3.1.2.2	<i>Generation of Monoclonal Mouse Fpr3 Antibodies</i>	44
3.1.3	Characterization of Two Novel Fpr3 Antibodies	46
3.2	Fpr3 Expression in the Murine Vomeronasal and Immune Systems	49
3.2.1	Fpr3 Protein is Expressed in Vomeronasal Sensory Neurons and in Immune Cells.....	49
3.2.2	Fpr3 Expression in Neutrophil Granulocytes is Enhanced by LPS Stimulation	53
3.3	Strain-Specific Variants of Murine Fpr3	58
3.3.1	Fpr3 Protein Expression Occurs in a Strain-Specific Manner	58
3.3.2	Loss of Fpr3 $\Delta_{424-435}$ Function Due to Diminished Receptor Expression	61
3.3.3	Lack of <i>Fpr3</i> $\Delta_{424-435}$ Expression in HEK Cells	63
3.3.4	Fpr3 $\Delta_{424-435}$ is Non-Functional in the Vomeronasal Organ	65
3.4	Comparative Characterization of Murine and Human Fpr3 Function.....	66
3.4.1	Orthology between Murine and Human Fpr3 is not Assessable by Sequence Comparison	67
3.4.2	Murine and Human Fpr3 Show Similar Functional Properties.....	67
3.4.3	Murine and Human Fpr3 are More Selective than Fpr1 and Fpr2	69
3.4.4	Specification of Fpr3 Function in Mouse and Human	71
3.4.5	Ligand Preferences of Murine and Human Fpr3 Differ Partially	73
4	DISCUSSION.....	76
4.1	Fpr3 of Mouse and Human are Functional Orthologs	77
4.1.1	Genetic Evidence for the Orthology between Fpr3 of Mouse and Human	77
4.1.2	Fpr3 of Mouse and Human Share Functional Similarities	78
4.1.3	Adaptations of Murine Fpr3 for a Function in Olfaction	79
4.2	Murine Fpr3 is Expressed in Multiple Tissues	80
4.2.1	Fpr3 Protein is Expressed in the Vomeronasal Organ	80
4.2.2	Fpr3 Protein is Expressed in Immune Cells	82
4.3	Strain-Specific Fpr3 Variants	83
4.3.1	Two Functionally Distinct Fpr3 Variants Exist in Mice	84
4.3.2	Truncation of Fpr3 $\Delta_{424-435}$ Protein Causes a Lack of Receptor Function	85
4.3.3	Distribution of the Fpr3 Variants Amongst Laboratory Mice.....	85
4.3.4	Fpr3 Variants Originated in Wild Living Mice.....	88
4.4	Outlook	89
5	LITERATURE.....	91
	Appendix	104
	Publications	
	Copyright Permission Policy of the American Society for Biochemistry and Molecular Biology	
	Einverständniserklärung	
	Acknowledgements	

List of Figures

Figure 1.	Olfactory perception is crucial for sick conspecific aversion	3
Figure 2.	Organization of the murine vomeronasal organ	5
Figure 3.	Receptors expressed in the vomeronasal organ	9
Figure 4.	Signal peptide structure	11
Figure 5.	Relationship and genomic organization of human and murine <i>Fpr</i> genes	11
Figure 6.	Schemata of the expression cassettes of pcDNA TM 3.1 ⁽⁺⁾ and pcDNA TM 5/FRT/TO	23
Figure 7.	Schema of the expression cassette of pcDNA TM 5/FRT/TO for <i>Fpr3</i> Δ ₄₂₄₋₄₃₅	24
Figure 8.	Representative responses in FLIPR experiments	29
Figure 9.	Test of the commercially available Fpr3 antibody N-20	41
Figure 10.	Characterization of the commercially available Fpr3 antibody M-20	42
Figure 11.	Epitopes of the commercially available Fpr3 antibody M-20	44
Figure 12.	Characterization of monoclonal mouse Fpr3 antibodies	45
Figure 13.	Epitopes of the two novel specific Fpr3 antibodies ECL1 and ECL2	47
Figure 14.	ECL1 and ECL2 detect Fpr3 and do not recognize other murine Fpr family members	48
Figure 15.	ECL1 and ECL2 show high sensitivity for Fpr3	49
Figure 16.	<i>Fpr3</i> mRNA is expressed in the vomeronasal organ	50
Figure 17.	Fpr3 protein is expressed by a small subset of vomeronasal cells	50
Figure 18.	Characterization of Fpr3-positive vomeronasal cells	52
Figure 19.	Molecular characteristics of the non-olfactory Fpr3-positive cells	53
Figure 20.	Fpr3 is expressed in mouse leukocytes	54
Figure 21.	Fpr3 protein is expressed in mouse neutrophil granulocytes	54
Figure 22.	<i>Fpr3</i> mRNA is absent in blood leukocytes	55
Figure 23.	<i>Fpr3</i> mRNA expression is induced by LPS stimulation	56
Figure 24.	Human neutrophil granulocytes express three Fprs	57
Figure 25.	Fpr3 protein levels rise with increasing mRNA levels upon LPS stimulation	57
Figure 26.	Strain-specific loss of Fpr3 expression in mice	59
Figure 27.	Sequence and distribution of the 12 nucleotide <i>in-frame</i> deletion in <i>Fpr3</i> Δ ₄₂₄₋₄₃₅	60

Figure 28.	Fpr3 $\Delta_{424-435}$ does not respond to the synthetic Fpr3 agonist W-peptide	62
Figure 29.	Fpr3 $\Delta_{424-435}$ does not respond to natural Fpr3 activators	63
Figure 30.	Expression of Fpr3 $\Delta_{424-435}$ and Fpr3 _{wt} in HEK293T cells	63
Figure 31.	Fpr3 $\Delta_{424-435}$ exhibits truncated expression in HEK293T cells	64
Figure 32.	Fpr3 agonists activate knobs of VSNs	66
Figure 33.	Sequence relationship between murine Fpr3 and human Fprs	67
Figure 34.	Murine and human Fpr3 show related agonist responses	69
Figure 35.	Mouse and human Fpr3 display similar agonist selectivity	71
Figure 36.	Mouse and human Fpr3 differ in their agonist sensitivity	72
Figure 37.	Calcium responses of murine and human Fpr3 saturate at 30 μ M ligand concentration	73
Figure 38.	The ligand recognition of murine and human Fpr3 partially differs	75
Figure 39.	Fpr3-positive leukocytes contain polymorphonuclear nuclei	82
Figure 40.	Distribution of the Fpr3 variants in the laboratory mouse genealogy using the example of Castle's mice	86

List of Tables

Table 1.	Synthetic ligands used in this study	15
Table 2.	Natural ligands used in this study	16
Table 3.	Used mouse strains	17
Table 4.	Sequencing primers	18
Table 5.	PCR primers	18
Table 6.	PCR templates	20
Table 7.	Cell culture media	26
Table 8.	Antibodies used in this study	33
Table 9.	Peptide fragments for the generation of monoclonal Fpr3 antibodies	46

Appendix

Table 10.	Peptide spot array epitopes	104
Table 11.	Mouse genes containing the AMKEK motif	105
Table 12.	Mouse genes containing the LNTA motif	105
Table 13.	Haplotype analysis of the <i>Fpr3</i> gene in different mouse strains	107

Abstract

Formyl peptide receptors (Fprs) are important and broadly tuned G protein-coupled pathogen-sensors. The murine and human *Fpr* gene families are comprised of seven and three genes, respectively. Fpr1 and Fpr2 of both species have been studied extensively, but the functions of murine and human Fpr3 are poorly understood. This study provides new insight into the expression and function of murine Fpr3 in the vomeronasal and immune systems and reports the existence of natural knockout strains of this receptor.

A key result of this thesis is the discovery of a large panel of distinct mouse strains that exhibit severely altered Fpr3 expression and function. Two Fpr3 receptor variants, such as Fpr3_{wt} and Fpr3 $\Delta_{424-435}$, which showed distinct expression patterns, were identified using two newly generated Fpr3-specific antibodies. Thereby, a lack of receptor expression was attributed to a 12 nucleotide *in-frame* deletion in the *Fpr3* $\Delta_{424-435}$ gene. The lack of four amino acids produced an unstable and truncated *Fpr3* $\Delta_{424-435}$ receptor protein. In line with these findings, calcium imaging in an *in vitro* expression system and in dendritic endings of vomeronasal sensory neurons showed a lack of function for this receptor variant. *Fpr3* $\Delta_{424-435}$ was present in at least 19 mouse strains, whereas *Fpr3*_{wt} was encoded in at least 13 other strains. These data suggest a large number of mouse strains with no known Fpr3 function. The discovery of a multitude of natural *Fpr3* knockout mouse strains will be valuable to study murine Fpr3 function in the context of various genetic backgrounds.

A second key finding is the dual detection of murine Fpr3 protein expression in chemosensory neurons of the olfactory system and in specific immune cells. Significant sequence overlap and common expression in immune cells suggested a similar biological role for murine and human Fpr3. In addition, comparative *in vitro* calcium imaging experiments showed that the functional properties of murine and human Fpr3 are similar but differed drastically from those of Fpr1 and Fpr2. Thereby, Fpr3 of both species shared strongly overlapping agonist response patterns. These data provide clear evidence that murine and human *Fpr3* are functional orthologous genes. However, concentration-response curves and structural derivative testing of a typical Fpr agonist revealed subtle tuning differences between murine and human Fpr3. Taken together, these data suggest a similar biological role for human and mouse Fpr3 with subtle functional adaptations in murine Fpr3 for olfactory system requirements.

Zusammenfassung

Formylpeptidrezeptoren (Fprs) sind wichtige G-Protein gekoppelte Pathogensensoren, die ein breites Ligandenspektrum aufweisen. Die *Fpr*-Genfamilie der Maus umfasst sieben Gene, während die des Menschen aus drei Genen besteht. Fpr1 und Fpr2 beider Spezies sind weitreichend erforscht, allerdings ist die Funktion des murinen und menschlichen Fpr3 unzureichend verstanden. Diese Arbeit liefert neue Erkenntnisse über die Expression und Funktion des Fpr3 der Maus im Vomeronasalorgan und Immunsystem, und zeigt das Vorkommen natürlicher Knockout-Stämme für diesen Rezeptor.

Ein Hauptergebnis dieser Studie ist die Entdeckung einer großen Anzahl an Mausstämmen, die gravierende Unterschiede in Expression und Funktion des Fpr3 aufweisen. Mit Hilfe von zwei neu generierten Fpr3-spezifischen Antikörpern konnten zwei Fpr3 Rezeptorvarianten identifiziert werden – Fpr3_{wt} and Fpr3 $\Delta_{424-435}$ –, die unterschiedliche Expressionsmuster zeigen. Dabei konnte fehlende Rezeptorexpression einer zwölf Nukleotide umfassenden *in-frame* Deletion im *Fpr3 $\Delta_{424-435}$* Gen klar zugeordnet werden. Das Fehlen von vier Aminosäuren führte zu einem instabilen und gekürzten *Fpr3 $\Delta_{424-435}$* Rezeptorprotein. Übereinstimmend mit diesen Feststellungen, zeigte Calcium-Imaging in einem *in vitro* Expressionssystem und in dendritischen Endungen vomeronasaler sensorischer Neurone einen Funktionsmangel für diese Rezeptorvariante. *Fpr3 $\Delta_{424-435}$* lag in mindestens 19 Mausstämmen vor, während *Fpr3_{wt}* von mindestens 13 anderen Stämmen kodiert wurde. Diese Daten weisen auf eine große Zahl an Mausstämmen ohne bekannte Fpr3 Funktion hin. Die Entdeckung einer Vielzahl natürlicher *Fpr3* Knockout-Mausstämme wird beitragen die Funktion des murinen Fpr3 im Kontext vielfältiger genetischer Hintergründe zu untersuchen.

Eine zweite Schlüsselentdeckung ist der duale Nachweis der Proteinexpression des murinen Fpr3 in chemosensorischen Neuronen des olfaktorischen Systems und in speziellen Immunzellen. Signifikante Sequenzübereinstimmungen und eine gemeinsame Expression in Immunzellen legen eine ähnliche biologische Rolle des murinen und menschlichen Fpr3 nahe. Darüber hinaus zeigten vergleichende *in vitro* Calcium-Imaging Experimente ähnliche funktionelle Eigenschaften für den murinen und menschlichen Fpr3, die sich drastisch von denen des Fpr1 oder Fpr2 unterscheiden. Dabei teilten Fpr3 beider Spezies stark überlappende Agonisten-Antwortmuster. Diese Daten liefern klare Hinweise dafür, dass die Gene des murinen und menschlichen *Fpr3* funktionell orthologe Gene sind. Jedoch zeigten Konzentrations-Antwortkurven und Strukturderivat-Tests eines typischen Fpr-Agonisten subtile Sensitivitätsunterschiede zwischen den beiden Rezeptoren. Zusammengefasst weisen die Daten auf eine ähnliche Rolle für den murinen und menschlichen Fpr3 mit subtilen

funktionellen Anpassungen des murinen Fpr3 an Anforderungen des olfaktorischen Systems hin.

Abbreviations

-NH ₂	functional amino group (-NH ₂) at the C-terminus of a protein
+RT	reverse transcription reaction with reverse transcriptase
-RT	reverse transcription control without reverse transcriptase
A ₂₆₀	absorption at a wavelength of 260 nm
A ₂₈₀	absorption at a wavelength of 280 nm
Aβ ₄₂	amyloid-beta 42
Ac2-26	annexin/lipocortin 1-mimetic peptide
AOB	accessory olfactory bulb
AP	alkaline phosphatase
ATG	start codon
ATP	adenosine triphosphate
BCIP	5-bromo-4-chloro-3-indolyl phosphate
BGH	bovine growth hormone poly-adenylation site
Bioimager	Bioimager BD Pathway 855
C1	physiological salt solution category 1
CCD	charge-coupled device
CD45R	R-isoform of the cluster of differentiation molecule 45
cDNA	complementary deoxyribonucleic acid
CFU	<i>colony forming units</i>
CMV	cytomegalovirus promoter sequence
Co.	company
CT	C-terminus
<i>cursive lettering</i>	gene (≠ normal lettering that describes a protein)
dATP	2'-deoxyadenosine 5'-triphosphate
dCTP	2'-deoxycytidine 5'-triphosphate
DEPC	diethyl dicarbonate
dGTP	2'-deoxyguanosine 5'-triphosphate
DIG	digoxigenin
DIOPT	DRSC Integrative Ortholog Prediction Tool
DMSO	dimethyl sulfoxide
DNA	deoxyribonucleic acid
dNTP	2'-deoxynucleoside 5'-triphosphate
dTTP	2'-deoxythymidine 5'-triphosphate

DTT	dichlorodiphenyltrichloroethane
EC ₅₀	half maximal effective concentration
ECL	extracellular loop
EDTA	ethylenediaminetetraacetic acid
ESP	exocrine gland-secreting peptide
f-	functional formyl group (-CHO) at the N-terminus of a protein
ΔF	maximal change in fluorescence
F ₀	baseline fluorescence
F _{max}	fluorescence maximum
F _{min}	fluorescence minimum
FCS	fetal calf serum
FL#	internal laboratory identifier number for ligands
FLIPR	fluorometric imaging plate reader
Fpr	(murine) formyl peptide receptor
FPR	human formyl peptide receptor
Fpr3Δ ₄₂₄₋₄₃₅	non-functional strain-specific receptor variant of (murine) formyl peptide receptor 3 containing a 12 nucleotide <i>in-frame</i> deletion from nucleotide 424 to 435
Fpr3 _{wt}	functional strain-specific receptor variant of (murine) formyl peptide receptor 3
Fpr-rs	formyl peptide receptor-related sequence
FuLe	full length
g	acceleration due to gravity
Gapdh	glyceraldehyde 3-phosphate dehydrogenase
Gα ₁₆	G protein alpha 16 subunit
Gα _{i2}	G protein alpha i2 subunit
Gα _o	G protein alpha o subunit
gene ID	gene identification number
Gγ2	G protein gamma 2 subunit
Gγ8	G protein gamma 8 subunit
h	hour
H2-Mv	gene encoding a major histocompatibility complex molecule
HBSS	Hank's balanced salt solution
HEK	human embryonic kidney

293T	cell line 293 that expresses the simian virus 40 large T antigen
HEPES	4-(2-hydroxyethyl)-1-piperazineethane-sulfonic acid
hFPR	human formyl peptide receptor
HGNC	HUGO Gene Nomenclature Committee
HIV-1	human immunodeficiency virus 1
hND	N-terminus of human NADH-ubiquinone oxidoreductase chain
HSV	herpes simplex virus derived fusion sequence
HSV-tag	11 amino acids derived from herpes simplex virus glycoprotein D
ICL	intracellular loop
LB	Luria-Bertani
LL-37	human antimicrobial peptide LL-37
LPS	lipopolysaccharide
Ly6G	lymphocyte antigen 6G
mATP6	N-terminus of murine ATP synthase A chain protein 6
mCOIII	N-terminus of murine Cytochrome c oxidase polypeptide III
MCS	multiple cloning site
mCytb	N-terminus of murine Cytochrome b
mFpr	murine formyl peptide receptor
MGI	mouse genome informatics
MHC	major histocompatibility complex
MHV	mouse hepatitis virus
min	minute
<i>M. m.</i>	<i>Mus musculus</i>
mND	N-terminus of murine NADH-ubiquinone oxidoreductase chain
MOB	main olfactory bulb
MOE	main olfactory epithelium
mRNA	messenger ribonucleic acid
MUP	major urinary protein
<i>n</i>	number of performed experiments
N-	N-terminus of a protein
NADH	reduced nicotinamide adenine dinucleotide
NBT	nitro blue tetrazolium
NCBI	national center for biotechnology information

OMP	olfactory marker protein
Order#	order number
ψ	pseudogene
PBS	phosphate-buffered saline
PCR	polymerase chain reaction
PDE4A	phosphodiesterase 4A
PH#	internal laboratory identifier number for primers
ppi	pixels per inch
PVDF	polyvinylidene difluoride
RFU	relative fluorescence units
Rho	rhodopsin-derived fusion sequence
Rho-Fpr3 $\Delta_{424-435}$ -HSV	fusion protein of the Fpr3 $\Delta_{424-435}$ receptor variant with an N-terminal Rho-tag and a C-terminal HSV-tag
Rho-Fpr3 _{wt}	fusion protein of the Fpr3 _{wt} receptor variant with an N-terminal Rho-tag
Rho-tag	the first 39 amino acids of bovine rhodopsin
RNA	ribonucleic acid
rpm	revolutions per minute
RPMI-1640	Roswell Park Memorial Institute medium
RT	room temperature
RT-PCR	reverse transcription polymerase chain reaction
S	septum
S.D.	standard deviation
SDS	sodium dodecyl sulfate
SDS-PAGE	sodium dodecyl sulfate polyacrylamide gel electrophoresis
SOC	super optimal broth with catabolite repression
SP	signal peptide
Sp6	Sp6 bacteriophage growing on <i>Escherichia coli</i>
SPase	signal peptidase
SSC	saline-sodium citrate
SV40	simian virus 40
T2R16-HSV	fusion protein of the human type 2 taste receptor 16 and a C-terminal HSV-tag
T7	T7 bacteriophage growing on <i>Salmonella typhimurium</i>

TASP	thermosensitive alkaline phosphatase
TE	Tris-EDTA
TGA	stop codon
TMHMM	transmembrane helix prediction based on a Markov model
TN	Tris-HCl, NaCl
TO	tetracycline operator
Tris	2-amino-2-(hydroxymethyl)propane-1,3-diol
U	enzyme unit
Vmn1r, V1r	vomeronasal type 1 receptor
Vmn2r, V2r	vomeronasal type 2 receptor
Vmn2r ⁺ H2-Mv ⁺	vomeronasal type 2 receptor coexpressed with a <i>H2-Mv</i> gene
Vmn2r ⁺ H2-Mv ⁻	vomeronasal type 2 receptor not coexpressed with a <i>H2-Mv</i> gene
VNO	vomeronasal organ
VSN	vomeronasal sensory neuron
YT	yeast extract and tryptone

1 INTRODUCTION

1.1 Social Recognition and Olfactory Pathogen Recognition

Important information about the social status of conspecifics is conveyed by olfactory cues in rodents (Restrepo *et al.*, 2006; Chamero *et al.*, 2007; Brennan, 2009; Li *et al.*, 2013). Chemical signals used to transmit information between conspecifics are commonly called pheromones. Pheromones are substances secreted to the outside by an individual and received by another individual of the same species that trigger distinct reactions, such as behaviors or developmental processes (Karlson and Lüscher, 1959).

The first ever described pheromone-mediated effect in mammals was the “Whitten effect”. In 1956, Wesley Whitten observed the induction of estrus in anestrus female mice upon exposure to male pheromones (Whitten, 1956). Soon after, the “Bruce effect” was demonstrated by Hilda Bruce in 1959 (Bruce, 1959). She described that newly mated female mice experience a pregnancy block and return to estrus if exposed to unfamiliar males prior to implantation of the embryo. A third mammalian pheromone effect that communicates the social status of an animal was discovered in 1969 by John Vandenbergh (Vandenbergh, 1969). The “Vandenbergh effect” portrays the acceleration of puberty in female mice upon exposure to male chemosignals. Interestingly, a delay in puberty could be induced by exposure to female pheromones (Cowley and Wise, 1972; Vandenbergh, 1973; Novotny *et al.*, 1986; Jemiolo and Novotny, 1994). Since then, many other important social behavioral effects induced by olfactory cues have been reported, including sexual behavior and preference, parental behavior, and discrimination of individuals (Jemiolo *et al.*, 1991; Leybold *et al.*, 2002; Haga *et al.*, 2010), parental behavior (Brouette-Lahlou *et al.*, 1999; Numan *et al.*, 2006), aggression (Stowers *et al.*, 2002; Chamero *et al.*, 2011), and the discrimination of individuals (Hurst *et al.*, 2001; Restrepo *et al.*, 2006; Kelliher *et al.*, 2006).

Despite the many benefits of social behaviors, close interactions among conspecifics increase the risk of parasite transmission and pathogenic infection (Altizer *et al.*, 2003; Kavaliers *et al.*, 2004). To prevent these events, mice and other rodents are able to recognize infected conspecifics and display aversive responses to contagious individuals. Behavioral and genetic evidence suggests the involvement of the sense of smell in this process (Penn and Potts, 1998; Kavaliers *et al.*, 2004). The best studied system is the health status-dependent choice of mating partners. In 1982, William Hamilton and Marlene Zuk first suggested that animals examine urine and fecal cues to identify disease and parasite-free mates (Hamilton and Zuk, 1982). Mice preferentially select parasite-free or parasite-resistant mating partners

(Hamilton and Zuk, 1982; Kavaliers *et al.*, 2000; Ehman and Scott, 2002). Female mice were shown to discriminate odors from healthy males against others infected with different parasites, such as nematodes, (Kavaliers and Colwell, 1995; Ehman and Scott, 2001; Kavaliers *et al.*, 2003a), protozoans (Kavaliers and Colwell, 1993; Kavaliers *et al.*, 1997), influenza virus (Penn *et al.*, 1998), or lice (Lehmann, 1993; Kavaliers *et al.*, 2003b). In all cases, the female mice actively avoided infected males or their odors (Kavaliers *et al.*, 2005). Male mice also showed aversion to urine odors of other males infected with parasites (Kavaliers *et al.*, 2004). They refused to copulate with females infected with nematodes (Edwards and Barnard, 1987) and displayed aversive behavior to them (Gourbal and Gabrion, 2004) or their odors (Kavaliers *et al.*, 1998). Resistance to the nematode *Heligomosomoides polygyrus* is heritable (Wahid *et al.*, 1989). Thus, this odor-based mate selection is considered an indicator of “good genes” (Kavaliers *et al.*, 2005).

Although many social interactions based on odors of infected conspecifics are known, the underlying molecular and cellular basis for perceiving an olfactory pathogen is unclear. The olfactory system of most mammals is subdivided into two principal subsystems, the main olfactory and the vomeronasal systems, which both trigger innate avoidance behaviors (Kobayakawa *et al.*, 2007; Papes *et al.*, 2010). Furthermore, two other olfactory structures, such as the septal organ of Masera and the Grueneberg ganglion, also play roles detecting pheromones and pheromone-driven behaviors (Roppolo *et al.*, 2006; Ma, 2007; Tirindelli *et al.*, 2009). One study provided clear evidence for involvement of the murine vomeronasal organ (VNO) mediating the avoidance of sick conspecifics (Boillat *et al.*, 2015). The authors demonstrated a preference of mice for healthy conspecifics over mice that were injected with lipopolysaccharide (LPS). LPS is an endotoxin produced by Gram-negative bacteria that activates the immune system and mimics a bacterial infection (Dantzer *et al.*, 2008). They also described aversive behavior to urine of mice infected with the mouse hepatitis virus (MHV) (Boillat *et al.*, 2015). Mice without a functional VNO showed no aversion (Figure 1). Hence, the VNO may function as a sensor of infection.

In line with the idea that the VNO is involved in pathogen sensing, odors from sick animals activate neurons in the vomeronasal pathway of wild-type mice (Boillat *et al.*, 2015). However, mice without a functional VNO lack this activation (Boillat *et al.*, 2015). In line with these experiments, sensory cells in the VNO detect inflammatory markers and bacterial peptides, which are typical activators of formyl peptide receptors (Fprs) found in the immune system (unpublished data). Furthermore, several members of the murine *Fpr* gene family are

expressed in the VNO (Liberles *et al.*, 2009; Rivière *et al.*, 2009). Thus, Fprs expressed in the VNO are prime candidates for olfactory pathogen sensing.

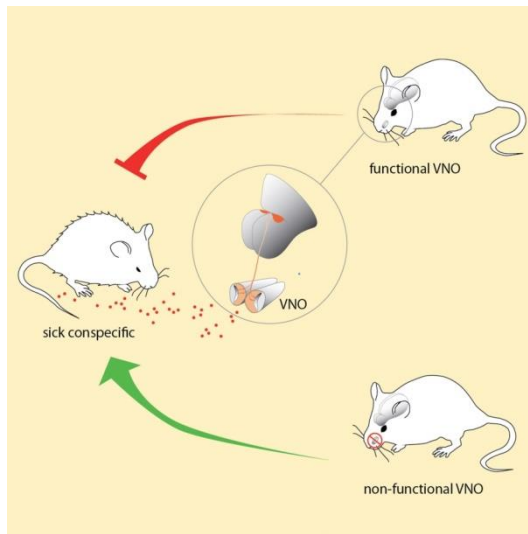


Figure 1. **Olfactory perception is crucial for sick conspecific aversion.** Mice with an intact VNO (upper right) avoid mice or urine infected with LPS or MHV (left). Mice with a non-functional VNO (lower right) show no aversion. Figure was adapted from Boillat *et al.*, 2015.

1.2 The Vomeronasal Organ

1.2.1 General Function of the Vomeronasal Organ

The VNO is the receptor organ of the accessory olfactory system. It contributes to social recognition and chemical communication – processes that are mediated by pheromones (Halpern and Martínez-Marcos, 2003). The crucial function of the VNO as a pheromone sensing system is well-established. Several studies examined mice after removal of the organ and reported the absence of typical pheromone-driven effects, such as the associated estrus induction (Whitten effect) (Sánchez-Criado and Gallego, 1979; Sánchez-Criado, 1982; Mora and Cabrera, 1997), pregnancy block (Bruce effect) (Reynolds and Keverne, 1979; Bellringer *et al.*, 1980), and puberty acceleration (Vandenbergh effect) (Lomas and Keverne, 1982). All these effects were still observable in control mice that possessed a functional VNO. Pheromone-driven effects and behaviors were also attenuated by ablation of different genes expressed in the VNO. Tissue-specific deletion of signal transduction elements, such as genes encoding the G protein alpha o subunit ($G\alpha_o$), the G protein gamma 8 subunit ($G\gamma 8$), or a family of nine nonclassical class I major histocompatibility complex (MHC) genes, the *H2-Mv* genes, severely reduced aggression (Chamero *et al.*, 2011; Montani *et al.*, 2013; Leinders-Zufall *et al.*, 2014). Additionally, $G\alpha_o$ gene removal impaired a wide range of reproductive pheromone-regulated behaviors in adult mice, including estrus induction

(Whitten effect) and puberty acceleration (Vandenbergh effect) (Oboti *et al.*, 2014). Furthermore, mice deficient for *Trpc2*, another essential signal transduction component for VNO function, showed striking behavioral defects in regulating a wide range of sexual and social behaviors (Zufall, 2005; Zufall *et al.*, 2005). In summary, these findings show that the VNO is a key element for pheromone perception.

An important function of the VNO beyond pheromone recognition is the detection of predator odors (Papes *et al.*, 2010; Isogai *et al.*, 2011). Specific substances contained in these odors, so-called kairomones, elicit powerful fear-like reactions in prey species that facilitate escape, induce freezing and avoidance, and can increase stress hormone levels (Apfelbach *et al.*, 2005). Known kairomones include trimethyl-thiazoline, a volatile component of fox odor (Kobayakawa *et al.*, 2007), several lipocalins found in rat urine and cat saliva (Papes *et al.*, 2010), and 2-phenylethylamine that is produced in many carnivore urines (Ferrero *et al.*, 2011). Kairomones can derive from different odor sources, such as urine, feces, saliva, and fur. Interestingly, different kairomones are detected by the VNO and the main olfactory epithelium and detection mechanisms may depend on stimulus volatility (Liberles, 2014).

In line with this observation, growing evidence emerges for the contribution of the main olfactory epithelium to the detection of social chemosignals (Spehr *et al.*, 2006a). Some non-volatile chemosignals established earlier as sensory stimuli of the VNO were shown to activate cells in the main olfactory epithelium (Ziesmann *et al.*, 2002; Lin *et al.*, 2004; Xu *et al.*, 2005; Spehr *et al.*, 2006b). Hence, the main olfactory epithelium is also involved in mediating social behaviors. In line with these thoughts, impairment of sexual behavior in mice lacking a functional main olfactory epithelium but possessing an intact VNO provided clear evidence for the involvement of the main olfactory epithelium in social behaviors (Keller *et al.*, 2006). However, behavioral tests using mice with genetic and surgical lesions showed that stimulation of each system by the same substance can result in differing behavioral effects. This suggests that the same chemosignals can convey distinct social behaviors through differential activation and processing through different olfactory systems (Spehr *et al.*, 2006a; Pérez-Gómez *et al.*, 2014).

1.2.2 Anatomy of the Vomeronasal Organ

The VNO was first described in 1813 by Danish anatomist Ludwig Jacobson (Jacobson, 1813). It is a sensory organ that is present in most mammals (Liberles, 2014). Anatomically, the VNO consists of a pair of bilateral symmetrical cylinders. It is located at the base of the anterior nasal septum. There, it is protected by a bony capsule that is formed by the vomer

bone. On the posterior side it ends blindly, whereas on the anterior side it is connected with the nasal cavity via a water-filled duct (Broman, 1920). Substances can enter the nasal cavity through sniffing (Halpern, 1987; Dulac and Torello, 2003; Liberles, 2014). Vomeronasal agonists dissolved in fluids have to be sucked actively into the nasal cavity. An active pumping mechanism generated by pulsing blood vessels located laterally of the lumen in the non-sensory epithelium creates a suction that transports the substances through the lumen to the crescent-shaped vomeronasal sensory epithelium (Figure 2) (Døving and Trotier, 1998). The vomeronasal sensory epithelium houses vomeronasal sensory neurons (VSNs). These are specialized nerve cells express distinct receptors that detect pheromone substances (Brennan and Zufall, 2006).

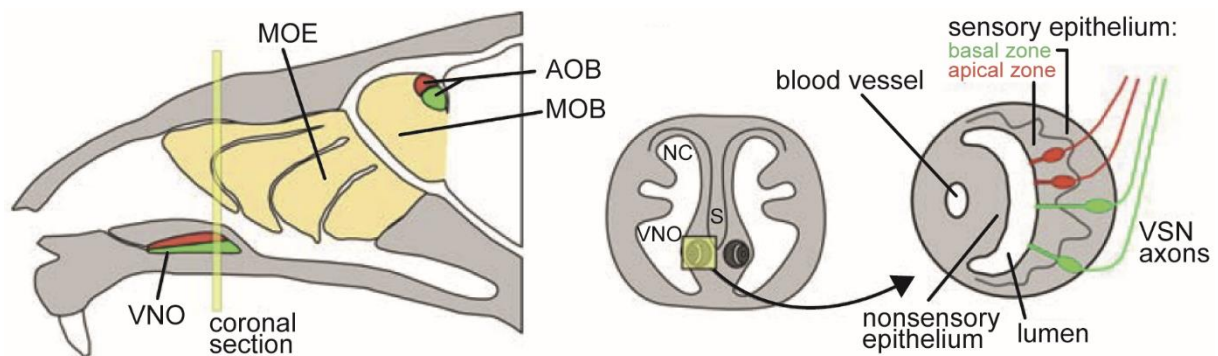


Figure 2. **Organization of the murine vomeronasal organ.** Midsagittal view of the nasal cavity and forebrain. Sensory neurons in the main olfactory epithelium (MOE) project their axons to glomeruli in the main olfactory bulb (MOB). Vomeronasal sensory neurons (VSNs) in the apical (red) or basal (green) layer of the vomeronasal organ (VNO), which is located at the base of the nasal septum (S), project to the anterior (red) or posterior (green) side of the accessory olfactory bulb (AOB). Figure was adapted and modified from Zufall *et al.*, 2005.

In 1970 the segregation of axon projections to the main olfactory bulb and the accessory olfactory bulb, specialized anterior brain areas, was documented in rodents (Winans and Scalia, 1970). The data suggested two parallel projection pathways to the brain, one for the VNO and one for the main olfactory epithelium (Raisman, 1972; Scalia and Winans, 1975). More than 20 years later, the separate projection of VSNs to the accessory olfactory bulb could be demonstrated by tracking axons with histological markers (Jia and Halpern, 1996; Belluscio *et al.*, 1999; Rodriguez *et al.*, 1999). Vomeronasal sensory neurons project to the accessory olfactory bulb (Figure 2). This structure serves as a first processing center for vomeronasal information (Munger *et al.*, 2009). On the molecular level the vomeronasal sensory epithelium can be subdivided into an apical and a basal layer (Halpern *et al.*, 1995; Dulac and Axel, 1995; Berghard and Buck, 1996). VSNs from different VNO layers project to different sides of the accessory olfactory bulb. VSNs located in the apical layer project to six

to 30 small glomeruli in the rostral half of the accessory olfactory bulb, whereas basal VSNs project to a similar amount of small glomeruli in the posterior half of the accessory olfactory bulb (Jia and Halpern, 1996; Belluscio *et al.*, 1999; Rodriguez *et al.*, 1999; Del Punta *et al.*, 2002a). From there, mitral cells interconnect the accessory olfactory bulb with higher brain regions, such as the amygdala and hypothalamic nuclei (Halpern, 1987).

1.2.3 Detection Mechanisms in the Vomeronasal Organ

Two main populations of VSNs are anatomically segregated into an apical and a basal zone that together form the vomeronasal sensory epithelium. These main populations differ in their expressed receptors (Herrada and Dulac, 1997; Matsunami and Buck, 1997; Ryba and Tirindelli, 1997) and down-stream signal transduction molecules (Dulac and Axel, 1995; Halpern *et al.*, 1995; Berghard and Buck, 1996).

The VNO detects many substances from different chemical classes (Zufall and Leinders-Zufall, 2007). Its ligand spectrum is complex and reaches from volatile substances to non-volatile peptides. Details are still under investigation, but the current view assigns detection of different ligand classes to specific zones of the vomeronasal sensory epithelium. VSNs of the apical zone expressing vomeronasal type 1 receptors (Vmn1rs) detect volatile substances, whereas basal VSNs expressing vomeronasal type 2 receptors (Vmn2rs) are responsible for the detection of peptide ligands (Liberles, 2014).

1.2.3.1 *Vmn1r* Expressing Vomeronasal Sensory Neurons

VSNs expressing Vmn1rs represent the vast majority of the apical VNO layer (Dulac and Axel, 1995; Pantages and Dulac, 2000; Leinders-Zufall, 2000). Vmn1rs are coexpressed with the G protein alpha i2 subunit (G α i2) (Berghard and Buck, 1996; Jia and Halpern, 1996) and the G protein gamma 2 subunit (G γ 2) (Rünnenburger *et al.*, 2002). In mouse, 191 intact of a total of 308 *Vmn1r* genes are known (Zhang *et al.*, 2007).

Vmn1r expressing cells can detect small volatile substances (Leinders-Zufall, 2000; Zufall and Leinders-Zufall, 2007). Electrovomeronasograms revealed activation of apical VSNs through substances, such as 2,5-dimethylpyrazine and 2-heptanone (Leinders-Zufall, 2000; Del Punta *et al.*, 2002b). Consistent with the notion that Vmn1rs are activated by volatiles, knockout of a ~600 kb genomic region that contains a cluster of 16 intact *Vmn1r* genes resulted in impaired recognition for volatiles, such as n-pentyl acetate and isobutylamine (Del Punta *et al.*, 2002b). However, this knockout did not give information about which of the deleted receptors were responsible for the perception of these substances. Further studies

addressing this question reported three specific receptor-ligand interactions for *Vmn1rs* (Boschat *et al.*, 2002; Haga-Yamanaka *et al.*, 2014; Haga-Yamanaka *et al.*, 2015). One study assigned the recognition of 2-heptanone to the receptor *V1r2b* by functional experiments on vomeronasal sensory neurons marked with green fluorescent protein (Boschat *et al.*, 2002). More recently, activation of tomato-labeled *V1rj2* or *V1rj3* expressing vomeronasal cells by sulfated steroids has been shown (Haga-Yamanaka *et al.*, 2014; Haga-Yamanaka *et al.*, 2015). *V1rj2* expressing cells responded to sulfated and glucuronidated estrogens, sulfated androgens, sulfated progesterones, and a corticosterone. *V1rj3* expressing cells were more selective in their responses and reacted only to sulfated estrogens, androgens, and progesterone (Haga-Yamanaka *et al.*, 2014; Haga-Yamanaka *et al.*, 2015).

1.2.3.2 Vmn2r Expressing Vomeronasal Sensory Neurons

VSNs expressing *Vmn2rs* are resident in the basal VNO zone. These receptors are coexpressed with $G\alpha_o$ (Berghard and Buck, 1996; Jia and Halpern, 1996) and $G\gamma 8$ (Rünnenburger *et al.*, 2002). In mouse, 122 of a total of 282 *Vmn2r* genes are intact genes (Martini *et al.*, 2001; Young and Trask, 2007). *Vmn2r* expressing VSNs can be further subdivided into VSNs coexpressing a *Vmn2r* with an *H2-Mv* gene ($Vmn2r^+ H2-M^+$) and VSNs expressing a *Vmn2r* without a *H2-Mv* gene ($Vmn2r^+ H2-Mv^-$). *H2-Mv* genes encode nine class I major histocompatibility complex (MHC) molecules. The associated MHC molecule is assumed to act as a co-factor, a chaperone, or a co-receptor for the given *Vmn2r* (Ishii *et al.*, 2003; Loconto *et al.*, 2003; Ishii and Mombaerts, 2008). A recent study deleted a 530 kb cluster of *H2-Mv* genes and showed lower sensitivity for a subset of VSNs lacking this cluster (Leinders-Zufall *et al.*, 2014).

Vmn2r expressing cells have been shown to detect class I MHC-binding peptides (antigens) that alter female reproductive function (Leinders-Zufall *et al.*, 2004; Leinders-Zufall *et al.*, 2009; Boehm and Zufall, 2006; Leinders-Zufall *et al.*, 2014). Related to this, pregnancy failure in freshly mated female mice (Bruce effect) could be evoked by the introduction of class I MHC-binding peptides of non-familiar males into familiar male urine that was given as stimulus (Leinders-Zufall *et al.*, 2004). It has been shown that *Vmn2r26* (*V2r1b*) expressing VSNs can be activated by antigens, such as SYFPEITHI, SEIDLILGY, and AYKDNRETI (Leinders-Zufall *et al.*, 2004). Distinct derivatives of these substances also activated the examined cells. Moreover, *Vmn2r81* (*V2rf2*) expressing cells reacted to the antigens SEIDLILGY and f-MFFINTLTTL (Leinders-Zufall *et al.*, 2014). These

findings provide support for an evolutionary link between recognition mechanisms in immune cells and subsets of VSNs.

Vmn2rs of the V2rp subfamily respond to exocrine gland-secreting peptides from tear fluid and saliva of mice (Kimoto *et al.*, 2005; Dey and Matsunami, 2011). These peptides form a family of 38 related peptides of which 15 have been shown to elicit electrical responses in the VNO (Kimoto *et al.*, 2007). Vmn2r116 (V2Rp5) is the best studied receptor detecting this substance class. VSNs that express Vmn2r116 are activated by exocrine gland-secreting peptide 1 (ESP1), a 7-kDa peptide secreted by the extraorbital lacrimal gland of male mice that enhances lordosis behavior in female mice. Knocking out the receptor gene abolishes VSN responses to ESP1 (Kimoto *et al.*, 2005; Haga *et al.*, 2010). Moreover, a single report described the activation of Vmn2r111 (V2rp2) by ESP5 and Vmn2r112 (V2rp1) by ESP5 and ESP6 (Dey and Matsunami, 2011). Recently, ESP22 that is present in tears of prepubertal mice was found to inhibit mating behavior of adult males (Ferrero *et al.*, 2013).

Another potent ligand group assigned to the basal VNO layer is composed of major urinary proteins (MUPs) (Sturm *et al.*, 2013). These proteins are proposed to operate as olfactory signals for conspecific recognition, due to their high polymorphism rate and the fact that they are genetically encoded (Cheetham *et al.*, 2007). MUPs may elicit inbreeding avoidance, countermarking behavior, and female sexual attraction (Hurst *et al.*, 2001; Sherborne *et al.*, 2007; Roberts *et al.*, 2010; Kaur *et al.*, 2014). Additional to this already wide recognition capacity, they also play an important role in mediating aggressive behavior, conditioned learned spatial preference, and the detection of predators (Chamero *et al.*, 2007, Chamero *et al.*, 2011; Papes *et al.*, 2010; Roberts *et al.*, 2012). To date, no specific Vmn2r could be assigned to this ligand class thus far.

1.2.3.3 Formyl Peptide Receptor Expressing Vomeronasal Sensory Neurons

Other important G protein-coupled receptors expressed in VSNs are Fprs. Mice encode seven *Fpr* genes (Gao *et al.*, 1998; Ye *et al.*, 2009). Two independent studies recently discovered five murine Fprs in subpopulations of VSNs (Liberles *et al.*, 2009; Rivière *et al.*, 2009). Four Fprs (*Fpr-rs3*, *Fpr-rs4*, *Fpr-rs6*, and *Fpr-rs7*) are located in the apical layer, where they coexpress with $G\alpha_i2$. Fpr3 (formerly known as Fpr-rs1; see MGI gene ID: 1194495) is the only Fpr expressed by basal VSNs and coexpresses with $G\alpha_o$ (Liberles *et al.*, 2009; Rivière *et al.*, 2009). Vomeronasal Fprs are not coexpressed with other types of vomeronasal receptors. Substances that are classified as Fpr agonists, such as the artificial W-peptide or the archetypical N-formylated peptide f-MLF, were shown to activate

vomeroneasal Fprs (Rivière *et al.*, 2009; Bufe *et al.*, 2012; Bufe *et al.*, 2015). However, their precise function is unknown, but some evidence suggests members of the Fpr family, particularly Fpr3, as current prime candidates for mediating vomeronasal pathogen sensing.

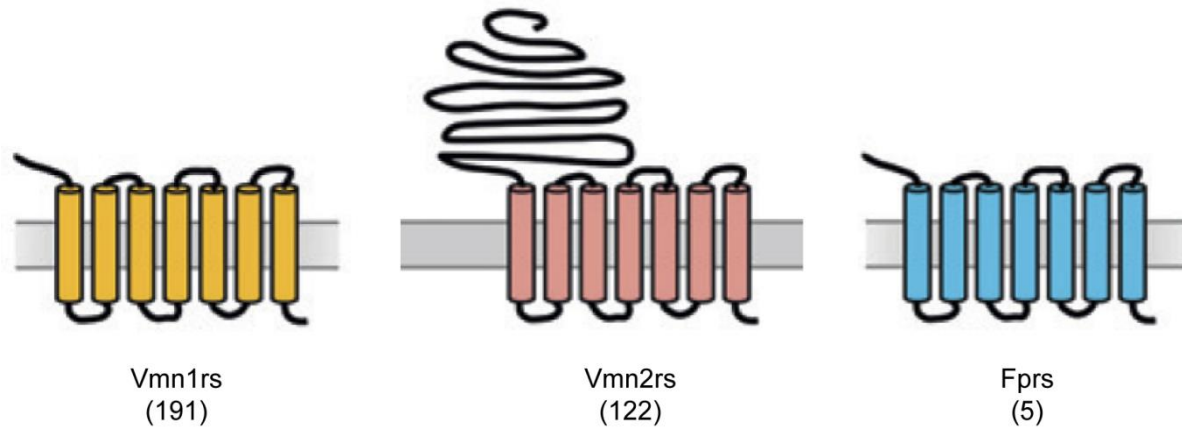


Figure 3. **Receptors expressed in the vomeronasal organ.** Schematic depiction of different receptor types expressed in murine VSNs. The number of known mouse genes is indicated below each structure. In the apical layer, 191 intact Vmn1r and four Fprs are expressed. In the basal layer, 122 intact Vmn2rs and Fpr3 are expressed. The receptors are expressed in non-overlapping subpopulations of VSNs. Figure was adapted and modified from Chamero *et al.*, 2012.

1.3 Formyl Peptide Receptors

1.3.1 General Function of Formyl Peptide Receptors

Fprs are chemotactic G protein-coupled receptors (Bufe and Zufall, 2016; Dahlgren *et al.*, 2016). They comprise a single 350 to 370 amino acid long polypeptide chain that forms seven transmembrane domains (Boulay *et al.*, 1990). The transmembrane segments of *Fpr* genes are more conserved than their extracellular domains, which display significant variability (Migeotte *et al.*, 2006; Fu *et al.*, 2006).

Little is known about Fpr function in the olfactory system. However, their function in the immune system is intensely studied. There they are involved in chemoattraction of phagocytic immune cells and contribute to the recruitment of cells from the bone marrow to the blood stream and from the blood stream to inflammatory sites (Ye and Boulay, 1997). They can detect a large spectrum of chemical attractants either secreted by invading pathogens or released during inflammatory processes (Migeotte *et al.*, 2006, Ye *et al.*, 2009). Upon activation, Fprs mediate a variety of host defense mechanisms against invading microorganisms (Fu *et al.*, 2006; Migeotte *et al.*, 2006; Ye *et al.*, 2009; Bloes *et al.*, 2015). Besides their prominent role in chemotaxis, Fprs are also involved in the mobilization of

adhesion molecules from intracellular storage granules, the secretion of proteolytic enzymes and in reactive oxygen species production (Holland, 2013; Parker and Winterbourn, 2013).

To fulfill this plethora of functions Fprs are very broadly tuned and promiscuous receptors that are capable of sensing many different ligands of different substance classes. Their functional promiscuity becomes clear when looking at the wide range of recognized substances. These include inflammatory markers, such as LL-37 (Yang *et al.*, 2000) and Annexin A1 (Ernst *et al.*, 2004), viral peptides, such as several viral HIV-1 envelope proteins (Su *et al.*, 1999a; Su *et al.*, 1999b; Le *et al.*, 2000), and host-derived peptides including mitochondrial peptides, such as different NADH-ubiquinone oxidoreductase chain, internal NADH dehydrogenase, and Cytochrome c oxidase subunit peptides (Rabiet *et al.*, 2005; Gripenberg and Miettinen, 2008; Bufe *et al.*, 2012). Furthermore, Fprs detect peptides associated to Alzheimer's disease, such as serum amyloid A (Ye *et al.*, 2009), A β ₄₂ (Le *et al.*, 2001a; Tiffany *et al.*, 2001), and humanin that protects cells from damage caused by A β ₄₂ (Harada *et al.*, 2004), as well as some host-derived non-peptide agonists. Moreover, they can detect a variety of synthetic peptides, such as the hexa-peptides W-peptide or M-peptide (Fu *et al.*, 2006; Ye *et al.*, 2009; Bae *et al.*, 2012; Bufe *et al.*, 2012; He *et al.*, 2013; Bufe *et al.*, 2015; Bylund *et al.*, 2014; Bufe and Zufall, 2016).

Currently best studied are bacterial peptide agonists with N-formylated peptides leading the way. Most known formylated peptides are derived from bacteria. f-MLF, derived from *Escherichia coli*, was one of the first characterized chemotactic peptides and has been studied extensively since its initial discovery in 1975 (Schiffmann *et al.*, 1975). f-MLF is the smallest formyl peptide that displays full agonistic activity for human FPR1 and FPR2. Other bacterial peptides, such as peptides derived from *Listeria monocytogenes* (Rabiet *et al.*, 2005; He *et al.*, 2013) and phenol-soluble modulins peptide toxins derived from *Staphylococcus aureus* (Wang *et al.*, 2007; Bloes *et al.*, 2015), have been also identified as Fpr agonists. The detection mechanism of Fprs relies on specific peptide motifs that are present in sensed peptides (Bufe *et al.*, 2012). Intriguingly, the motifs found in many formerly identified bacterial peptides are prime components of bacterial signal peptides (Bennet *et al.*, 1980; Bufe and Zufall, 2016). In line with these findings, recent systematic structure-function studies of Fprs from six mammalian species revealed clear evidence that Fprs primarily focus on the detection of formylated signal peptides from bacteria. This is due to specific evolutionarily conserved pathogen associated molecular patterns that possibly allow for detection of more than 100,000 distinct formyl peptides (Bufe *et al.*, 2015).

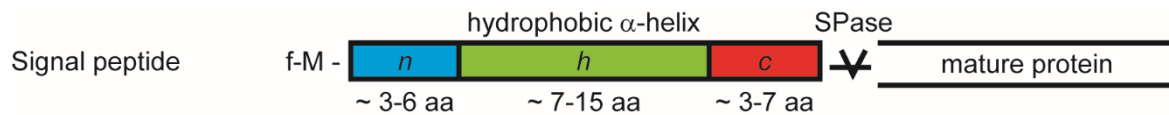


Figure 4. **Signal peptide structure.** Signal peptides are the first natural agonists identified for murine Fpr3. They guide newly synthesized proteins to the membrane transport machinery of a bacterium. Besides their differing amino acid sequences they share a conserved secondary structure that is largely α -helical (von Heinje, 1985). They exhibit a typical motif combining a high degree of sequence flexibility and a conserved three-dimensional topology. Bacterial signal peptides comprise three typical domains: a 3-6 amino acid long N-terminal region (blue) starting with a methionine (M), an α -helical hydrophobic h-region (green), and a C-terminal region (red), that contains a conserved signal peptidase (SPase) recognition motif (von Heinje, 1985; Dalbey *et al.*, 2012). Figure was adapted from Bufo *et al.*, 2015.

1.3.2 Genetics of Formyl Peptide Receptors

Fprs can be found in mammals (Liberles *et al.*, 2009) and in other phylogenetic classes, such as birds and fish (Panaro *et al.*, 2007; Bufo and Zufall, 2016). The human genome encodes three *Fpr* genes, *FPR1*, *FPR2*, and *FPR3*, in a cluster located on chromosomal region 19q13.3 (Figure 5B) (Bao *et al.*, 1992; Alvarez *et al.*, 1994). All three human *Fpr* genes are single copy genes with intron-less open reading frames, but they encode introns in their untranslated regions (Perez *et al.*, 1992; Ye *et al.*, 1992; Bao *et al.*, 1992; Murphy *et al.*, 1992).

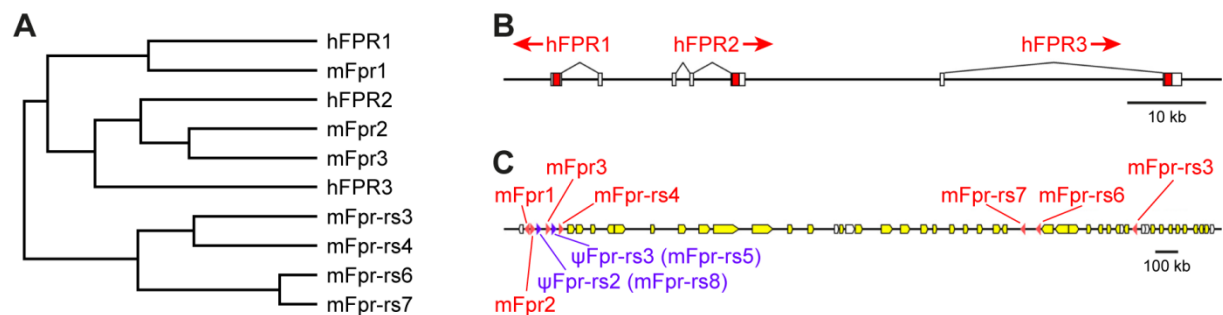


Figure 5. **Relationship and genomic organization of human and murine *Fpr* genes.** **A**, dendrogram depicting amino acid sequence similarities between human and murine Fprs. **B**, organization of the three human *Fpr* genes located on chromosome 19q13.3. White and red boxes indicate non-coding or coding exonic sequence segments, respectively. **C**, organization of the nine functional and non-functional *Fpr* genes of the mouse located on chromosome 17A3.2. Red, purple, yellow, and white arrows represent presumably functional *Fpr* genes, pseudogenes, vomeronasal receptor genes, or other genes, respectively. hFPR = human Fpr; mFpr = murine Fpr. Figure was adapted from Migeotte *et al.*, 2006.

Looking at the organization of *Fpr* genes in other species than human, the complex history and evolution of the receptor family becomes clear. In rodents, the *Fpr* gene cluster has undergone species-specific expansion (Gao *et al.*, 1998; Wang and Ye, 2002). Thus, the mouse genome encodes seven full-length *Fpr* genes – *Fpr1*, *Fpr2*, *Fpr3*, *Fpr-rs3*, *Fpr-rs4*, *Fpr-rs6*, and *Fpr-rs7* – and two pseudogenes ψ *Fpr-rs2* (*Fpr-rs8*) and ψ *Fpr-rs3* (*Fpr-rs5*) with

premature stop codons on chromosome 17A3.2 (Figure 5C) (Gao *et al.*, 1998; Migeotte *et al.*, 2006). *ψFpr-rs2* has an open reading frame and its expression could be induced by LPS stimulation in spleen and bone marrow, which are both leukocyte accumulating organs (Tiffany *et al.*, 2011). This suggests that the protein product of *ψFpr-rs2* may fulfill a biological function.

1.3.3 Tissue Distribution of Formyl Peptide Receptors

Fpr expression is described in a variety of leukocytes. Human *FPR1* has been described in tissue-residing neutrophil granulocytes, macrophages, microglia, dendritic cells, monocytes, and lymphocytes (Durstin *et al.*, 1994; Lacy *et al.*, 1995; Migeotte *et al.*, 2005; Migeotte *et al.*, 2006). Expression of human *FPR1* was also reported for multiple non-immune organs and tissues including epithelial cells in organs with secretory functions, thyroid and cortical cells of the adrenal gland, liver, smooth muscle, brain, spinal cord, and both motor and sensory neurons (Becker *et al.*, 1998; Ye *et al.*, 2009). Human *FPR2* expression has been reported for neutrophil granulocytes, monocytes, macrophages, T- and B-lymphocytes, microglial cells, platelets, hepatocytes, epithelial cells, microvascular endothelial cells, and fibroblasts (Le *et al.*, 2001b; VanCompernelle *et al.*, 2003; Czapiga *et al.*, 2005; Migeotte *et al.*, 2006). Expression of human *FPR3* is less studied. This receptor has been found in fewer cell types than the other human Fprs (Ye *et al.*, 2009). mRNA of the receptor has been detected in monocytes and dendritic cells, where it is thought to be the dominant formyl peptide receptor (Yang *et al.*, 2001; Yang *et al.*, 2002; Migeotte *et al.*, 2005). RNA of human *FPR3* has also been detected in a wide variety of tissues including lung, spleen, lymph nodes, trachea, placenta, liver, adrenal gland, small intestine, and in some other tissues at minor levels, by using quantitative reverse transcription polymerase chain reaction (RT-PCR) (Harada *et al.*, 2004; Migeotte *et al.*, 2006).

Expression of murine Fprs is not studied to the extent of human Fprs. Murine *Fpr1* is expressed in dendritic cells, neutrophil granulocytes, and bone marrow cells (Gao *et al.*, 1998; Lee *et al.*, 2004; Southgate *et al.*, 2008; Chiu *et al.*, 2013). Moreover, transcripts for murine *Fpr1* have been reported for spleen, lung, kidney, liver, the trigeminal nerve, and bone marrow cells (Migeotte *et al.*, 2006; Chiu *et al.*, 2013). Murine *Fpr2* has been found in the same cells and organs as *Fpr1*, except for liver (Gao *et al.*, 1998; Lee *et al.*, 2004; Migeotte *et al.*, 2006; Southgate *et al.*, 2008; Chiu *et al.*, 2013).

Investigations on murine *Fpr3* expression are more ambiguous. One report described *Fpr3* expression in the leukocyte accumulating organs spleen and lung, as well as in

peripheral blood-derived leukocytes by northern blot analyses (Gao *et al.*, 1998). However, the performed experiments lacked a cellular resolution and technical issues, such as cross-hybridization with other *Fprs*, could not be completely excluded. Moreover, several other studies could not confirm the finding of murine *Fpr3* expression in leukocytes (Lee *et al.*, 2004; Southgate *et al.*, 2008; Rivière *et al.*, 2009; Chiu *et al.*, 2013).

The expression of the *Fpr-rs* genes is even less understood. Besides *Fpr3*, all of them are expressed in the VNO (Liberles *et al.*, 2009; Rivière *et al.*, 2009). Small amounts of *Fpr-rs3* RNA were also found in skeletal muscle by northern blot analyses (Gao *et al.*, 1998). *Fpr-rs4* expression outside the olfactory system has not been reported yet. *Fpr-rs6* RNA has been detected in brain, spleen, testis, and skeletal muscle. *Fpr-rs7* expression has been described in heart, liver, lung, spleen, smooth muscle, pancreas by RT-PCR (Wang and Ye, 2002). Moreover, transcripts for *Fpr-rs6* and *Fpr-rs7* were identified from bone marrow-derived dendritic cells (Lee *et al.*, 2004).

1.3.4 Relationship between Murine and Human Formyl Peptide Receptors

The evolutionary relationship between murine *Fprs* and their human counterparts are not understood in their entirety. In agreement with several publications, the mouse genes *Fpr1* and *Fpr2* are orthologs of human *FPR1* and *FPR2*, respectively (Migeotte *et al.*, 2006; Önnheim *et al.*, 2008; Dahlgren *et al.*, 2016). Functionally, murine and human *Fpr1* and *Fpr2* are very similar. Receptors of both species are very promiscuous (see chapter 1.3.1). Thus, it is not surprising that many ligands activating human *Fprs* also activate their mouse orthologs.

The relationship between murine *Fpr3* and the human *Fpr* genes is insufficiently examined. Its sequence is most similar with that of human *FPR2* with a significant overlap to human *FPR3* (Hartt *et al.*, 1999; Ye *et al.*, 2009). The high sequence similarity of murine *Fpr3* to these human immune receptors provides evidence for a possible expression of murine *Fpr3* in the immune system. Furthermore, its orientation and position on the chromosome resembles that of human *FPR3* (Figure 5B, C). Murine *Fpr3* has only recently been deorphanized (Bufe *et al.*, 2012; He *et al.*, 2013; Bufe *et al.*, 2015). Functionally, murine *Fpr3* seems to share a high similarity with human *FPR3* since both receptors are less promiscuous than *Fpr1* and *Fpr2* of both species. Calcium imaging experiments showed responses for murine and human *Fpr1* and *Fpr2* to a wide panel of bacterial signal peptides whereas *Fpr3* of both species was much more narrowly tuned. These data provide first evidence for a functional orthology between murine and human *Fpr3*. However, to substantiate the definite relationship of murine *Fpr3* to a possible human counterpart, further

functional investigations must be done. *Fpr-rs3*, *Fpr-rs4*, *Fpr-rs6*, and *Fpr-rs7* seem to have no direct counterparts in the human genome (Figure 5A) (Migeotte *et al.*, 2006).

1.4 Aims of this Work

Recently, formyl peptide receptors have been discovered in the mouse vomeronasal organ (Liberles *et al.*, 2009; Rivière *et al.*, 2009). However, the biological role of these vomeronasal Fprs is poorly understood but they are candidate pathogen sensors based on the function of structurally related Fprs in immune cells (Liberles *et al.*, 2009; Rivière *et al.*, 2009). Murine Fpr3 was the first vomeronasal Fpr that was recently deorphanized (Bufe *et al.*, 2012). Furthermore, several studies have reported functional similarities between murine Fpr3 and the immune receptor human FPR3. Both receptors sense peptides of bacterial origin (Harada *et al.*, 2004; Ernst *et al.*, 2004; Bufo *et al.*, 2015). However, differences in their expression patterns argue against a similar function for the two receptors. Murine Fpr3 is expressed in the vomeronasal organ, but reports about its presence in immune cells are controversial (Gao *et al.*, 1998; Lee *et al.*, 2004; Southgate *et al.*, 2008; Rivière *et al.*, 2009; Chiu *et al.*, 2013). Human FPR3 is found in immune cells but adult humans lack a functional vomeronasal organ (Yang *et al.*, 2001; Yang *et al.*, 2002; Migeotte *et al.*, 2005; Liman and Innan, 2003; Zhang and Webb, 2003). Thus, it is questionable if both receptors fulfill similar functions. Three main questions were proposed to understand the biological relationship between murine and human Fpr3:

1. What is the evolutionary relationship between murine and human Fpr3?
2. What is the functional relationship between murine and human Fpr3?
3. What is the precise expression pattern of murine Fpr3 in different tissues?

Careful characterization of murine Fpr3 expression with two newly generated antibodies showed that the receptor is expressed in the vomeronasal organ and immune system. Functional studies using heterologous calcium imaging provided clear evidence for similarities in the agonist responses of murine and human Fpr3.

Additionally, a large panel of natural *Fpr3* knockout mouse strains that lack expression and function of this receptor are presented.

2 EXPERIMENTAL PROCEDURES

2.1 Ligands

To achieve the main goals of this work, it was relevant to gain insight into the function of murine and human Fpr3. Therefore, many different ligands of different origins and with different properties were used for functional experiments.

2.1.1 Synthetic Ligands

A major ligand group used in this study consisted of synthetic peptides, comprising W- and M-peptide in D- and L-conformation, and various W-peptide derivatives. Table 1 lists all synthetic peptide ligands used in this study with their primary structure, the company they were purchased from, their purity, the solvent they were diluted in, and the FL-number (FL#), which is the internal laboratory identifier.

Table 1. Synthetic ligands used in this study

Ligand	Primary Structure	Company	Purity (%)	Solvent	FL#
W-Peptide Library					
D-W-Peptide	WKYMVm-NH ₂	Innovagen	>95.00	C1	FL21
L-W-Peptide	WKYMVM-NH ₂	Tocris	>99.20	C1	FL22
D-M-Peptide	MMHWAm-NH ₂	GenScript Corporation	>99.60	C1	FL57
L-M-Peptide	MMHWAM-NH ₂	GenScript Corporation	>96.80	C1	FL56
W-Library Peptide 13b	WKYMV C -NH ₂	GenScript Corporation	>97.20	C1	FL46
W-Library Peptide 14	WKYMV a -NH ₂	GenScript Corporation	>98.50	C1	FL47
W-Library Peptide 29	WKYMV i -NH ₂	GenScript Corporation	>97.30	C1	FL81
W-Library Peptide 30	WKYMV o -NH ₂	GenScript Corporation	>99.90	C1	FL82
W-Library Peptide 28	WKYMV f -NH ₂	GenScript Corporation	>98.60	C1	FL80
W-Library Peptide 13	WKYMV c -NH ₂	GenScript Corporation	>95.00	C1	FL32
W-Library Peptide 33	WKYMV [hcy]-NH ₂	GenScript Corporation	>95.20	C1	FL85
W-Library Peptide 45	WKYMV q -NH ₂	GenScript Corporation	>97.70	C1	FL106
W-Library Peptide 27	WKYMV k -NH ₂	GenScript Corporation	>99.70	C1	FL79
W-Library Peptide 46	WKYMV e -NH ₂	GenScript Corporation	>97.50	C1	FL107
W-Library Peptide 92	WKYMAm-NH ₂	VCPBIO	>95.19	C1	FL177
W-Library Peptide 93	WKYMI m -NH ₂	VCPBIO	>98.11	C1	FL178
W-Library Peptide 94	WKYMF m -NH ₂	VCPBIO	>98.52	C1	FL179
W-Library Peptide 91	WKYAV m -NH ₂	VCPBIO	>97.45	C1	FL176
W-Library Peptide 87	WKYW V m-NH ₂	VCPBIO	>95.26	C1	FL172
W-Library Peptide 88	WKYF V m-NH ₂	VCPBIO	>95.31	C1	FL173
W-Library Peptide 89	WKYK V m-NH ₂	VCPBIO	>95.75	C1	FL174
W-Library Peptide 90	WKYE V m-NH ₂	VCPBIO	>95.93	C1	FL175
W-Library Peptide 17	WK AM Vm-NH ₂	GenScript Corporation	>99.00	C1	FL50
W-Library Peptide 16	WK FM Vm-NH ₂	GenScript Corporation	>96.70	C1	FL49
W-Library Peptide 36	WK QM Vm-NH ₂	GenScript Corporation	>96.70	C1	FL97
W-Library Peptide 34	WK KM Vm-NH ₂	GenScript Corporation	>96.80	C1	FL95
W-Library Peptide 35	WK EM Vm-NH ₂	GenScript Corporation	>97.20	C1	FL96

2.1.2 Natural Ligands

Besides the synthetic ligands, various natural peptide ligands comprising murine, human, and bacterial peptides were used in this study. Table 2 displays all natural peptide ligands with their primary structure, their origin, the company they were acquired from, their purity, the solvent they were diluted in, and the FL-number (FL#), which is the internal laboratory identifier.

Table 2. Natural ligands used in this study

Ligand	Primary Structure	Origin	Company	Purity (%)	Solvent	FL#
Murine Peptides						
Ac2-26	Ac- AMVSEFLKQAWFIENEEQEYVQTVK	Immune system	Tocris	>95.00	C1	FL19
mATP6	f-MNENLF	mitochondria	VCPBIO	>95.44	C1	FL196
N-terminus of mND2	f-MNPITL	mitochondria	VCPBIO	>95.33	C1	FL188
N-terminus of mND3	f-MNLYTV	mitochondria	VCPBIO	>95.52	C1	FL133
N-terminus of mND4	f-MLKIIL	mitochondria	VCPBIO	>95.63	C1	FL189
N-terminus of mND4L	f-MPSTFF	mitochondria	VCPBIO	>95.21	C1	FL190
N-terminus of mND5	f-MNIFFT	mitochondria	VCPBIO	>95.42	C1	FL191
N-terminus of mND6	f-MNNYIF	mitochondria	VCPBIO	>96.54	C1	FL192
N-terminus of mCytb	f-MTNMRK	mitochondria	VCPBIO	>95.33	C1	FL195
N-terminus of mCOIII	f-MTHQTH	mitochondria	VCPBIO	>95.74	C1	FL194
Human Peptides						
N-terminus of hND4	f-MLKLIV	mitochondria	VCPBIO	>96.96	C1	FL142
N-terminus of hND5	f-MTMHTT	mitochondria	VCPBIO	>98.00	C1	FL113
N-terminus of hND6	f-MMYALF	mitochondria	VCPBIO	>95.97	C1	FL141
Bacterial Peptides						
f-MIVILY	f-MIVILY	<i>Listeria monocytogenes</i>	VCPBIO	>96.34	C1	FL140
Bacterial Signal Peptide Fragments (N-termini)						
<i>Streptococcus</i> -SP1	f-MGFFIS	<i>Streptococcus suis</i>	VCPBIO	>95.43	C1	FL134
<i>Psychromonas</i> -SP6	f-MLFYFS	<i>Psychromonas ingrahamii</i>	VCPBIO	>95.59	DMSO	FL207
<i>Clostridium</i> -SP13	f-MKKNLV	<i>Clostridium perfringens</i>	United Biosystems	>95.67	C1	FL239
<i>Hydrogenobacter</i> -SP16	f-MKKFLL	<i>Hydrogenobacter thermophilus</i>	United Biosystems	>95.78	C1	FL245
<i>Staphylococcus</i> -SP22	f-MKKFNI	<i>Staphylococcus aureus</i>	VCPBIO	>95.30	C1	FL170
<i>Salmonella</i> -SP24	f-MKKFRW	<i>Salmonella enterica</i>	VCPBIO	>98.34	C1	FL185
Bacterial Signal Peptides (full length)						
<i>Staphylococcus</i> -SP22 FuLe	f-MKKFNILIALLFFTSLVISPLNVKA	<i>Staphylococcus aureus</i>	VCPBIO	>96.83	C1	FL180

2.2 Mouse Strains

In this thesis, experiments with a variety of different mouse strains were performed. For strain names, the nomenclature employed by the Mouse Genome Informatics database (ftp://ftp.informatics.jax.org/pub/reports/MGI_Strain.rpt) was used.

Table 3. Used mouse strains

Strain	Origin	Inbred Type	Source
C57Bl/6N	England	Classical	Trese Leinders-Zufall (Saarland University School of Medicine) Dieter Bruns (Saarland University School of Medicine)
NZB/Ola	England	Classical	Reinhart Kluge (German Institute of Human Nutrition)
129X1/Sv	England	Classical	Trese Leinders-Zufall (Saarland University School of Medicine)
BALB/cJ	England	Classical	
FVB/NCrI	Switzerland	Classical	Frank Kirchhoff (Saarland University School of Medicine)
SPRET/EiJ	Spain	Wild-derived (spretus)	
CAST/EiJ	Thailand	Wild-derived (castaneus)	
KAZ/DT	Kazakhstan	Wild-derived (musculus)	Diethard Tautz (Max-Planck-Institut für Evolutionsbiologie)
CZE/DT	Czech Republic	Wild-derived (musculus)	
GER/DT	Germany	Wild-derived (domesticus)	
FRA/DT	France	Wild-derived (domesticus)	

Mouse inbred strains can be classified into two groups: classical and wild-derived. While the genome of the classical inbred strains derived of only a few progenitors (Tucker *et al.*, 1992; Beck *et al.*, 2000) and comprises a mosaic of different *mus musculus* subspecies (Bonhomme *et al.*, 1987), the genome of wild-derived inbred strains consists of wild living mice caught at different times and locations (Beck *et al.*, 2000), and thus mostly represent the genome of the respective wild caught *mus musculus* subspecies.

2.3 Molecular Biology

2.3.1 Oligonucleotides

For this study, two types of primers were used – sequencing primers and polymerase chain reaction (PCR) primers. Sequencing primers were used in sequencing reactions to verify the nucleotide sequences of cloned genes. PCR primers were used for amplification of murine and human *Fprs* for cloning purposes. The housekeeping genes encoding glyceraldehyde 3-phosphate dehydrogenase (*Gapdh*) and β -actin were also amplified with PCR primers as controls in PCR reactions. All primers were purchased from Sigma-Aldrich.

2.3.1.1 Sequencing Primers

Internal sequencing primers bind inside of a gene. Additionally, sequencing primers targeting the cytomegalovirus (CMV) promoter before the start codon (ATG) and the bovine growth hormone (BGH) polyadenylation site behind the stop codon (TGA) were used to ensure covering the complete amplified gene in order to obtain comprehensive analyses. Sequencing primers with their binding targets, their sequences and their PH-numbers (PH#), which are the internal laboratory identifiers are listed in table 4.

Table 4. Sequencing primers

Binding Target	Sequencing Primer Sequences [5' > 3']	PH#
<i>Murine Fpr3</i>	Forward: GCTAGAAATGTGGTTGTTGGGTCC	PH473
	Forward: GATCAGATGTGGTGATCTATGATTCTAC	PH692
	Forward: CTGAATCTAGCATTGGCTGACTTC	PH693
	Forward: CATTGCAGTAGATGTAAACCTATTGG	PH694
	Reverse: AGGAAGTGAAGCCAAATTGGT	PH695
<i>CMV promoter</i>	Forward: CGCAAATGGGCGGTAGGCGTG	PH1
<i>BGH polyadenylation site</i>	Reverse: TAGAAGGCACAGTCGAGG	PH2

2.3.1.2 PCR Primers





Primers for amplification of complete coding regions were designed to cover the start (ATG) and the stop codon (TGA). Forward primers comprised the start codon, whereas reverse primers included the stop codon. Primers that were used for gene amplification in PCR experiments, their targeted genes, and accession numbers are listed in table 5.





Table 5. PCR primers

Gene	Accession Numbers*	Synonyms*	Gene-Specific Primer Sequences [5' > 3']	PH#
<i>Murine Fpr3</i>	NM_008042.2	<i>ALX; Fpr-rs1; Fpr-s1; Fprl1; LXA4-R; Lxa4r</i>	Forward: ATGGAAACCAACTACTCTATCCCTTTGAAT	PH354
			Reverse: TATTGCCTTTATTCAATGTCTTCAGGA	PH355
			RNA Probe Primers for <i>In Situ</i> Hybridization:	
			Forward: CACTACAAAGATTCACAAAAAAGCCTTTG	PH558
			Reverse: AATATTCTAGGCCCTTTGACTTTTACTTTTTT	PH559
<i>Human FPR1</i>	NM_001193306.1	<i>FMLP; FPR</i>	Forward: ATGGAGACAAATTCCTCTCTCCC	PH462
			Reverse: CTTTGCCTGTAACCTCCACCTCTGC	PH463
<i>Human FPR2</i>	NM_001462.3	<i>ALXR; FMLP-R-II; FMLPX; FPR2A; FPRH1; FPRH2; FPRL1; HM63; LXA4R</i>	Forward: ATGGAAACCAACTTCTCCACTCCTC	PH464
			Reverse: CATTGCCTGTAACCTCAGTCTCTGCA	PH465
<i>Human FPR3</i>	NM_002030.4	<i>FML2_HUMAN; FMLP-R-II; FMLPY; FPRH1; FPRH2; FPRL2; RMLP-R-I</i>	Forward: ATGGAAACCAACTTCTCCATTCTCCT	PH467
			Reverse: CATTGCTTGTAACCTCCGTCTCCTC	PH468
<i>β-actin</i>	NM_007393.5	<i>Actx; beta-actin; E430023M04Rik</i>	Forward: CTGGAACGGTGAAGGTGACA	PH153
			Reverse: AAGGGACTTCCTGTAACAATGCA	PH154
<i>Gapdh</i>	NM_001289726.1	<i>Gapd</i>	Forward: ACCACAGTCCATGCCATCAC	PH11
			Reverse: TCCCACCACCTGTTGCTGTA	PH12




* = National Center for Biotechnology Information (NCBI) data.




For cloning, PCR primers were attached to a sequence with several restriction sites to ensure directed insertion into expression vectors. To forward primers a *HindIII*- (AAGCTT), a *SbfI*-site (CCTGCAGG), and a KOZAK sequence (GCCACC) was added upstream of the start codon (ATG) at the 5' end.

- forward primers: 5'–     – 3'

 = *HindIII*-site
 = *SbfI*-site
 = KOZAK sequence
 = start codon

To reverse primers a stop codon (TGA), a *SacI*- (GAGCTC), and a *NotI*-site (GCGGCCGC) was added downstream of the stop codon (ATG) at the 3' end.

- reverse primers: 3'–    – 5'

 = *NotI*-site
 = *SacI*-site
 = stop codon

2.3.2 Polymerase Chain Reaction

PCR was performed with Phusion High-Fidelity DNA Polymerase (New England Biolabs Inc.) according to the manufacturer's protocol. For each reaction, 0.5 µl cDNA and 10 pM of a forward and reverse primer were added to 10 µl 2× Phusion Master Mix, respectively, and filled up to a total volume of 20 µl with de-ionized water. The whole reaction was pipetted and mixed on ice. Reaction conditions for all primers were 98°C for 15 s followed by 35 cycles (denaturation: 98°C for 10 s, annealing: 64°C for 10 s, elongation: 72°C for 40 s), and 72°C for 20 s. Subsequently, PCR products were purified.

2.3.3 PCR Templates

PCR templates for this study were obtained via RNA isolation (see chapter 2.3.4), subsequent cDNA synthesis (see chapter 2.3.5), and by direct extraction of genomic DNA (see chapter 2.3.6). Templates were collected from different mouse strains and different

tissues. Table 6 outlines all used PCR templates, the organs and mouse strains they were gathered from, and the providers of the used mice.

Table 6. PCR templates

Template	Organ	Mouse Strain	Source
RNA	Blood	C57	Purchased from Zyagen
cDNA	VNO Bone Marrow Cells	C57Bl/6NCrl	Trese Leinders-Zufall and Dieter Bruns (Saarland University School of Medicine)
	VNO	NZB/Ola	Reinhart Kluge (German Institute of Human Nutrition)
	VNO	129X1/Sv	Trese Leinders-Zufall (Saarland University School of Medicine)
	VNO	BALB/cJ	Trese Leinders-Zufall (Saarland University School of Medicine)
	VNO	FVB/NCrl	Frank Kirchhoff (Saarland University School of Medicine)
Genomic DNA	Ear	SPRET/EiJ CAST/EiJ KAZ/DT CZE/DT GER/DT FRA/DT	Diethard Tautz (Max-Planck-Institut für Evolutionsbiologie)

2.3.4 RNA Isolation

RNA from VNO and bone marrow of mice was obtained with the innuPREP RNA Mini Kit (Analytik Jena AG) according to the manufacturer's protocol. For lysis, tissue was incubated in 400 µl RL buffer for 2 min at room temperature (RT) and subsequently fully resuspended. For removal of genomic DNA, the suspension was transferred to a Spin Filter D and centrifuged at 10,000× g for 2 min and 400 µl 70% (v/v) ethanol was added to the filtrate. Binding of RNA was achieved by transferring the sample to Spin Filter R and subsequent centrifugation at 10,000× g for 2 min. For on-column DNase I digestion, 300 µl Washing Solution HS were added to the filter and centrifuged at 10,000× g for 1 min. A DNase I/Digestion Buffer mix (40 Kunitz Units innuPREP DNase I in 80 µl DNase I Digestion Buffer) was applied to the filter and incubated for 15 min at RT. Subsequently, 300 µl Washing Buffer HS were added and centrifuged at 10,000× g for 1 min. For washing, 750 µl LS Buffer were added and centrifuged at 10,000× g for 1 min. Ethanol was removed by spinning the column again after discarding the flow-through at 10,000× g for 3 min. RNA was eluted with RNase-free water after incubation of 1 min at RT and subsequent centrifugation at 6,000× g for 1 min. Quality was assessed by gel electrophoresis and photometric measurements. After isolation, RNA was used to synthesize cDNA.

2.3.5 cDNA Synthesis

cDNA was synthesized from 0.5 µg total RNA using the Smart cDNA Synthesis protocol (Clontech) and Superscript II Reverse Transcriptase (Invitrogen). Therefore, 5 µl reverse transcriptase buffer (2µl 5× First Strand Buffer, 4 mM dichlorodiphenyltrichloroethane (DDT), 12.5 mM dNTP-Mix (3.125 mM of dATP, dTTP, dGTP, and dCTP), 40 Units MMLV reverse transcriptase RNase H⁻ (Gibco), 10 Units RiboLock RNase Inhibitor (Thermo Scientific), and 1.15 µl water treated with diethyl dicarbonate (DEPC)) were added to 0.1 µg to 1 µg RNA including 2 µM CDS Primer and 2 µM Smart II Primer. The whole reaction was pipetted and mixed on ice. Synthesis was achieved by increasing heating steps starting at 42°C for 30 min, followed by 45° for 10 min, 50°C for 10 min, 55°C for 10 min, and 65°C for 5 min. After synthesis, cDNA was diluted in 100 µl de-ionized water and subsequently used as template in PCR reactions.

2.3.6 Extraction of Genomic DNA

Genomic DNA was extracted from the VNO or ear stamps of mice with the Blood DNA Mini Kit (PEQLAB) according to the manufacturer's protocol. For lysis 250 µl PBS, 25 µl OB-Protease, and 250 µl BL-Buffer were added to the tissue in a 1.5 ml Safe-lock tube (Eppendorf) and vortexed for 10 s. Afterwards, it was incubated at 70°C for 10 min. For binding of DNA, 260 µl isopropanol was added and mixed. Subsequently, the sample was transferred to the filter column and centrifuged at 8,000× g for 1 min. Flow-through was discarded. The column was washed twice with 600 µl washing buffer supplemented with ethanol. Flow-through was discarded. To remove ethanol, the column was centrifuged at 8,000× g for 2 min. Genomic DNA was eluted in 200 µl Elution-Buffer after 2 min via centrifugation at 5,000× g for 1 min and afterwards used as template in PCR reactions.

2.3.7 Purification of PCR Products

PCR products were purified with the MinElute PCR Purification Kit (Qiagen) according to the manufacturer's protocol. Briefly, PCR products were diluted 1:5 with binding buffer, mixed via pipetting up and down and transferred on centrifugation columns. After centrifugation for 1 min at 14,000 rpm and RT the reactions were rinsed with 750 µl washing buffer. Subsequently, the reactions were centrifuged again, to eliminate alcohol remains. Purified DNA was eluted in 15 µl elution buffer via centrifugation for 1 min at 14,000 rpm and RT. Afterwards, purified PCR products were analyzed by separation with agarose gel electrophoresis.

2.3.8 Gel Electrophoresis

DNA was size separated in 1% (m/v) agarose gels. As electrophoresis buffer 0.5× TBE (de-ionized water containing 44.5 mM Tris base, 44.5 mM boric acid, 1 mM EDTA- Na_2 (pH 8)) and ethidium bromide (Carl Roth®) was used. To obtain a gel agarose was added to the buffer. 10 μl DNA solution (1 μl in the case of a PCR sample) were adjusted to 12 μl with 6X Orange DNA Loading Dye (Thermo Scientific). Reference was 6 μl FastRuler™ Middle Range DNA Ladder (Thermo Scientific). The duration of an electrophoresis was 30 min under constant voltage of 80 V.

2.3.9 RNA Quantification

Quantification of RNA probes was performed in gel electrophoresis chambers pretreated with 0.3% (v/v) H_2O_2 for 24 h and RNase-free agarose was used. References, to determine RNA probe concentration, were 20 ng, 40 ng, 60 ng, 80 ng, and 100 ng of non-labeled probes that were loaded on the gel. Molecular weight standard was the RiboRuler™ High Range RNA Ladder (Thermo Scientific).

2.3.10 Enzymatic DNA Digestion

Subcloning of PCR products into vectors was performed by digesting purified PCR products and vectors with different restriction enzymes. PCR products were digested with *Sbf*I and *Not*I. Digestions were performed after the Thermo Scientific™ FastDigest™ (Thermo Scientific) protocol. Therefore, 1 μl 10X FastDigest buffer, 0.5 μl of each used restriction enzyme, and ~200 ng purified PCR product or 1 μg plasmid vector were adjusted to 10 μl with de-ionized water. Additional 0.5 μl thermosensitive alkaline phosphatase (TSAP; Promega) were added to vector digestions. The reaction was incubated for 1 h at 37°C and could be afterwards used for ligation into expression vectors.

To identify bacterial clones carrying the desired receptor, restriction analyses were performed with the purified plasmids. Restriction analyses were performed with *Eco*RI and *Sac*I. Digestion reactions were analyzed for specific band patterns on agarose gels. Restriction sites were predicted with the Vector NTI® software (life technologies).

2.3.11 Expression Vectors

PCR products containing the complete coding sequence of a gene were ligated into mammalian expression vectors in 5' → 3' orientation. For calcium imaging experiments, *Fprs*

were inserted into a slightly modified version of pcDNATM3.1⁽⁺⁾ (Thermo Scientific) that contained a *SbfI* restriction site.

For immunocytochemical detection, *Fprs* were inserted into the pcDNATM5/FRT/TO vector (Thermo Scientific), a tetracycline inducible plasmid that can be used in mammalian cells with the Flp-In T-RExTM system (Thermo Scientific). It was also modified in its multiple cloning site (MCS) by adding an extra *SbfI* restriction site. In addition, the plasmid contains the sequence for the first 39 amino acids of bovine rhodopsin (Rho-tag). When the inserted gene is expressed, the Rho-tag is fused to the N-terminus of the receptor gene and can be detected by an anti-Rho antibody. This allows examination of protein expression for the inserted receptor via immunofluorescence analyses. *Fpr* genes were cloned into *SbfI* and *NotI* sites within the modified pcDNATM3.1⁽⁺⁾ and pcDNATM5/FRT/TO vectors. Figure 6 shows the altered cloning sites of the two vectors.

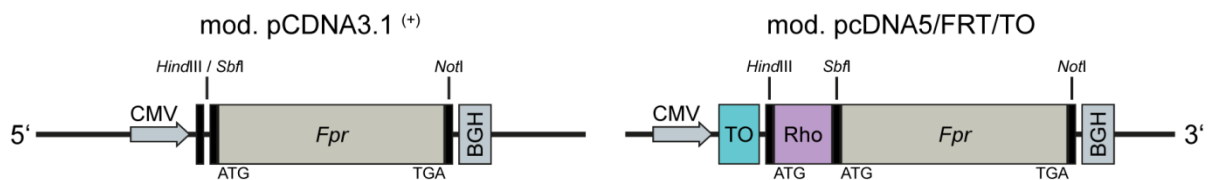


Figure 6. **Schemata of the expression cassettes of pcDNATM3.1⁽⁺⁾ and pcDNATM5/FRT/TO.** **Left panel:** For calcium imaging experiments in transiently transfected HEK293T cells, murine *Fpr3* was cloned into a version of the vector with an extra *SbfI* restriction site. **Right panel:** For expression analysis during immunocytochemistry experiments performed in transiently transfected HEK293T cells, *Fprs* were cloned into pcDNA5/FRT/TO carrying an upstream fusion sequence of the first 39 amino acids of bovine rhodopsin (Rho-tag). Start (ATG) and Stop (TGA) codons are indicated below. Restriction sites are shown as black bars. Corresponding restriction enzymes are shown above the gene cassettes. BGH = Bovine Growth Hormone polyadenylation site; CMV = cytomegalovirus promoter sequence; Rho = rhodopsin-derived fusion sequence; TO = tetracycline operator.

Fpr3 $\Delta_{424-435}$ was subcloned from the modified pcDNATM5/FRT/TO vector to an existing pcDNATM5/FRT/TO vector containing 11 amino acids derived from herpes simplex virus glycoprotein D (HSV-tag) downstream of its multiple cloning site. This subcloning was realized with *HindIII* and *NotI* and resulted in an *Fpr3* $\Delta_{424-435}$ receptor with an N-terminal Rho-tag and a C-terminal HSV-tag that was expressed as fusion protein. Thereby, the extent of the expression of *Fpr3* $\Delta_{424-435}$ in transiently transfected HEK293T cells could be examined in immunocytochemistry experiments targeting the Rho- and HSV-tag. Figure 7 shows the altered cloning site of the described expression vector. All plasmids carry an ampicillin resistance gene for selective growth in bacteria.

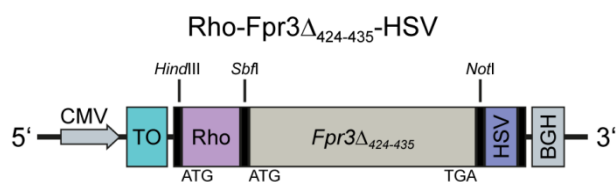


Figure 7. **Schema of the expression cassette of pcDNA™5/FRT/TO for *Fpr3*Δ₄₂₄₋₄₃₅.** *Fpr3*Δ₄₂₄₋₄₃₅ was subcloned into pcDNA5/FRT/TO carrying an upstream Rho-tag and downstream 11 amino acids of the herpes simplex virus glycoprotein D (HSV-tag). Start (ATG) and Stop (TGA) codons are indicated below. Restriction sites are shown as black bars. Corresponding restriction enzymes are shown above the gene cassettes. BGH = Bovine Growth Hormone poly-adenylation site; CMV = cytomegalovirus promoter sequence; HSV = herpes simplex virus derived fusion sequence; Rho = rhodopsin-derived fusion sequence; TO = tetracycline operator.

2.3.12 DNA Ligation

Ligation of digested and purified DNA (plasmids and PCR products) was performed with the Fast-Link™ DNA Ligation Kit (LK0750H; Epicentre Biotechnologies) according to the manufacturer's protocol. Therefore, 0.5 µl 10× Fast-Link™ Ligation Buffer, 0.5 µl ATP, 0.5 µl Fast-Link™ DNA Ligase, 10 ng to 20 ng insert DNA, and 5 ng to 10 ng vector DNA were adjusted to 5 µl with de-ionized water. Reactions were incubated overnight at 4°C or 1 h at RT. Ligation products may be used for transformation of competent *Escherichia coli*.

2.3.13 Transformation of Competent *Escherichia coli*

Ligation products were transformed via heat-shock into competent *Escherichia coli* 10-β bacteria (competence > 10⁹ CFU; New England Biolabs). Stocks of *Escherichia coli* 10-β were stored at -80°C and thawed on ice. 1 µl ligation product was added to a 15 µl bacteria aliquot and incubated on ice for 10 min. Heat-shock was performed for 30 s at 42°C in the water bath. Afterwards, bacteria were held on ice for 1 min. 150 µl SOC-medium (2% (m/v) casein hydrolyzate, 5% (m/v) yeast extract, 0.05% (m/v) NaCl, 2.5 mM KCl, 10 mM MgCl₂, and 20 mM D-Glucose, adjusted to pH 7.4) were given to the bacteria for regeneration and shaken at 220 rpm and 37°C for 1 h. Subsequently, bacteria were spread on agar plates containing 50 µg/ml ampicillin and incubated overnight at 37°C.

2.3.14 Isolation of Plasmid DNA from Bacterial Cultures

At least three bacteria colonies were picked for each genetic construct for restriction analysis. Clones positive for the restriction analysis were inoculated in 5 ml of 2× YT-medium (1.6% (m/v) casein hydrolyzate, 1% (m/v) yeast extract, 0.5% (m/v) NaCl, adjusted to pH 7.4) containing 50 µg/ml ampicillin and kept shaking overnight at 37°C. Grown bacteria cultures were harvested by centrifugation for 10 min at 3,200× g and RT.

Isolation of plasmid DNA from the bacteria was realized with the Wizard® Plus SV Minipreps DNA Purification System (Promega) according to the manufacturer's protocol.

2.3.15 Determining DNA and RNA Concentration

Concentration and purity of DNA and RNA solutions were determined with the Ultrospec 2100 *pro* photometer (Amersham Biosciences). Therefore, light absorption at 260 nm (A_{260}) and 280 nm (A_{280}) was measured. Solutions were diluted 1:25 and measured in a 10 mm path length quartz cuvette. Values were determined in comparison to blank reference. Only DNA solutions with an $A_{260/280}$ quotient between 1.7 and 1.9, and RNA solutions with an $A_{260/280}$ quotient between 1.8 and 2.0 were used in experiments.

2.3.16 DNA Sequencing

DNA sequencing of PCR amplicates was performed by the SeqLab Co. (Göttingen, Germany) according to their guidelines. Primers used for generation of PCR products were also used for sequencing (see chapter 2.3.1.2; Table 5). Newly produced constructs were also sequenced with primers against sites resident in the cloning vectors: the human cytomegalovirus promoter sequence (CMV) and the bovine growth hormone poly-adenylation site (BGH). Sequencing reactions typically spanned ~1,000 bp. To cover the whole length of a given sequence, genes >1,000 bp were also sequenced with internal sequencing primers (see chapter 2.3.1.1; Table 4).

2.3.17 Generation of Bacterial Glycerol Stocks

Glycerol stocks of bacteria were acquired from 1 ml of an overnight culture. It was centrifuged at 5,000 rpm for 3 min. After discarding the supernatant the bacteria pellet was resuspended in 1 ml LB-medium (1% (m/v) casein hydrolyzate, 0.5% (m/v) yeast extract, 1% (m/v) NaCl, adjusted to pH 7.4) with 15% (v/v) glycerol and stored at -80°C.

2.3.18 Formyl Peptide Receptor Genes

Murine *Fpr1* corresponds to the NCBI Reference Sequence NM_013521.2 with exchanges of T879C and G408A. Murine *Fpr2* resembles the sequence of NM_008039.2 with a C192T exchange. Murine *Fpr3* isolated from vomeronasal cDNA corresponds perfectly to NM_008042.2. *Fpr3* $\Delta_{424-435}$ is identical to *Fpr3* except for a 12 nucleotide *in-frame* deletion spanning base pairs 424 to 435. *Fpr-rs3* and *Fpr-rs6* are identical to NM_008040.2 and

NM_177316.2, respectively. *Fpr-rs4* corresponds to NM_008041.2 but with A69T and G577A exchanges. *Fpr-rs7* corresponds to AF437513 with T441G and T500C exchanges. These deviations were also observed in genomic DNA of C57BL/6J mice. Human *FPR1* resembles to NM_001193306.1 with V111L, R163H, and N192K exchanges. Human *FPR2* and human *FPR3* correspond to NM_001462.3 and NM_002030.3, respectively. Sequences for the full coding regions of all used receptors have been annotated (Bufe *et al.*, 2015).

2.4 HEK293T Cell Culture

2.4.1 HEK293T Cells

HEK293T PEAKrapid cells (ATCC[®]; CRL-11268[™]) were used to investigate Fprs in a heterologous cell system. HEK293T PEAKrapid cells constitutively express the simian virus 40 (SV40) large T antigen and thus support the replication of recombinant plasmids with the SV40 origin of replication. The plasmid vectors used in this study provide the SV40 origin of replication.

2.4.2 Cell Culture Media

Table 7. Cell culture media

HEK293T Culture Medium		Cryopreservation Medium
Basic Medium	Dulbecco's Modified Eagle Medium (DMEM; D6429; Sigma-Aldrich)	DMEM
Penicillin/Streptomycin (Sigma-Aldrich)	1% (v/v) = 10,000 Units/ml Penicillin, 10 mg/ml Streptomycin	1% (v/v) = 10,000 Units/ml Penicillin, 10 mg/ml Streptomycin
L-Glutamine (Sigma-Aldrich)	2 mM	2 mM*
FCS (Sigma-Aldrich)	10% (v/v) (heat inactivated for 20 min at 56°C in a water bath)	20% (v/v)*
DMSO	/	10% (v/v)
Storage	4°C	4°C

2.4.3 Cultivating Culture Cells

Cells were grown in 75 cm² culture flasks in 20 ml of appropriate culture medium (see chapter 2.4.2) and kept until 80% to 90% confluency. Propagation was realized by rinsing with 10 ml of Dulbecco's Phosphate Buffered Saline (Sigma-Aldrich). Afterwards, cells were incubated in 5 ml Trypsin-EDTA for 3 min at RT until they detached from the flask bottom. Digestion was stopped by adding 5 ml appropriate culture medium. Separation of cells was performed by pipetting carefully up and down. After centrifugation at 900× g for 3 min cells were resuspended gently in 10 ml fresh culture medium. 1 ml of the suspension

was used to inoculate a new 75 cm² flask. HEK293T PEAKrapid cells were propagated until 30 passages. Then a new cell stock aliquot was thawed (see chapter 2.4.5).

For heterologous calcium imaging and immunocytochemistry experiments, black 96 well μ CLEAR-Plates (Greiner bio-one) were coated by incubation with 50 μ l 10 μ g/ml poly-*D*-lysine dissolved in PBS for 30 min at RT. Afterwards, cells were seeded at 20% to 30% confluency in each well and incubated for 24 h (37°C, 5% (v/v) CO₂).

2.4.4 Transient Transfection of Culture Cells

When reaching 50% to 70% confluency, cells were transfected with the poly cationic DNA transfection reagent JetPEI™ (PEQLAB) according to the manufacturer's protocol. Per well (96-well plate) a total of 0.25 μ g DNA were diluted in 10 μ l of 150 mM NaCl (4°C). In another tube, 0.5 μ l JetPEI™ were added to another 10 μ l of 150 mM NaCl (4°C). DNA was added to JetPEI™, briefly mixed, and incubated for 30 min at RT. Afterwards, the total 20 μ l were added to a well containing seeded cells in 100 μ l HEK293T culture medium (see chapter 2.4.2). For immunocytochemical analyses 0.25 μ g plasmid DNA encoding a receptor were transfected. For calcium imaging experiments 0.125 μ g DNA plasmid encoding a receptor were cotransfected with equal amounts of a plasmid encoding the G protein alpha 16 subunit (G α_{16}). The total amount of transfected DNA was kept constant. Cells were dye loaded and imaged 48 h after transfection, with cell density of approximately 50,000 cells/well.

2.4.5 Thawing of Cryopreserved Culture Cells

For inoculation of new cell passages, stored cells were briefly thawed at 37°C in the water bath and quickly transferred to a 10 cm² culture flask (Sarstedt) filled with 37°C warm HEK293T culture medium (see chapter 2.4.2). After 4 h, the medium was replaced with fresh medium to wash out remaining DMSO and cell debris. When reaching 80% confluency, cells were carefully detached from the flask bottom, transferred to a 75 cm² culture flask (Sarstedt) and cultivated in appropriate culture medium (see chapter 2.4.2).

2.4.6 Storage of Culture Cells

HEK293T PEAKrapid cells were stored in cryopreservation medium (see chapter 2.4.2) and frozen to -80°C at -1 K/min using a Nalgene® Mr. Frosty cryo container (Sigma-Aldrich). Afterwards, they were stored in liquid nitrogen at -196°C.

2.5 High-Throughput Calcium Imaging

2.5.1 Cell Population Calcium Imaging

2.5.1.1 Dye Loading of HEK293T Cells for Cell Population Calcium Imaging

For calcium imaging measurements of cell populations, transiently transfected HEK293T cells (see chapter 2.4.4) were loaded with the fluorescence dye Fluo-4, AM (Molecular Probes). 48 h after transfection culture medium of each well of a given 96-well plate was exchanged to loading buffer (50 μ l C1 buffer (130 mM NaCl, 5 mM KCl, 10 mM Na-HEPES, 2 mM CaCl_2 , and 10 mM D-Glucose, adjusted to pH 7.4 with NaOH) containing 0.07% (m/v) Probenecid (Sigma-Aldrich) and 2 μ M Fluo-4, AM). Cells were incubated for 2 h at RT in the dark. Subsequently, they were washed three times with C1 buffer using the ELx50 ELISA cell-washer (BioTek) and measured.

2.5.1.2 Data Acquisition for Cell Population Calcium Imaging with the FLIPR

For heterologous high-throughput calcium imaging on cell populations the fluorometric imaging plate reader (FLIPR; Molecular Devices) was used. This device is equipped with an automated overhead pipetting unit that can apply fluids (*e.g.* ligands) to all wells of a 96-well plate simultaneously. It can detect fluorescence signals in all wells and allows the examination of up to 96 stimuli for different transfection conditions simultaneously. Because of this, the FLIPR is well-suited for ligand screening and the examination of concentration-dependent responses of receptors upon different stimuli. Excitation of prepared cells is achieved with a water-cooled argon laser at 488 nm. The fluorescence detection technology is based on a charge-coupled device (CCD) camera setup whose detection optics are optimized for signals from a cell monolayer at the bottom of the well. The overall fluorescence adds up to one single signal that constitutes the response of the whole cell population in the well. Fluorescence is measured from each well independently and converted into a numerical value.

2.5.1.3 Analysis of FLIPR Experiments

Cell population responses of transfected HEK293T cells (~50,000 cells/well) were recorded using the FLIPR system. Response amplitudes ($\Delta F/F_0$) were calculated by dividing the maximal change in fluorescence after ligand application ($\Delta F = F_{\text{max}} - F_{\text{min}}$) by baseline fluorescence (F_0) (Figure 8A). In all experiments, a buffer control was measured in separate

wells to determine the maximal baseline variations without stimulation. The mean amplitude of control wells determined in a given experiment was then subtracted from all mean amplitudes obtained upon stimuli. This procedure prevented baseline variations in negative wells from being interpreted as signal amplitudes. In FLIPR experiments, quantifications and resulting bar charts represent signal amplitudes. Concentration-response curves were performed applying decreasing concentrations of a ligand to different wells (Figure 8B) and calculated with Graph Pad Prism 5.0 (GraphPad Software) (see chapter 2.9.2) (Figure 8C). All experiments were performed at least in duplicate wells using at least three independent transfections.

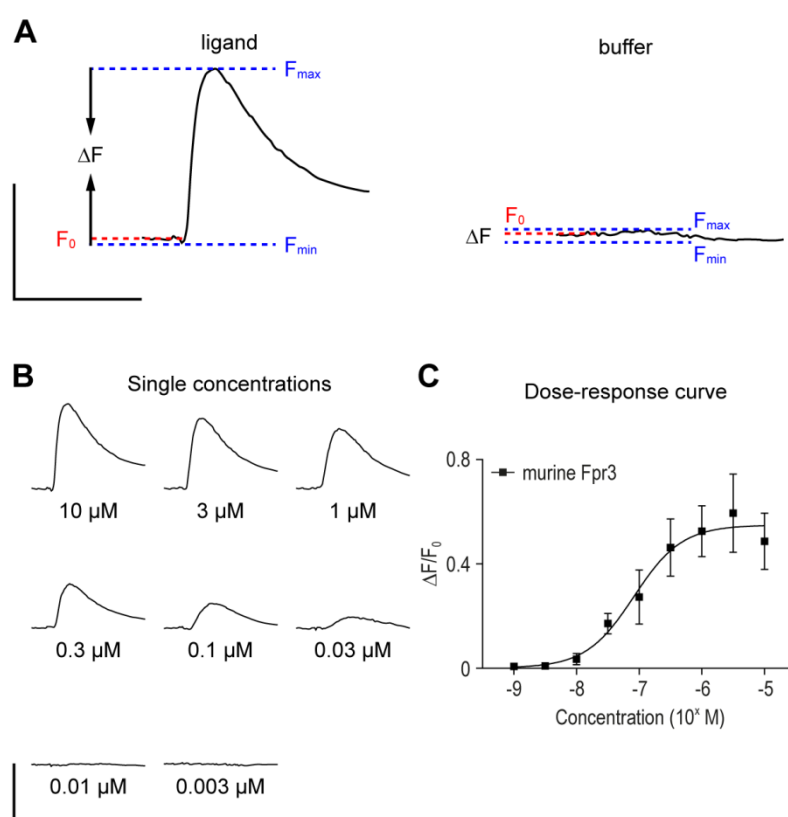


Figure 8. Representative responses in FLIPR experiments. **A**, maximal change in fluorescence after ligand (left panel) or buffer (right panel) application. Shown is the fluorescence minimum (F_{min}) and the fluorescence maximum (F_{max}) in blue, and the baseline fluorescence (F_0) in red. The maximal change in fluorescence is represented by ΔF . Response amplitudes were calculated with the formula $\Delta F/F_0$. **B**, representative individual signals of a concentration-response curve obtained with decreasing ligand-concentrations in individual wells. **C**, Concentration-response curve calculated with the values of three independent experiments. Scale bars, vertical 5,000 RFU; horizontal 100 s.

2.5.2 Single Cell Calcium Imaging

2.5.2.1 Dye Loading of HEK293T Cells for Single Cell Calcium Imaging

For single cell calcium imaging measurements, transiently transfected HEK293T cells (see chapter 2.4.4) were loaded with the ratiometric calcium sensitive dye Fura-2, AM (Molecular Probes). 48 h after transfection culture medium of each well of a given 96-well plate was exchanged with Fura-2 loading buffer (100 μl C1 buffer containing

5 mM Trypan Red Plus™ (AAT Bioquest) and 2 μ M Fura-2, AM). Afterwards, cells were incubated for 2 h at RT in the dark and washed three times with C1 buffer using the ELx50 ELISA cell-washer (BioTek).

2.5.2.2 Data Acquisition for Single Cell Calcium Imaging with the Bioimager

Heterologous calcium imaging in single cell resolution was performed with the Bioimager BD Pathway 855 (Bioimager; BD Biosciences). This device is a fully automated confocal microscope with an automated pipetting unit. It allows high-throughput live cell analyses of living cells with optional confocal imaging. Automated sequences of liquid (*e.g.* ligand) applications on 96-well plates with simultaneous single cell resolution live imaging can be programmed. Because of its resolution, responses of single cells can be detected in a well. Therefore, the Bioimager is well-suited for examination of signals that would be overlooked in cell population measurements and for high-throughput immunocytochemistry experiments that require single cell resolution. 103 W mercury short arc lamps (Chroma) provide a broad excitation spectrum of 330 nm to 900 nm. A set of dichroitic mirrors, excitation and absorption filters enable various settings for excitation and absorption. Pictures are taken with a high resolution ORCA-ER CCD camera (Hamamatsu). The optical apparatus contains several Olympus objectives that deliver magnifications of 4 \times to 60 \times .

2.5.2.3 Analysis of Bioimager Experiments

For automated single cell calcium imaging of transfected HEK293T cells (~50,000 cells/well) the BD Pathway 855 Bioimaging system was used. Calcium-dependent ratiometric fluorescence signals were recorded at 0.5 Hz. 30 μ M ATP were applied after the stimulus and served as a positive control to monitor cell viability. Prior to the stimulus, C1 buffer was applied to control for mechanical artifacts. Cells that responded to C1 buffer (negative control) or lacked response to ATP (positive control) were excluded from the analysis. Images were taken with the Bioimaging system and quantified using Attovision Software (BD Biosciences) and Excel2010. In quantifications of Bioimager experiments, bar heights represent the percentage of responding cells.

2.6 Immunocytochemistry

2.6.1 Preparation of Samples for Immunocytochemistry

2.6.1.1 Dissociation of Vomeronasal Tissue

VNO epithelium of 8-12 week old mice was detached from the cartilage and minced in PBS at 4°C (Chamero *et al.*, 2011; Pérez-Gómez *et al.*, 2015). Pooled tissue from three to five mice was incubated for 20 min at 37°C in 1 ml PBS supplemented with papain (0.22 U/ml; Worthington), 1.1 mM EDTA (Thermo Scientific), and 5.5 mM L-cysteine hydrochloride (Sigma-Aldrich). Subsequently, cells were kept on ice for 5 min in 1 ml DNase buffer (600 µl PBS with 400 µl 5× Colorless GoTaq® Reaction Buffer (Promega) and 50 U DNase I (Thermo Scientific)). Thereafter, the reaction was stopped by adding 10 ml DMEM (Invitrogen) supplemented with 10% (v/v) FCS, and centrifuged for 5 min at 1,000× g and 4°C. After removal of supernatant, cells were resuspended in 200 µl DMEM supplemented with 10% (v/v) FCS and gently extruded by pipetting. Supernatant containing dissociated cells was seeded on coverslips coated with concanavalin-A (0.5 mg/ml, overnight at 4°C; Sigma-Aldrich) and incubated for 1 h at 37°C and 5% (v/v) CO₂.

2.6.1.2 Preparation of Blood Cells

Blood samples were obtained from 8-12 week old mice that were euthanized with CO₂. Blood (10 µl) was deposited on a microscope slide (Superfrost Plus; Menzel-Gläser) and smeared immediately. After drying blood smears were ready for experiments.

2.6.1.3 Preparation of Bone Marrow Cells

Isolation of bone marrow cells was performed as described (Boxio *et al.*, 2004). 8-12 week old mice were euthanized with CO₂ and decapitated. Femoral bones were isolated and stored in ice-cold calcium/magnesium-free Hank's balanced salt solution (HBSS) buffer (Gibco) containing 10 mM 4-(2-hydroxyethyl)-1-piperazineethane-sulfonic acid (HEPES) for 10 min. Epiphysis was removed from both ends of the bone and 1-2 ml HBSS with HEPES were forced through the bone shaft with a syringe (needle: 20G) to flush out the bone marrow. Bone marrow suspension was counted with a MOXI Z cell counter (Orflo) using Type S Moxi Z Cassettes (Orflo) and centrifuged at 300× g (brake on lowest level) for 8 min at 4°C. Supernatant was discarded and the cell pellet was resuspended in Roswell Park Memorial Institute medium (RPMI-1640, Gibco) containing 100 U/ml penicillin,

0.1 mg/ml streptomycin, 5 mM L-glutamine, and 10% (v/v) FCS (at a concentration of 4×10^6 cells/ml. Cells were seeded on petri dishes ($\sim 1 \times 10^7$ cells/dish) and incubated for 2 h at 37°C and 5% (v/v) CO₂. Stimulation of bone marrow cells was achieved by adding 150 µg/ml lipopolysaccharide of *Salmonella enteritidis* (Sigma-Aldrich) into culture medium of seeded cells. Stimulated and unstimulated samples were incubated for additional 8 h at 37°C and 5% (v/v) CO₂ before use in experiments.

2.6.2 Immunostaining Protocol

Cells were fixed for 4 min in 4% (m/v) methanol-free paraformaldehyde (Polyscience), rinsed in PBS, and treated with a blocking solution (PBS supplemented with 5% (v/v) FCS) and 0.25% (v/v) Triton-X100 for 30 min at RT. Thereafter, cells were incubated overnight at 4°C with primary antibody in blocking solution. After rinsing with PBS, staining was obtained by sample incubation for 60 min at RT with fluorescence-conjugated secondary antibody in blocking solution containing Hoechst33342 (1 µg/ml; Hoechst) to counterstain cell nuclei. The same immunocytochemistry protocol was used for HEK293T cells, dissociated VNO cells, and leukocytes from blood and bone marrow.

2.6.2.1 Image Acquisition and Data Analysis for General Immunostainings

All representative images from vomeronasal, blood, and bone marrow cells were taken with an Olympus BX61 fluorescence microscope with an X-Cite[®] SERIES 120PC (EXFO) light source. Representative pictures of HEK293T cells and montage pictures for quantification were taken with the BD Pathway 855 Bioimaging system (BD Biosciences). Quantifications were evaluated with BD-image Explorer software (BD Biosciences).

2.6.3 Antibodies

2.6.3.1 Used Antibodies

Primary antibodies binding at the target proteins varied in their applied concentration. The two generated and affinity purified ECL1 and ECL2 had a stock solution of 2 µg/ml. All secondary antibodies that were used for fluorescence stainings also had a stock concentration of 2 mg/ml and were used at 2 µg/ml.

Table 8 summarizes the used primary and secondary antibody combinations, antibody names, clonality, working concentrations of the primary antibodies, order numbers (Order#),

the company they were purchased from, and the fluorescence conjugate for each secondary antibody.

Table 8. Antibodies used in this study

Primary Antibodies						Associated Secondary Antibodies				
Name	Primary Antibody	Clonality	Working Concentration	Order#	Company	Secondary Antibody	Clonality	Conjugate	Order#	Company
M-20	Rabbit anti-Fpr3	Polyclonal	0.2 mg/ml	sc-18195	Santa Cruz	Goat anti-rabbit	Polyclonal	Alexa Fluor 488	A-11034	Invitrogen
N-20	Rabbit anti-Fpr3	Polyclonal	0.5 mg/ml	orb100776	Biorbyt	Goat anti-rabbit	Polyclonal	Alexa Fluor 488	A-11034	Invitrogen
ECL1	Rabbit anti-Fpr3	Polyclonal	2.0 µg/ml	-/-	-/-	Goat anti-rabbit	Polyclonal	Alexa Fluor 488	A-11034	Invitrogen
ECL2	Mouse anti-Fpr3	Monoclonal	0.2 µg/ml	-/-	-/-	Goat anti-mouse ¹	Polyclonal	Alexa Fluor 546	A-11003	Invitrogen
						Goat anti-mouse ²	Polyclonal	Alexa Fluor 488	A-11029	Molecular Probes
						Donkey anti-mouse ²	Polyclonal	Alexa Fluor 647	A-31571	Invitrogen
OMP	Goat anti-OMP	Polyclonal	2.0 µg/ml	544-10001	Wako	Donkey anti-goat	Polyclonal	Alexa Fluor 555	A-21432	Invitrogen
Gα _c	Rabbit anti-Gα _c	Polyclonal	0.2 µg/ml	sc-387	Santa Cruz	Donkey anti-rabbit	Polyclonal	Alexa Fluor 555	A-31572	Invitrogen
PDE4A	Rabbit anti-PDE4A	Polyclonal	0.5 µg/ml	PD4-112AP	FabGennix	Donkey anti-rabbit	Polyclonal	Alexa Fluor 555	A-31572	Invitrogen
V2R2	Rabbit anti-V2R2	Polyclonal	1:10,000	-/-	Gift from R. Tirindelli*	Donkey anti-rabbit	Polyclonal	Alexa Fluor 555	A-31572	Invitrogen
CD45R	Rat anti-CD45R	Polyclonal	0.25 µg/ml	2553087	BD Pharmingen	Donkey anti-rat	Polyclonal	Alexa Fluor 488	A-21208	Invitrogen
Ly6G	Rat anti-Ly6G	Polyclonal	0.25 µg/ml	127601	BioLegend	Donkey anti-rat ³	Polyclonal	CF633	20137	Biotium
						Donkey anti-rat ⁴	Polyclonal	Alexa Fluor 488	A-21208	Invitrogen
Rho	Mouse anti-rhodopsin	Monoclonal	1:500	-/-	Gift from R. Molday**	Goat anti-mouse	Polyclonal	Alexa Fluor 546	A-11003	Invitrogen
HSV	Mouse anti-HSV	Monoclonal	0.1 µg/ml	69171	Novagen	Goat anti-mouse	Polyclonal	Alexa Fluor 546	A-11003	Invitrogen

* R. Tirindelli, University of Parma, Parma, Italy; ** Dr. R. Molday, Centre for Macular Research, University of British Columbia, Canada; ¹ used for stainings in HEK293T cells; ² used for stainings on VNO and blood samples; ³ used for colocalization experiments with ECL1; ⁴ used for colocalization experiments with ECL2

2.6.3.2 Generation of Fpr3 Antibodies

The polyclonal rabbit antibody ECL1 was generated based on the commercially available murine Fpr3 antibody M-20 (see chapter 2.6.3.1). Epitope mapping via peptide-spot assay analysis (see chapter 2.6.3.3) of M-20 revealed two epitopes. For each epitope, a peptide was synthesized and used to immunize a rabbit. Subsequent immunocytochemistry experiments with both rabbit sera on HEK293T cells expressing murine Fpr3 revealed best results for the serum of the rabbit injected with AMKEKWPFGWFLCKL. After 12 weeks serum was obtained and antibody was purified by affinity chromatography with the sulfo-linked AMKEKWPFGWFLCKL peptide and adjusted to a stock concentration of 2 mg/ml.

The monoclonal mouse antibody ECL2 was developed in cooperation with the Abmart Co. Epitope scoring of the Fpr3 sequence of the mouse was used to determine four peptide sequences (WGNSVEERLNTA, LSEDSGHISDTR, HSLSSRLQRALS, and ITTKIHKKAFV) spanning intracellular, extracellular, and C-terminal epitopes on Fpr3. For immunogen production these epitopes were over-expressed in *Escherichia coli* and purified by nickel-affinity chromatography. Each immunogen was then injected into three 8-12 week old female BALB/C mice. For hybridoma cell generation spleen cells from the best

responding mice were fused to SP2/0 myeloma cells and single parent cell colonies were obtained and tested by ELISA for their ability to bind the antigen. The nine most productive and stable clones were injected into the peritoneal cavity of mice. After 10–14 days ascites fluid was obtained and tested. Immunocytochemistry experiments on HEK293T cells expressing murine Fpr3 showed the highest sensitivity for the antibodies produced with the cell line for WGNSVEERLNTA. Antibodies produced by the corresponding hybridoma cell line were used for all ECL2 immunochemistry experiments.

2.6.3.3 Peptide-Spot Array Analysis for Antibody Characterization

For peptide-spot array analysis, 69 peptides covering the whole sequence of murine Fpr3 were synthesized. Each peptide consisted of 15 amino acid residues and overlapped by ten residues with its predecessor. All peptides were subjected to sodium dodecyl sulfate polyacrylamide gel electrophoresis (SDS-PAGE) on acid hardened polyvinylidene difluoride (PVDF) cellulose membranes derivatized with a polyethylene glycol spacer. Membranes were equilibrated in 150 mM NaCl, 50 mM Tris/HCl (pH 7.5) for 30 min at RT. Each antibody (M-20, ECL1, and ECL2; see chapter 2.6.3.1) was solved at a concentration of 4 µg/ml in PBS containing 5% (m/v) milk powder. Then they were added to the membrane and incubated overnight at 4°C. After washing with PBS, the membrane was incubated with the corresponding peroxidase-coupled secondary antibody overnight at 4°C. Thereafter, the membrane was washed twice with PBS for 10 min and incubated with enhanced chemiluminescence solution until pronounced signal was visible. Analysis was performed using the Fusion SL (Peqlab) luminescence imaging system. Captured images were used for quantification. Therefore, picture colors were inverted in Photoshop CS5 (Adobe). Each spot was analyzed with a marker circle having a diameter of 3.9 cm (1528 pixels). The average signal value for each spot was then determined with the histogram option.

2.6.3.4 Blocking Peptides

Peptides that were used for antibody generation, AMKEKWPFGWFLCKL for ECL1 and WGNSVEERLNTA for ECL2, were also used as blocking peptides. 10 µg/ml of the respective peptide were pre-incubated with antibody for 1 h at RT and then given to the preparation as first antibody application. Thus, the specific binding sites of the antibodies were blocked. Subsequently, all steps of the normal immunostaining protocol were performed (see chapter 2.6.2).

2.7 *In Situ* Hybridization

2.7.1 Coronal Slices of the Vomeronasal Organ for *In Situ* Hybridization

Mice were anesthetized with an injection of 2 ml of 6.6% (v/v) Ketamine (Pfizer) and 2.2% (v/v) Rompun® (Bayer) in PBS into the abdominal cavity. They were perfused with ice-cold 4% (m/v) paraformaldehyde (pH 7.4). The VNO was dissected and incubated overnight in 4% (m/v) paraformaldehyde at 4°C. Subsequently, it was incubated in increasing sucrose gradients of 10% (m/v; 2 h), 20% (m/v; 2 h), and 30% (m/v; overnight) at 4°C. Afterwards, the VNO was embedded in Tissue-Tek O.C.T. (Sakura Finetek), frozen in 2-methylbutan that was cooled by liquid nitrogen, and stored at -80°C. For *in situ* hybridization 12 µm thick slices were cut and collected on microscope slides (Superfrost Plus; Menzel-Gläser).

2.7.2 Design and Generation of RNA Probes

Nucleotide 672 to 1056 from NCBI accession number NM_008042.2 plus 153 bp of the 3' UTR was used for murine *Fpr3* RNA probe design. Additional 153 bp of the 3' UTR of *Fpr3* increased the specificity and minimized overlap with other *Fpr* genes. Based on these specifications, the DNA template for the *Fpr3* probes was amplified with the primers CACTACAAAGATTCACAAAAAAGCCTTTG and AATATTCTAGGCCCTTTGACTTTTACTTTTTT, and subsequently cloned into a pGEM-T Easy Vector (A1360; Promega) via TA-cloning. Antisense and sense probes were generated by the use of T7 and Sp6 RNA polymerases, respectively. The antisense and sense probes were labeled with Digoxigenin (DIG; Roche) according to the manufacturer's instructions. Therefore, 1 µg template DNA, 4 µl 5× First Strand Buffer (Invitrogen), 2 µl DTT (0.1 M; Invitrogen), 2 µl 10× DIG-Mix (Roche), 1 µl RiboLock RNase Inhibitor (Thermo Scientific), and 7 µl H₂O were mixed and incubated for 90 min at 37°C and taken on ice. Probes were DNase digested by incubation with 2.5 µl 10× DNase buffer (Thermo Scientific) and 1 µl DNase I (50 U/µl; Thermo Scientific) for 15 min at 37°C. Addition of 2.5 µl EDTA (0.2 M; Thermo Scientific) stopped the enzyme reaction. DNase was inactivated by incubation of 10 min at 65°C. Precipitation of the probes was reached by adding 2 µl 4 M LiCl and 60 µl 100% (v/v) ethanol with subsequent overnight incubation at -20°C. Probes were centrifuged at 10,000× g for 20 min at 4°C. Supernatant was discarded and the pellet was washed three times with 100 µl 80% (v/v) ethanol. The RNA pellet was dried and resolved in 25 µl TE buffer (10 mM Tris-Cl pH 7.0, 1 mM EDTA).

2.7.3 Hybridization

Coronal VNO slices were thawed and dried for 15 min at RT. They were fixed for 4 min in 4% (m/v) paraformaldehyde and washed twice for 3 min with PBS at RT. Slides were treated with 0.2 M HCl for 10 min at RT and washed twice for 3 min with PBS. Slices were incubated for 10 min with acetylation solution (0.1 M triethanolamine, 1.75 μ l/ml acetic acid (99.9% (v/v)), 2.5 μ l/ml acetic anhydride) at RT and washed twice for 3 min with PBS at RT. Afterwards, slices were incubated with pre-hybridization solution (50% (v/v) formamide and 600 mM NaCl) for 2 h at 65°C in a sealed chamber filled with formamide. Hybridization solution (50% (v/v) formamide, 10 mM Tris-Cl pH 8.0, 200 μ g/ml yeast tRNA, 1 \times Denhardt's, 600 mM NaCl, 0.25% (v/v) SDS, 1 mM EDTA pH 8.0) was preheated for 10 min at 85°C. 0.2 ng/ μ l DIG-labeled probes were added to the preheated hybridization solution and heated for 3 further min. Hybridization solution containing probes was given on the slices and incubated overnight (>12 h) at 65°C in a chamber filled with formamide.

2.7.4 Washing

After hybridization, slices were washed once with 5 \times SSC at 65°C for 30 min, and once with 2 \times SSC, 0.2 SSC, and 0.1 \times SSC at RT for 20 min, each. Afterwards, slices were blocked with TN-blocking solution (100 mM Tris pH 7.5, 150 mM NaCl, 2% (v/v) FCS) for 30 min. Slices were incubated with anti-DIG antibody (Roche, 1:5,000) in TN-blocking solution overnight at 4°C. They were washed three times with TN buffer (100 mM Tris pH 7.5, 150 mM NaCl) for 5 min at RT. Slices were equilibrated in AP buffer (100 mM Tris base pH 9.5, 100 mM NaCl, 50 mM MgCl₂) for 5 min at RT.

2.7.5 Detection with Alkaline Phosphatase

For detection of hybridized RNA, slices were incubated with detection buffer (175 μ g/ml 5-bromo-4-chloro-3-indolyl phosphate (BCIP), 300 μ g/ml nitro blue tetrazolium (NBT), 1 mM levamisole in AP buffer at RT in a chamber filled with TN buffer until the staining was well-developed. The staining reaction was stopped at 4°C and slices were mounted with fluorescence mounting medium (DAKO).

2.8 Software and Web Tools

2.8.1 Software

2.8.1.1 *Adobe Photoshop CS5*

Adobe Photoshop CS5 (Adobe) was used to adjust brightness and contrast of immuno images. Every pixel in a picture was adjusted in the same way. Images showing staining and respective negative controls were also adjusted in the same way. Pictures were also rotated and cropped in Photoshop.

2.8.1.2 *Adobe Illustrator CS6*

All figures were created in Adobe Illustrator CS6 (Adobe) to maintain a minimum pixel density of 300 ppi (pixels per inch) that is suitable for high resolution printing.

2.8.1.3 *Microsoft Office 2010*

This thesis was written and edited in Microsoft Word2010. All quantitative data analyses were performed in Excel2010.

2.8.1.4 *VectorNTI Suite 9*

VectorNTI Suite 9 (Thermo Scientific) including VectorNTI, ContigExpress, and AlignX was used to design all vector constructs and to analyze chromatographs of sequenced genes. Diverse genealogies for determining sequence relationship between genes were compiled in AlignX.

2.8.1.5 *FLIPR system software v2.1.2*

Data acquisition and evaluation for FLIPR experiments was performed with FLIPR system software v2.1.2 (Molecular Devices).

2.8.1.6 *BD AttoVision™ software v1.6*

Data acquisition and evaluation for Bioimager experiments was performed with BD AttoVision™ software v1.6 (BD Biosciences).

2.8.1.7 *Graph Pad Prism*

Graph Pad Prism 5.0 (GraphPad Software) was used to calculate concentration-response curves.

2.8.1.8 *Cell^P*

Immuno pictures taken with the Olympus BX61 fluorescence microscope were saved with the Cell^P software.

2.8.2 Web Tools

2.8.2.1 *Gene Information Gathering*

The U.S. government-funded national resource for molecular biology information (NCBI, <http://www.ncbi.nlm.nih.gov/>), was used to gather information about genes and their coding regions. Information on the 3' and 5' regions was gathered with the Ensembl genome browser (<http://www.ensembl.org/>). Database analyses on which *Fpr3* gene variant is expressed by which mouse strain was performed via consulting the Mouse Genomes Project (<http://www.sanger.ac.uk/science/data/mouse-genomes-project>).

2.8.2.2 *Prediction of Gene Orthology*

Assessment of orthology between murine and human *Fpr3* based on sequence comparison was performed with DIOPT (DRSC Integrative Ortholog Prediction Tool; (Version 5.3 May 2016) (http://www.flyrnai.org/cgi-bin/DRSC_orthologs.pl) of the Harvard Medical School. This Tool provides an integrative search algorithm combining orthology search results from 12 renowned ortholog prediction tools. These include Compara (<http://www.ensembl.org/info/docs/api/compara>), the HUGO Gene Nomenclature Committee (HGNC; <http://www.genenames.org>), HomoloGene (<http://www.ncbi.nlm.nih.gov/homologene>), InParanoid (<http://inparanoid.sbc.su.se/cgi-bin/index.cgi>), Isobase (Singh *et al.*, 2008; Liao *et al.*, 2009; Park *et al.*, 2011; <http://groups.csail.mit.edu/cb/mna/isobase>), the OMA Browser (Altenhoff *et al.*, 2014; <http://omabrowser.org>), OrthoDB (<http://cegg.unige.ch/orthodb6>), OrthoMCL (<http://orthomcl.org>), Panther (<http://pantherdb.org>), PhylomeDB (<http://phylomedb.org>), Roundup (DeLuca *et al.*, 2006; DeLuca *et al.*, 2012; <http://wall-lab.stanford.edu/projects/roundup/>), and TreeFam (<http://www.treefam.org>).

2.8.2.3 Prediction of Transmembrane Domains (TMHMM)

Prediction of the transmembrane domains for murine Fpr3 was performed with the online tool for “Prediction of transmembrane helices in proteins” (TMHMM Server v. 2.0) of the Center for Biological sequence Analysis, Technical University of Denmark (<http://www.cbs.dtu.dk/services/TMHMM>).

2.8.2.4 Calculation of Primer Melting Temperatures

All melting temperatures of primers were calculated with the Sigma-Genosys DNA Calculator tool (<http://www.sigma-genosys.com/calc/DNACalc.asp>).

2.8.2.5 Mouse Haplotype Analyses

Haplotype analyses were performed with the Mouse Phylogeny Viewer (<http://msub.csbio.unc.edu/>) as presented by Yang and colleagues (Yang *et al.*, 2011). According to the Ensembl genome browser, murine *Fpr3* is present on chromosome 17 with an exon reaching from nucleotide 17,970,458 to 17,971,677. To include strain specific variations in the gene position, subspecific origins were examined in the nucleotide range from 17,970,000 to 17,972,000.

2.9 Statistics and Mathematics

2.9.1 Average and Standard Deviation

Sample average was calculated with the basic calculation for arithmetic mean for each experiment. Subsequently, the mean values of all associated experiments (*e.g.* independent transfection or dissociation) were averaged with the basic calculation for the arithmetic mean.

Standard deviation (Excel2010; STDEV) was calculated using the formula $\sqrt{\frac{\sum (x - \bar{x})^2}{(n-1)}}$, with \bar{x} being the sample's arithmetic mean and n being the sample size. Resulting error bars show the empirical standard deviation of the sample average. Calculations of sample average and standard deviation were used for quantification of cells in immunocytochemistry- and calcium imaging experiments. Quantification was calculated and evaluated after the same criteria.

2.9.2 Concentration-Response Curves

Curves were calculated with Graph Pad Prism 5.0 (GraphPad Software) using the equation

for sigmoidal concentration-response with variable slope,
$$Y = \text{Bottom} + \frac{(\text{Top} - \text{Bottom})}{1 + 10^{(\text{LogEC50} - X) \cdot \text{HillSlope}}},$$

with “Bottom” being the Y value at the bottom plateau, “Top” being the Y value at the top plateau, LogEC50 being the X value when the response is halfway between Bottom and Top, and the Hill-Slope describing the steepness of the curve. For statistical analysis, only curves with calculated R^2 -values > 0.95 were used. The absolute sum of squares for normalized curves was < 900 . The highest ligand concentration used to create concentration-response curves was $30 \mu\text{M}$. Empirical average and standard deviation were calculated from independent measurements.

3 RESULTS

3.1 Generation and Characterization of Two Novel Fpr3 Antibodies

An immunofluorescence analysis with different antibodies was performed to gain new insight into the murine Fpr3 expression pattern. The goal was to study Fpr3 expression in different mouse tissues via immunohisto- and cytochemistry. First, two commercially available polyclonal antibodies specifically designed against Fpr3 were tested. It was important that they specifically detected Fpr3 and did not cross-react with other proteins, particularly with close members of the murine Fpr family. Therefore, I first characterized the two antibodies in a heterologous expression system using HEK cells transiently transfected with murine Fpr3 as an established standard laboratory procedure (Bufe *et al.*, 2012).

3.1.1 Characterization of Commercially Available Fpr3 Antibodies

To test if both commercially available Fpr3 antibodies, M-20 (sc-18195; Santa Cruz Biotechnology, Inc.; see chapter 2.6.3.1) and N-20 (orb100776; Biorbyt; see chapter 2.6.3.1), specifically bind Fpr3, they were applied to HEK cells transiently transfected with the receptor at dilutions of 1:50–1:500.

First, I tested the N-20 antibody for its specific detection of murine Fpr3 (Figure 9). Cells were transfected with Fpr3 attached to an N-terminal rhodopsin-epitope (Rho-tag) (Figure 9A). The Rho-tag was detected with an antibody directed against this epitope, which controlled for expression of the receptor. Representative images of N-20 showed no staining at any of the tested dilutions (Figure 9B). Even the highest concentration 10 $\mu\text{g/ml}$ (1:50) showed no specific signal. Cells were transfected with the empty vector (mock) as a negative control. The positive Rho-tag stained control showed pronounced Fpr3 expression, despite no staining with the N-20 antibody.

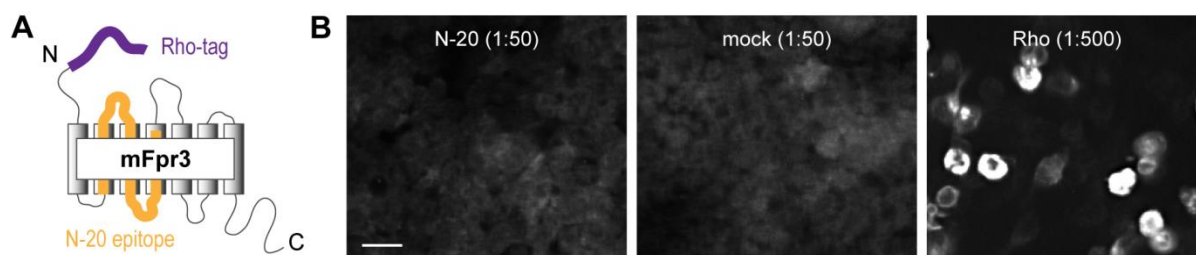


Figure 9. Test of the commercially available Fpr3 antibody N-20. **A**, model of the murine G protein coupled receptor Fpr3 with its seven transmembrane domains, three external and three internal loops, and N- and C-terminus. The exact epitope for N-20 on Fpr3 is proprietary to Biorbyt. It is located within the range of the residues 61 and 160 and is marked with an orange line. The N-terminally attached Rho-tag is indicated in purple. **B**, immunocytochemistry on HEK293T cells transiently expressing either Fpr3 or an N-terminal Rho-tagged

version of the receptor performed with the polyclonal rabbit antibody N-20 and a Rho-tag antibody. Shown are representative images of N-20 at 10 $\mu\text{g/ml}$ (1:50) and of the Rho-tag antibody used 1:500. mFpr = murine Fpr. Scale bar, 20 μm .

This result demonstrates a lack of proper detection of Fpr3 using N-20, although the antibody was originally designed to detect this receptor. Therefore, the N-20 antibody was not suitable for investigating Fpr3 expression.

Representative immunostainings using the M-20 antibody showed specific Fpr3 staining for M-20 up to 0.4 $\mu\text{g/ml}$ (1:500) (Figure 10). The signal was only visible at high antibody concentrations but suffered from a high signal to noise ratio. Staining intensity decreased rapidly at lower antibody concentrations (Figure 10A). Quantification revealed a drastic drop from $9.3\% \pm 1.4\%$ to $2.9\% \pm 1.7\%$ stained cells from the 4 $\mu\text{g/ml}$ (1:50) to 2 $\mu\text{g/ml}$ (1:100) dilutions, and almost no specific signal was detected at 0.4 $\mu\text{g/ml}$ (1:500). Moreover, the M-20 antibody showed high non-specific staining that increased at higher antibody concentrations, and the specific signal was only two-fold higher than that of the non-specific background at 4 $\mu\text{g/ml}$ (1:50) (Figure 10B), which would have been the best concentration for immunohistochemistry. This was not sensitive enough for use on native cells.

These results show that M-20 was limited to an analysis of murine Fpr3 in a heterologous overexpression system and demonstrate that neither of the commercially available Fpr3 antibodies was suitable for examining the Fpr3 protein in native cells.

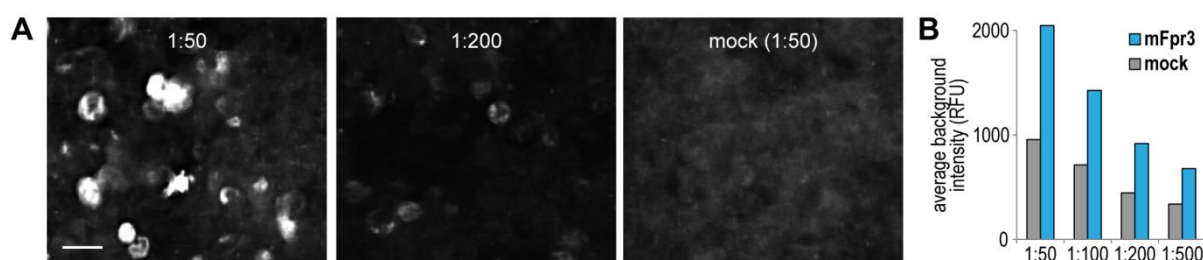


Figure 10. **Characterization of the commercially available Fpr3 antibody M-20.** Immunocytochemistry on murine Fpr3 and mock (empty vector) transfected HEK293T cells with the polyclonal rabbit antibody M-20. **A**, representative images of the dilutions 1:50 and 1:200. Scale bar, 20 μm . **B**, quantification of the average background intensity in relative fluorescence units (RFU) for all used concentrations of M-20. mFpr = murine Fpr.

3.1.2 Generation of Fpr3 Antibodies

Because neither commercially available Fpr3 antibody produced satisfying results, I decided to generate own antibodies for the detection of murine Fpr3. I planned the production of two antibodies to increase the chances of successfully establishing one or more reliable

Fpr3 antibodies. The first antibody was a polyclonal Fpr3 antibody made in rabbits based on the commercial M-20 antibody. However, it should have improved sensitivity and should produce less background staining. Because an efficient Fpr3 antibody was very important for this work, I generated a monoclonal mouse antibody directed against Fpr3, in parallel. This should maximize the chances of producing a functioning antibody that can be used for stainings in native tissue. Different species of origin should allow greater versatility in the design of later experiments and to bypass species-related background issues. The monoclonal antibodies were prepared in cooperation with the Abmart Co. in a mouse hybridoma cell line.

3.1.2.1 Generation of Polyclonal Rabbit Fpr3 Antibodies

An epitope map of the M-20 antibody was prepared by peptide-spot array analysis (see chapter 2.6.3.3) in cooperation with Dr. Martin Jung to identify suitable epitopes on murine Fpr3 to produce the immunization peptide. A set of 69 peptides, including all 351 amino acid residues of murine Fpr3, was prepared and spotted on a membrane. Each peptide was 15 amino acids in length and overlapped 10 residues with the preceding peptide. The antibody was applied to the synthesized peptides at a 1:50 dilution (Figure 11).

The peptide-spot assay revealed several epitopes on the N-terminus, C-terminus, transmembrane domains, and extracellular loops of murine Fpr3 (Figure 11A). Only the epitopes on the extracellular loops were of interest because the Fpr family has the strongest sequence diversity in these areas. The main peptide fragments AMKEKWPFGWFLCKL and MQFSGSYKIIGRLVN in the Fpr3 extracellular loops were detected by the M-20 antibody (Figure 11B, C). Two rabbits were immunized with each peptide, and the sera were applied to HEK cells transfected with Fpr3 over 16 weeks. The antibody sera obtained from the animal immunized with the AMKEKWPFGWFLCKL peptide showed specific staining that increased weekly, whereas the sera obtained with MQFSGSYKIIGRLVN did not produce any staining. Thus, the AMKEKWPFGWFLCKL serum was collected. The antibody was purified by affinity chromatography (see chapter 2.6.3.2) to increase sensitivity and decrease non-specific staining. The resulting polyclonal rabbit antibody directed against murine Fpr3 was called ECL1 because its peptide for immunization, AMKEKWPFGWFLCKL, is present on the first extracellular loop of the receptor (in short ECL1). A subsequent immunocytochemical analysis confirmed that ECL1 was more sensitive than M-20.

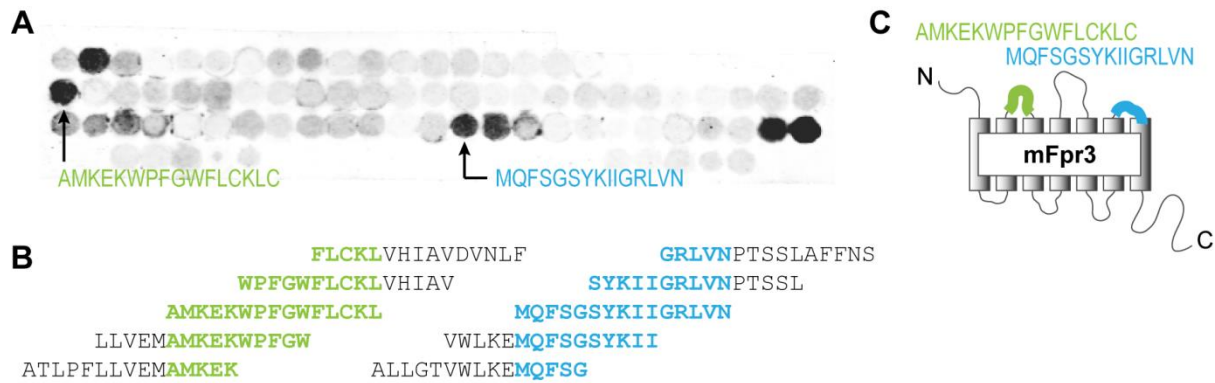


Figure 11. **Epitopes of the commercially available Fpr3 antibody M-20.** Peptide spot array analyses of M-20. **A**, original array visualized by enhanced chemiluminescence. **B**, the commercially available Fpr3 antibody M-20 was tested against peptides comprising the complete sequence of murine Fpr3. Each spot consists of a 15 amino acid peptide overlapping by ten residues with its predecessor. Therefore, parts of every 15 amino acid motif are present in five spot-peptides. Shown are the peptide sequences that comprise both main epitopes on Fpr3. **C**, model of murine Fpr3 with its seven transmembrane domains, three external and three internal loops, and N- and C-terminus. The two epitopes identified for M-20 on the first and third extracellular loop are marked with green (AMKEKWPFGWFLCKLC) and blue (MQFSGSYKIIGRLVN) lines. Peptide spot arrays were performed by Dr. Martin Jung, Department of Medical Biochemistry and Molecular Biology, Saarland University. mFpr = murine Fpr.

3.1.2.2 Generation of Monoclonal Mouse Fpr3 Antibodies

Nine mouse antibodies were generated in hybridoma cell lines from BALB/c mice based on four peptide fragments from murine Fpr3 whose sequences had low similarities with the sequences of the other six members of the murine Fpr family. Epitopes were chosen based on peptides with a possible low consensus of Fpr3 with the other six members of the murine Fpr family. The four selected Fpr3 epitopes were WGN SVEERLNTA from the second extracellular loop, ITTKIHKKAFV from the third intracellular loop, and HSLSSRLQRALS and LSEDSGHISDTR from the C-terminus. Three antibodies were generated with the first peptide (ECL2-1, ECL2-2, and ECL2-3), one with the second (ICL3), three with the third (CT1-1, CT1-2, and CT1-3), and two with the fourth (CT2-1 and CT2-2) peptide (Table 9).

To figure out which antibody was best suited to examine murine Fpr3 expression, I performed immunocytochemistry experiments with all nine antibodies at 1 µg/ml on Fpr3 and mock transfected HEK cells (Figure 12).

ICL3, CT2-1, and CT2-2 showed no staining for Fpr3, whereas ECL2-1, ECL2-2, ECL2-3, CT1-1, CT1-2, and CT1-3 clearly detected the receptor (Figure 12A). Quantification revealed that ECL2-1 and ECL2-2 were the most sensitive of the nine antibodies (Figure 12B). They detected $11.7\% \pm 0.6\%$ and $11.6\% \pm 2.1\%$ of the cells, respectively. ECL2-3, CT1-1, CT1-2, and CT1-3 only detected $5.1\% \pm 0.6\%$ to $7.1\% \pm 2.3\%$ of the Fpr3-expressing cells. Because

ECL2-1 combined the best staining intensity with the lowest background in the mock, it was used for further experiments and called ECL2.

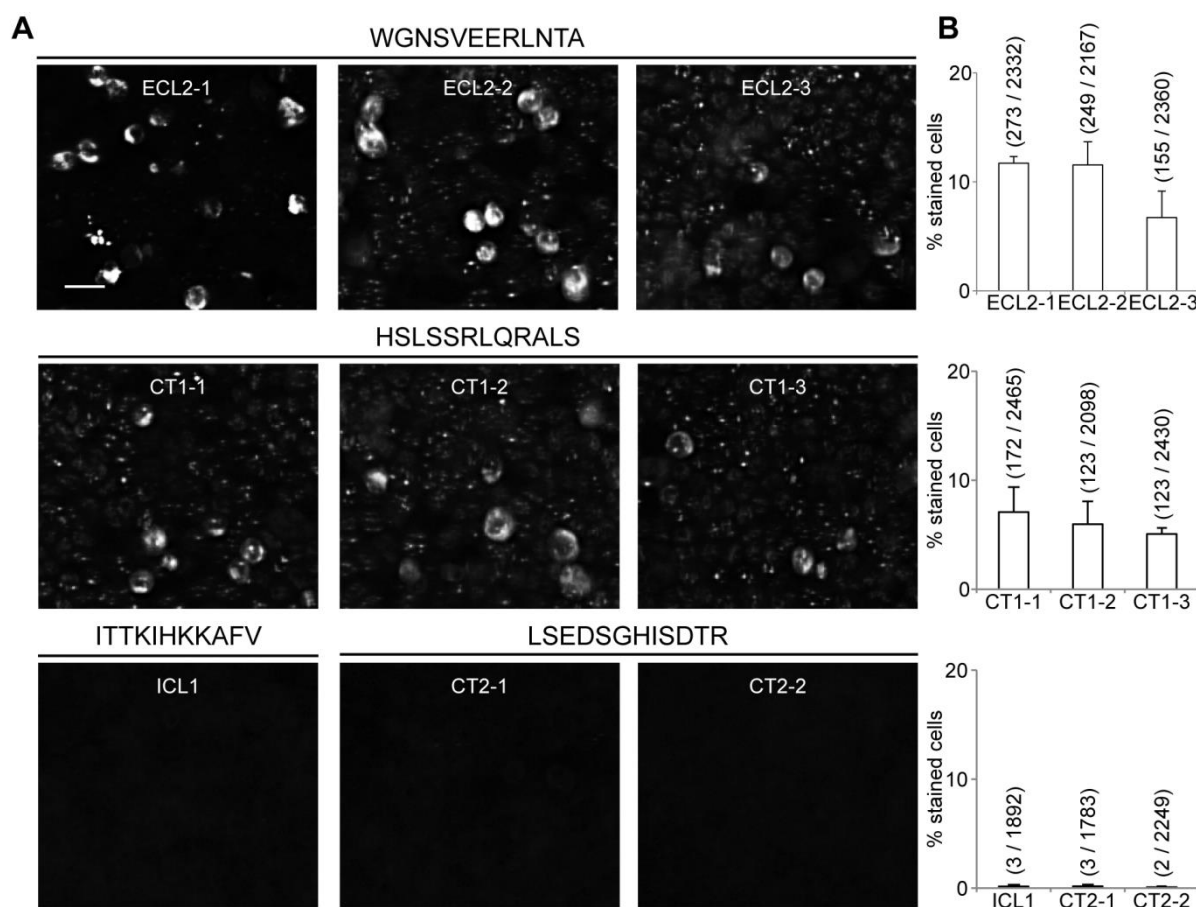
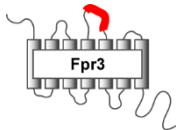
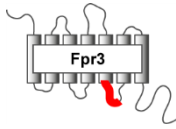
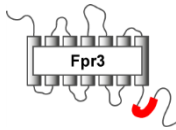
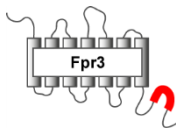


Figure 12. **Characterization of monoclonal mouse Fpr3 antibodies.** Immunocytochemistry on HEK293T cells transfected with murine Fpr3 with the nine monoclonal mouse antibodies (1:2,000). **A**, representative images of all nine monoclonal mouse antibodies. *Scale bar*, 20 μ m. **B**, Quantification of the average stained cells for each antibody. Numbers in parentheses denote positive *versus* total cells. *Error bars*, S.D.

In summary, these data demonstrate that the ECL1 polyclonal rabbit and ECL2 monoclonal mouse antibodies stained in a heterologous overexpressing system. However, it was unclear whether these antibodies would work in complex immunohistochemistry reactions in the VNO or on immune cells, as many other receptors and possible targets for non-specific antibody binding are present in native tissues. To further consolidate the functionality and specificity of the Fpr3 antibodies, they were characterized in HEK cells on Fpr3 and all other members of the murine Fpr family.

Table 9. Peptide fragments for the generation of monoclonal Fpr3 antibodies

Epitope	Position	Amino Acids	Location	Antibodies
WGNSVEERLNTA		183-194	2 nd extracellular loop	ECL2-1 ECL2-2 ECL2-3
ITTKIHKKAFV		224-235	3 rd intracellular loop	ICL3
HSLSSRLQRAIS		315-326	C-terminal	CT1-1 CT1-2 CT1-3
LSEDSGHISDTR		325-336	C-terminal	CT2-1 CT2-2

3.1.3 Characterization of Two Novel Fpr3 Antibodies

ECL1 and ECL2 were generated with peptides representing non-overlapping sites of murine Fpr3. Their epitopes were on two different extracellular loops of the receptor, which possess the highest sequence divergence among the members of the murine Fpr family. Antibodies can occasionally recognize more than one domain within a protein. Multiple recognition sites and unfavorable epitopes can increase the chance for non-specific binding or cross-reactivity. The binding sites on murine Fpr3 were characterized to ensure that ECL1 and ECL2 only recognized the epitopes used for their generation (Figures 13, 14).

First, a peptide-spot array analysis was performed to precisely determine the recognition sites of both antibodies (Figure 13). ECL1 and ECL2 were tested at 4 µg/ml (1:500) on 69 peptides covering the entire murine Fpr3 sequence spotted on a membrane, as described previously (see chapter 3.1.2).

Both antibodies showed strong immunoreactivity to the sequences used for their generation (AMKEKWPFGWFLCKL and WGNSVEERLNTA) and only weakly interacted with other receptor domains. The secondary antibody controls did not react with any of the domains. Parts of the peptide sequences were present in five of the 69 spotted peptides due to a five amino acid shift from the peptide to its predecessor (Figure 13). However, the antibodies did not react with all five peptides. Each antibody bound strongly to only one spot. Surprisingly, the particular spot did not comprise the full-length peptide used for

immunization. Instead, only a small portion of the respective original peptide was bound by the antibodies and led to strong staining in the peptide-spot assay. The peptide-spot containing the AMKEK C-terminal showed the highest staining intensity for ECL1, whereas the peptide containing the LNTA N-terminal showed the strongest reaction for ECL2. A comparison between signal intensities and the peptide sequences revealed that the key ECL1 and ECL2 binding residues were AMKEK and LNTA, respectively (Figure 13A, B). Surprisingly, both motifs were also contained in neighboring peptide spots to which the antibodies showed no strong immunoreactivity, indicating recognition of only a very specific conformation of the respective peptide epitopes for both antibodies. A database analysis of approximately 20,000 mouse genes (Church *et al.*, 2009) revealed the presence of the AMKEK and LNTA motifs in only 0.08% (17) and 0.6% (119) of all mouse genes, respectively (Tables 11 and 12; Appendix). Thus, both motifs are reasonably specific for murine Fpr3. Moreover, they were absent in most Fprs of the mouse, except Fpr2, which has 88.5% sequence identity with Fpr3.

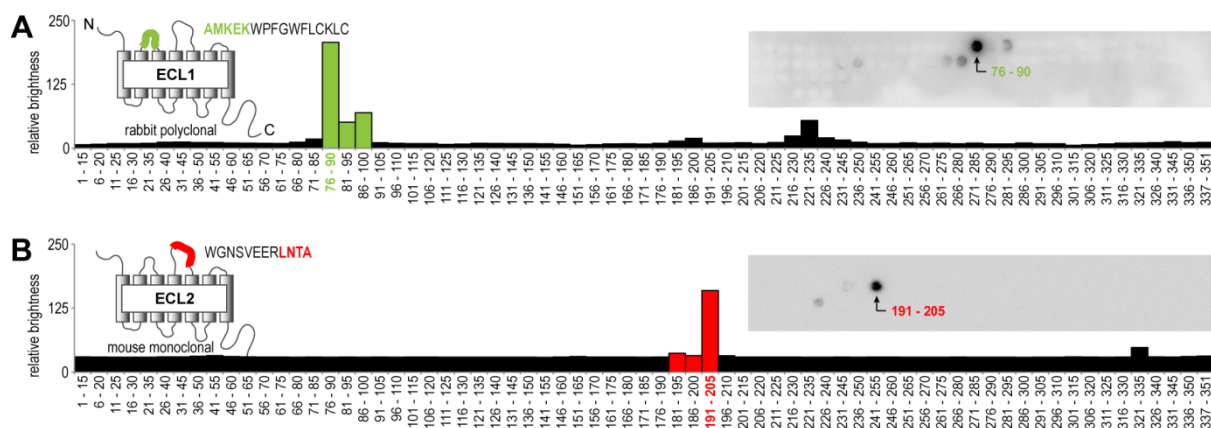


Figure 13. Epitopes of the two novel specific Fpr3 antibodies ECL1 and ECL2. Peptide spot array analyses of the polyclonal rabbit antibody ECL1 (A, green) and the monoclonal mouse antibody ECL2 (B, red). Models indicate the positions and sequences of the immunization peptides used for antibody generation. Both antibodies were tested against peptides comprising the complete sequence of murine Fpr3. Each spot consists of a 15 amino acid peptide overlapping by ten residues with its predecessor. Insets show original arrays visualized by enhanced chemiluminescence. The charts show the quantification of staining intensities; bars containing the AMKEK or LNTA motif are colored. Numbers denote the peptide positions in the receptor protein; the part of the immunization peptide sequences that are recognized by the antibodies are colored.

The antibodies were applied to HEK cells transiently transfected with either Fpr3 or another member of the murine Fpr family to test whether the antibodies cross-reacted with Fpr2 or any other murine Fpr (Figure 14).

Both antibodies recognized Fpr3-expressing cells in a nearly identical manner and stained exclusively for this receptor. No cross-reactivity to any other member of the murine Fpr family, such as Fpr1, Fpr2, Fpr-rs3, Fpr-rs4, Fpr-rs6, or Fpr-rs7, was detected. Moreover,

no non-specific staining was observed on any of the HEK cells transfected with these receptors. Quantification revealed a nearly identical percentage of cells stained with ECL1 and ECL2 (Figure 14B). ECL1 stained $11.6\% \pm 2.7\%$ and ECL2 stained $11.2\% \pm 1.7\%$ of the Fpr3 transfected cells. Although all receptors were well-expressed in HEK cells, I did not observe any specific reactivity to Fpr2 or any other murine Fpr.

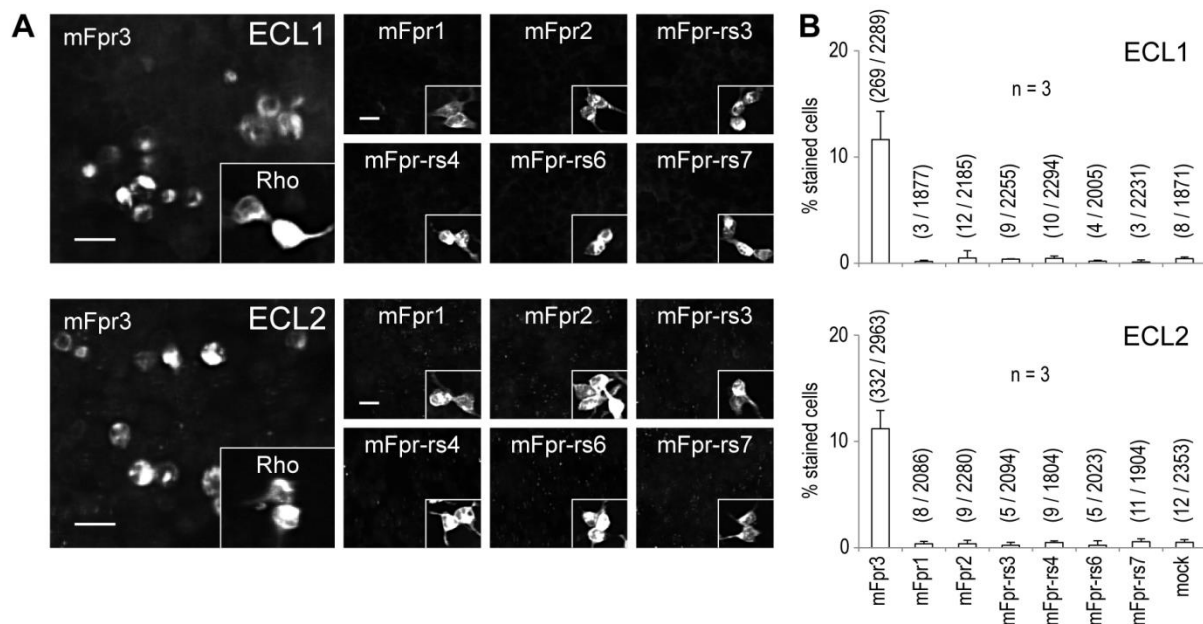


Figure 14. **ECL1 and ECL2 detect Fpr3 and do not recognize other murine Fpr family members.** **A**, immunostaining of HEK293T cells to test the cross-reactivity of ECL1 (upper panel) and ECL2 (lower panel) for the indicated receptors. Insets show stainings with an anti-rhodopsin-epitope (Rho) as a positive control for expression of the given receptors. Scale bars, 20 μm. **B**, averaged percentage of stained cells from three independent experiments. Numbers in parentheses denote positive *versus* total cells. mFpr = murine Fpr. Error bars, S.D.

Both newly generated antibodies were specific for murine Fpr3. Next, I was interested in determining whether one antibody was more sensitive than the other. Therefore, the sensitivities of both antibodies were tested by serial dilutions from 20 μg/ml (1:100) to 0.002 μg/ml (1:1,000,000) on HEK cells expressing Fpr3 (Figure 15).

Reactivity of the polyclonal ECL1 was optimal up to 2 μg/ml (1:1,000), but decreased with further dilution (Figure 15A). ECL1 stained 61% and 44% of the cells at 0.67 μg/ml (1:3,000) and 0.2 μg/ml (1:10,000), respectively. Further dilution showed very little to no staining. The antibody had no reactivity over background at ≤ 0.02 μg/ml (1:100,000). The monoclonal ECL2 antibody was even more sensitive and showed full activity up to 0.2 μg/ml (1:10,000) (Figure 15B). Further dilution revealed little staining. ECL2 had reactivity of 63% at 0.067 μg/ml (1:30,000), which decreased to background at ≤ 0.02 μg/ml (1:100,000).

Taken together, these results demonstrate the specificity and sensitivity of the newly developed Fpr3 antibodies, indicating their suitability for immunohisto- and cytochemical experiments with native tissues.

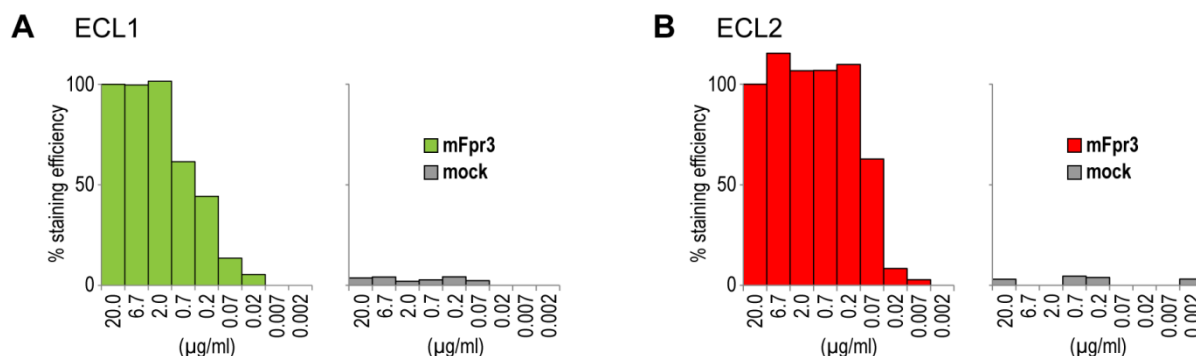


Figure 15. **ECL1 and ECL2 show high sensitivity for Fpr3.** Antibody dilution experiment examining the sensitivity of ECL1 (**A**) and ECL2 (**B**) in HEK293T cells tested in decreasing concentrations from 1:100 to 1:1,000,000. Signals were normalized to 1:100 dilution. Immunoreactivity was compared to mock transfected cells (gray). mFpr = murine Fpr.

3.2 Fpr3 Expression in the Murine Vomeronasal and Immune Systems

The expression pattern of murine *Fpr3* throughout the body is only partially understood. Expression of this receptor is best understood in the vomeronasal system, whereas in other tissues *Fpr3* expression is currently subject of controversy (see chapter 1.3.3). Two independent studies (Liberles *et al.*, 2009, Rivière *et al.*, 2009) provided clear evidence for *Fpr3* expression in a small subpopulation (<1%) of vomeronasal sensory neurons by quantitative RT-PCR and *in situ* hybridization. However, direct detection of Fpr3 protein is still missing. With the new Fpr3 antibodies ECL1 and ECL2, I planned to examine Fpr3 expression in the VNO and immune system of the mouse.

3.2.1 Fpr3 Protein is Expressed in Vomeronasal Sensory Neurons and in Immune Cells

For the detection of murine Fpr3 protein in native cells I initially wanted to focus on a well-studied tissue. I decided that the VNO should be excellently suited to first examine Fpr3 expression with the novel antibodies based on the consistent reports on *Fpr3* expression and the challenging amount of target cells. To be absolutely sure about the presence of Fpr3 in the VNO, I used *in situ* hybridization and RT-PCR to independently prove expression of *Fpr3* mRNA (Figure 16).

With RT-PCR experiments a band of the correct size for murine *Fpr3* from VNO cDNA was reproducibly ($n = 5$) detected (Figure 16A). The control reaction lacking reverse

transcriptase showed no band at all. Sequencing indeed revealed *Fpr3* as the amplification product. Next, *in situ* hybridization was performed to achieve cellular resolution (Figure 16B). In line with previous reports (Liberles *et al.*, 2009, Rivière *et al.*, 2009) *Fpr3* mRNA in a small subset of VSNs from C57Bl/6NCrl mice was observed in the antisense reaction. The sense reaction showed no specific signal.

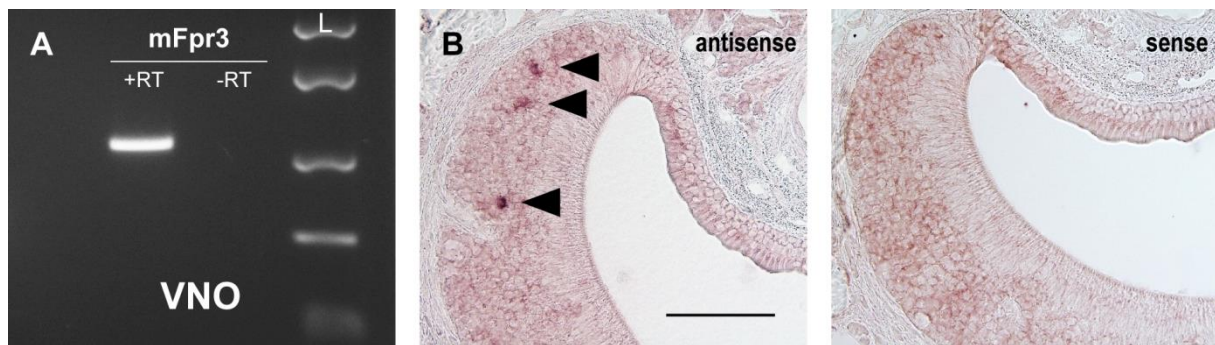


Figure 16. ***Fpr3* mRNA is expressed in the vomeronasal organ.** **A**, RT-PCR analysis of murine *Fpr3* expression in the vomeronasal organ (VNO). A band of the correct size and sequence was observed in VNO cDNA (+RT) but not in the negative control lacking reverse transcriptase (-RT). Similar results were obtained in five independent experiments. (L) FastRuler Middle Range DNA Ladder. **B**, *in situ* hybridization with sense and antisense probes for *Fpr3* on coronal slices of the vomeronasal organ. Black triangles mark *Fpr3*-positive cells. mFpr = murine Fpr. Scale bar, 100 μ m.

After having confirmed the presence of *Fpr3* mRNA in the VNO, expression of Fpr3 protein in dissociated VNO cells was examined (Figure 17). For these experiments, the monoclonal mouse antibody ECL2 was used because of its superior sensitivity over the polyclonal ECL1 antibody (Figure 15).

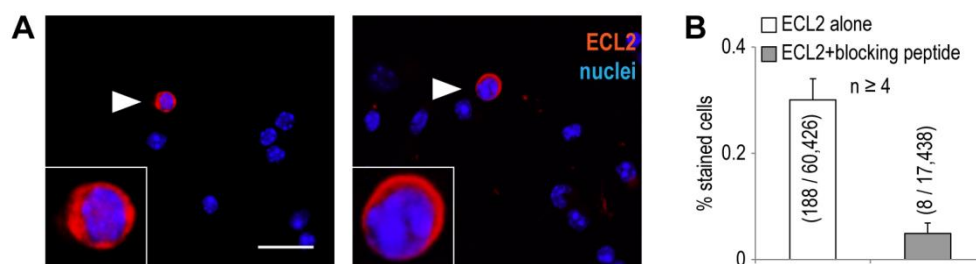


Figure 17. ***Fpr3* protein is expressed by a small subset of vomeronasal cells.** **A**, representative immunostaining with ECL2 on dissociated vomeronasal cells of C57Bl/6NCrl mice. The white triangle marks an Fpr3-positive cell (red). **B**, quantification of murine Fpr3 immunoreactivity. Average frequency of Fpr3 expression was analyzed in a total of 60,426 cells from six independent experiments. Antibody specificity was demonstrated by blocking the specific binding site through preincubation with 10 μ g/ml of the peptide used for antibody generation. Error bars, S.D.

Staining reactions with ECL2 produced a clear and convincing signal in a subset of VNO cells (Figure 17A). Only very little non-specific staining was visible. Quantitative analysis of 60,426 cells from seven independent experiments revealed Fpr3 expression in 188 cells, which corresponds to an average expression rate of 0.3% (Figure 17B). Specificity of the staining was controlled by the blocking peptide.

mRNA of murine *Fpr3* has been found in sensory neurons of the basal VNO layer that also express $G\alpha_o$ (Liberles *et al.*, 2009) but are negative for the basal Vmn2rs and the apical marker $G\alpha_i2$ (Liberles *et al.*, 2009). With regard to these findings, I performed colocalization immunocytochemistry experiments with the ECL2 antibody and antibodies for the cellular marker $G\alpha_o$, Vmn2r1 (V2R2), a marker for Vmn2r-positive VSNs (Martini *et al.*, 2001), and phosphodiesterase 4A (PDE4A), a molecular marker of apical VSNs (Lau and Cherry, 2000) (Figure 18).

According to the previous report (Liberles *et al.*, 2009), I expected coexpression with $G\alpha_o$ and none with PDE4A or V2R2. First, colocalization of Fpr3 with PDE4A and Vmn2rs was examined. The expression pattern for Fpr3 protein in my experiments was consistent with my expectation as there was virtually no colocalization between Fpr3 and PDE4A or V2R2. As expected, a pronounced overlap for Fpr3 and $G\alpha_o$ protein was detected. Quantification revealed colabeling in 56% (61/108) of the cells. Because of the assumption that the $G\alpha_o$ -positive cells were mature VSNs that also expressed olfactory marker protein (OMP), which is present in all mature VSNs (Margolis, 1982), the experiment was repeated with this particular protein. Staining for OMP confirmed the result obtained for $G\alpha_o$, as pronounced coexpression for Fpr3 and OMP was visible. 54% (93/171) of the Fpr3-positive cells coexpressed with the marker for mature VSNs. Interestingly, only about half of the Fpr3-positive cells coexpressed with the markers that labeled them as VSNs. Hence, nearly half of the cells positive for Fpr3 in this preparation did not express specific markers of mature VSNs ($G\alpha_o$ and OMP), indicating that they could comprise non-olfactory cell types.

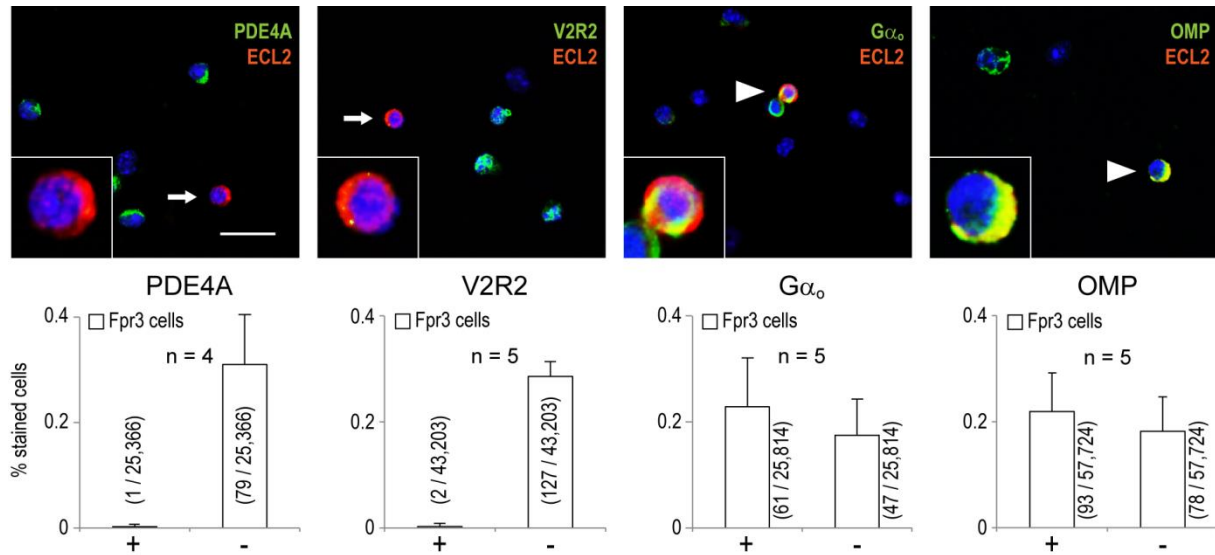


Figure 18. **Characterization of Fpr3-positive vomeronasal cells.** Colocalization of murine Fpr3 (red) with different cellular markers (green) on dissociated vomeronasal cells from C57Bl/6NCrl mice. Fpr3 staining colocalized with phosphodiesterase 4A (PDE4A), as a marker for the apical zone of the VNO, vomeronasal type 2 receptor 1 (V2R2), as a marker for V2R2 expressing cells, the G protein alpha o subunit ($G\alpha_o$), as a marker for the basal zone, and the olfactory marker protein (OMP), as a marker for mature vomeronasal sensory neurons. The colocalizing cells are marked with a white triangle, non-colocalizing with a white arrow. All cells were counterstained with the nuclear dye Hoechst33342 (blue). Insets show Fpr3-positive cells in a 3 \times magnification. Scale bars, 20 μ m. The bar chart below each picture denotes the quantification from four to five experiments, analyzing the colocalizations in a total of 25,000 to 57,000 cells. Precise numbers are given in the graphs. Fpr3-positive cells that coexpress the marker are labeled by (+), while cells not coexpressing the marker are labeled with (-). Values in parentheses denote positive *versus* total cells. Error bars, S.D.

Consistent with these findings, there are hints in the literature for murine Fpr3 expression in immune cells. Thus, I assumed that the OMP- and $G\alpha_o$ -negative cells may have been leukocytes. As my cell preparation was likely to contain trace contaminations from white blood cells, I hypothesized that the Fpr3 antibody detected some leukocytes in addition to VSNs. To evaluate this, coexpression of two immune cell markers with Fpr3 was tested (Figure 19). An antibody directed against the lineage-specific R-isoform of the cluster of differentiation molecule 45 (CD45R), a plasma membrane phosphatase and one of the most commonly used pan-B cell markers, which is expressed in most leukocytes, was used. However, this molecule is not expressed by neutrophil granulocytes. Thus, for detection of this cell type, an antibody detecting the lymphocyte antigen 6G (Ly6G), a marker exclusively expressed by neutrophil granulocytes, was used (Ballas and Rasmussen, 1993; Rolink *et al.*, 1996; Lai *et al.*, 1998).

Both immune cell marker antibodies produced clear and robust stainings. Expression of Ly6G was examined first because it is only expressed by one cell type and would therefore deliver more specific results. For this molecule, marked overlap of Fpr3 and Ly6G protein was observed in 28 of 64 (44%) of the analyzed cells. Subsequently, CD45R expression was

examined to evaluate if any other immune cell type also expressed murine Fpr3. Virtually no coexpression with Fpr3 was detected for CD45R. These results provide first evidence for a dual expression of Fpr3 protein in specific subsets of neurons in the VNO and in immune cells and prove expression of *Fpr3* mRNA and protein in murine vomeronasal sensory neurons that also express $G\alpha_o$ and OMP.

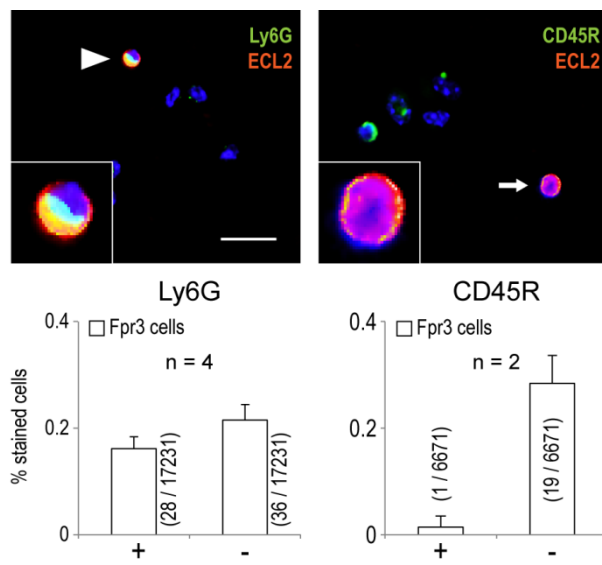


Figure 19. Molecular characteristics of the non-olfactory Fpr3-positive cells. Colocalization of murine Fpr3 (red) with immune cell markers (green) on dissociated VNO cells. Fpr3 staining colocalized with Ly6G (lymphocyte antigen 6G), a neutrophil granulocyte marker. No colocalization was seen for CD45R (cluster of differentiation molecule 45R), that is expressed by most immune cells but absent in neutrophil granulocytes. The colocalizing cells are marked with a white triangle, non-colocalizing with a white arrow. All cells were counterstained with the nuclear dye Hoechst33342 (blue). Insets show Fpr3-positive cells in a 3× magnification. Scale bars, 20 μ m. The bar chart below each picture denotes the quantification from two to five experiments, analyzing the colocalizations in a total of 7,000 to 17,000 cells. Precise numbers are given in the graphs. Values in parentheses denote positive *versus* total cells. Error bars, S.D.

3.2.2 Fpr3 Expression in Neutrophil Granulocytes is Enhanced by LPS Stimulation

Mouse blood cells were analyzed by immunocytochemical and RT-PCR to characterize Fpr3-positive immune cells in greater detail. First, the newly generated antibodies were used to directly test leukocytes from murine blood smears for Fpr3 expression (Figure 20).

ECL2 and ECL1 produced clear stainings on nucleated blood cells with little to no non-specific staining (Figure 20A, B; *left panel*). Staining was observed in 182/1377 leukocytes for ECL2 and in 907/7844 leukocytes for ECL1, resulting in mean percentages of $13.4\% \pm 0.6\%$ and $13.2\% \pm 2.6\%$, respectively (Figure 20C). Furthermore, the signals of both antibodies colocalized to $89.0\% \pm 4.8\%$ (Figure 21C). The stainings of both antibodies could be abolished by blocking of the epitope specific antibody binding sites with the peptides that were used for their generation. The number of Fpr3-expressing leukocytes corresponded well to the typically range of neutrophil granulocytes in mouse blood, which is between 9% to 18% (Gowen and Calhoun, 1943). Moreover, Fpr3-positive leukocytes showed a multi-lobed nucleus that is typical for mature neutrophil granulocytes (Figure 20A, B; *right panel*). This result suggests that the Fpr3-expressing leukocytes are neutrophil granulocytes.

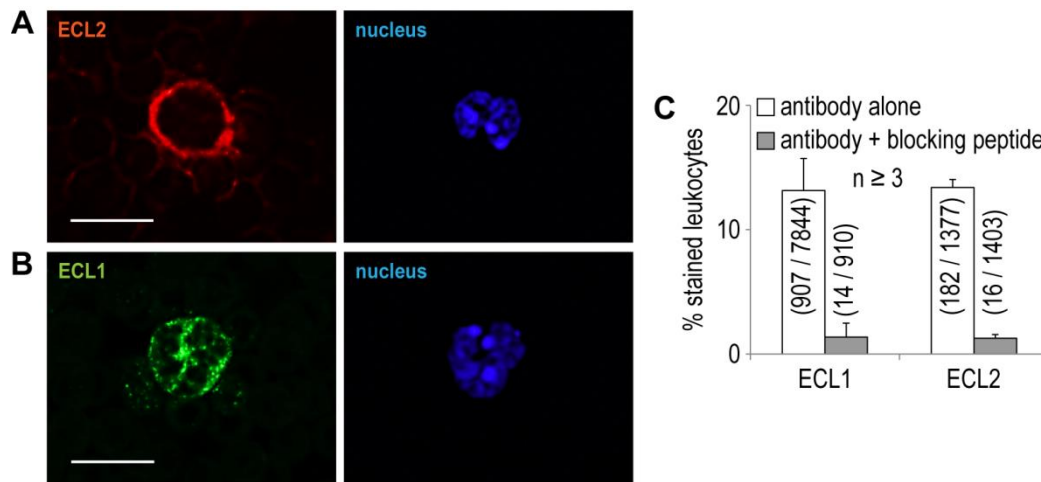


Figure 20. **Fpr3 is expressed in mouse leukocytes.** Representative immunostainings of blood cells from C57Bl/6NCr1 mice with the monoclonal mouse antibody ECL2 (A) or the polyclonal rabbit antibody ECL1 (B). For nuclear staining Hoechst33342 was used (right). Scale bars, 10 μ m. C, quantification and specificity of ECL2 and ECL1 immunoreactivity in leukocytes. Antibody specificity was demonstrated by blocking the specific binding site through preincubation with 10 μ g/ml of the peptide used for antibody generation.

To prove this, I performed colocalization experiments between murine Fpr3 and the neutrophil granulocyte marker Ly6G (Figure 21). They should have given definite information about whether these Fpr3-expressing cells are neutrophil granulocytes.

Staining with the Ly6G antibody colocalized with Fpr3 protein expression determined with ECL2 and ECL1 (Figure 21A, B). Quantification revealed colabeling between Ly6G and ECL1 or ECL2 of $83.1\% \pm 9.3\%$ and $86.7\% \pm 3.1\%$, respectively (Figure 21C). Hence, these results unambiguously demonstrate the presence of Fpr3 protein in mouse neutrophil granulocytes.

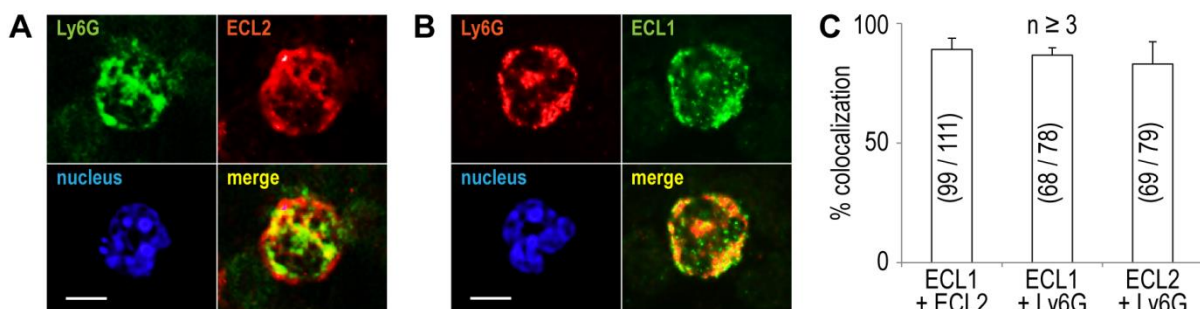


Figure 21. **Fpr3 protein is expressed in mouse neutrophil granulocytes.** Colocalization between the monoclonal mouse antibody ECL2 (A) and the polyclonal rabbit antibody ECL1 (B) with the neutrophil granulocyte marker Ly6G. Cell nuclei are shown in blue. Scale bar, 5 μ m. C, colocalization between Fpr3 and Ly6G immunoreactivity in leukocytes. Bars show average percentage of colocalizing cells from at least three independent experiments. Numbers in parentheses denote positive versus total cells. Error bars, S.D.

In line with the presence of Fpr3 protein in mouse blood cells, *Fpr3* mRNA should have also been detectable in those cells. First, PCR experiments were performed to investigate *Fpr3* mRNA expression in blood cells (Figure 22).

Surprisingly, no band proving *Fpr3* mRNA in mouse blood was visible. To exclude technical problems, a number of positive controls were performed. Glyceraldehyde 3-phosphate dehydrogenase (*Gapdh*), an essential enzyme in glycolysis that is present in all cells and control for cDNA quality, was readily amplified from blood and vomeronasal cDNA. Furthermore, a band for *Fpr3* from vomeronasal cDNA was easily detected. In general, mRNA from blood cells was detectable without a problem and therefore I could largely exclude any technical problems as the reason for this unexpected result. A possible explanation for this rather surprising result was the relatively low RNA amount in mature neutrophil granulocytes circulating in the blood. Indeed, these cells possess 10-fold to 20-fold less RNA per cell than monocytes or lymphocytes (Cassatella, 1999). Thus, I concluded that the detection limit of the RT-PCR was too low to amplify *Fpr3* from neutrophil granulocyte RNA.

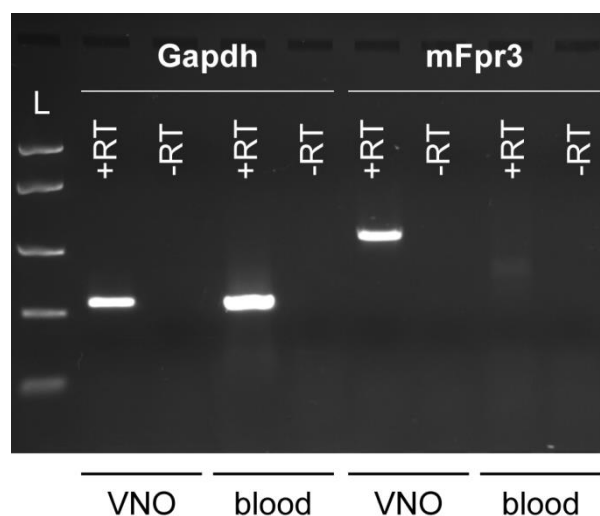


Figure 22. *Fpr3* mRNA is absent in blood leukocytes. **A**, RT-PCR analysis of murine *Fpr3* expression in mouse blood. Receptor expression was only detected in the positive control reaction from vomeronasal cDNA. Glyceraldehyde 3-phosphate dehydrogenase (*Gapdh*, reverse transcription control) was amplified from vomeronasal and blood cDNA. Similar results were obtained in three independent experiments. Size marker (L) FastRuler Middle Range DNA Ladder. mFpr = murine *Fpr*.

In blood only mature neutrophil granulocytes are present. Their maturation and proliferation takes place in the bone marrow. Hence, it was possible that the mRNA levels for *Fpr3* were much higher in maturing neutrophil granulocytes. Moreover, it is well-known that mRNA levels of specific genes in leukocytes, such as *Fpr1* (Mandal *et al.*, 2005) and *Fpr2* (Cui *et al.*, 2002; Iribarren *et al.*, 2003), increase after stimulation with bacterial stimuli. Thus, I assumed that this could also be true for *Fpr3*. To test this, bone marrow cells were

stimulated with lipopolysaccharide (LPS) from *Salmonella enteritidis* prior to mRNA isolation and both preparations were examined for *Fpr3* expression (Figure 23).

LPS stimulation of bone marrow cells in RT-PCR experiments fulfilled my assumptions. When stimulating cells with 150 µg/ml LPS from *Salmonella enteritidis*, *Fpr3* mRNA expression was detected in all LPS-stimulated samples (Figure 23; *left panel*). A strong band for murine *Fpr3* was amplified. Controls with β -actin, a cytoskeletal protein present in each cell, and without reverse transcriptase showed the expected results. In line with my hypothesis, a band for *Fpr3* from mRNA of unstimulated bone marrow cells was not observed (Figure 23; *right panel*), although the controls showed the desired results. Hence, *Fpr3* mRNA levels in unstimulated cells were relatively low and LPS stimulation induced an increase in *Fpr3* expression, which explained why most previous RT-PCR studies failed to detect it. These results show that murine *Fpr3* is upregulated upon LPS stimulation.

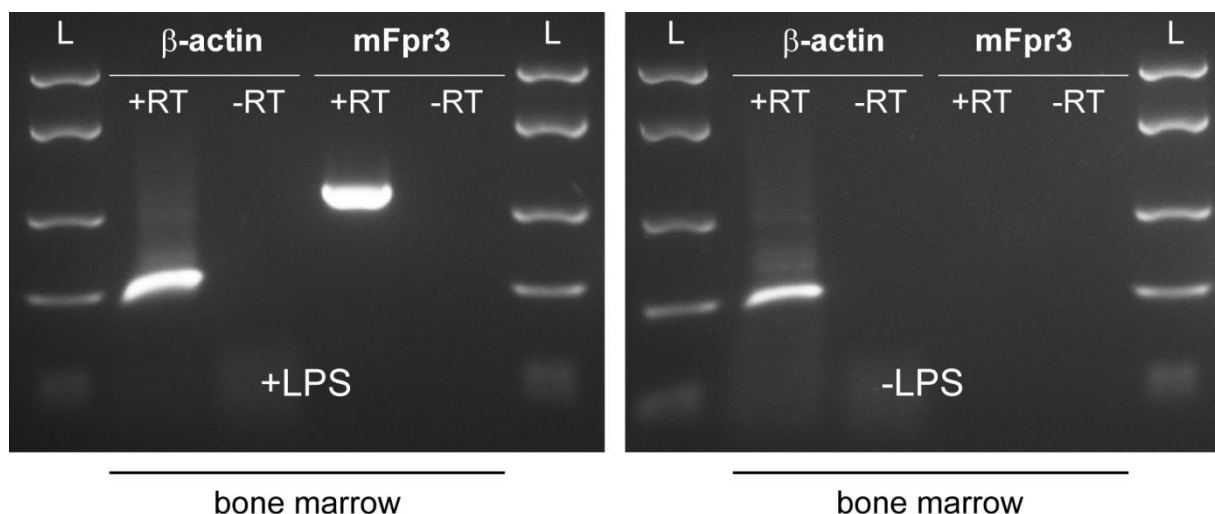


Figure 23. ***Fpr3* mRNA expression is induced by LPS stimulation.** RT-PCR analysis of murine *Fpr3* expression in bone marrow. Receptor expression was observed upon stimulation with 150 µg/ml lipopolysaccharide (LPS) from *S. enteritidis* (left). *Fpr3* was not detected from unstimulated mouse bone marrow cDNA (right). β -actin was amplified from all cDNAs. Similar results were obtained in two independent experiments. Size marker (L) FastRuler Middle Range DNA Ladder. mFpr = murine *Fpr*.

Assuming a similar biological role for murine and human FPR3, I was interested in determining whether both receptors are present in the same cell type. Because of the successful detection of murine *Fpr3* in neutrophil granulocytes, I next investigated human FPR3 expression in this cell type (Figure 24). RT-PCR experiments with human neutrophil granulocytes that were stimulated with 150 µg/ml LPS from *Salmonella enteritidis* showed human *FPR3* mRNA expression. A marked band for human *FPR3* was amplified. Positive controls with *Gapdh*, human *FPR1*, and human *FPR2* that have been reported to be

expressed in neutrophil granulocytes (see chapter 1.3.3) all showed distinct bands. Negative controls without reverse transcriptase showed no bands. These results demonstrate human *FPR3* expression in neutrophil granulocytes.

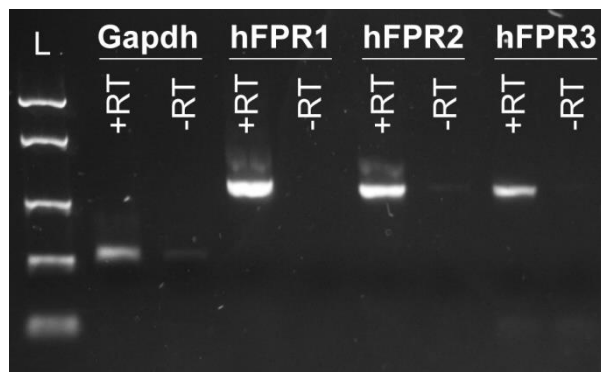


Figure 24. **Human neutrophil granulocytes express three Fprs.** RT-PCR analysis of *FPR1*, *FPR2*, and *FPR3* expression in human neutrophil granulocytes. Bands of the correct sizes and sequences for all three receptors were observed in human neutrophil granulocyte cDNA (+RT) but not in the negative control without reverse transcriptase (-RT). Glyceraldehyde 3-phosphate dehydrogenase (Gapdh) was used as reverse transcription control. Similar results were obtained in three independent experiments. Size marker (L) FastRuler Middle Range DNA Ladder. hFPR = human Fpr.

I reasoned that the increase in RNA through LPS stimulation indicates increased levels of receptor protein, which should have been detectable in corresponding immunocytochemistry experiments. Thus, unstimulated and LPS-stimulation mouse bone marrow cells were examined using ECL2 to detect murine Fpr3 protein (Figure 25).

ECL2 produced reliable stainings on bone marrow cells, as before on blood cells (Figure 25A). Staining was visible in unstimulated and LPS-stimulated cells. Representative images depicted increased cell amounts positive for Fpr3 after LPS stimulation. Quantification revealed that the number of Fpr3-positive cells indeed almost doubled from $5.1\% \pm 0.7\%$ to $9.5\% \pm 0.3\%$ (Figure 25B). Thus, expression of Fpr3 protein in mouse neutrophil granulocytes can be induced by LPS.

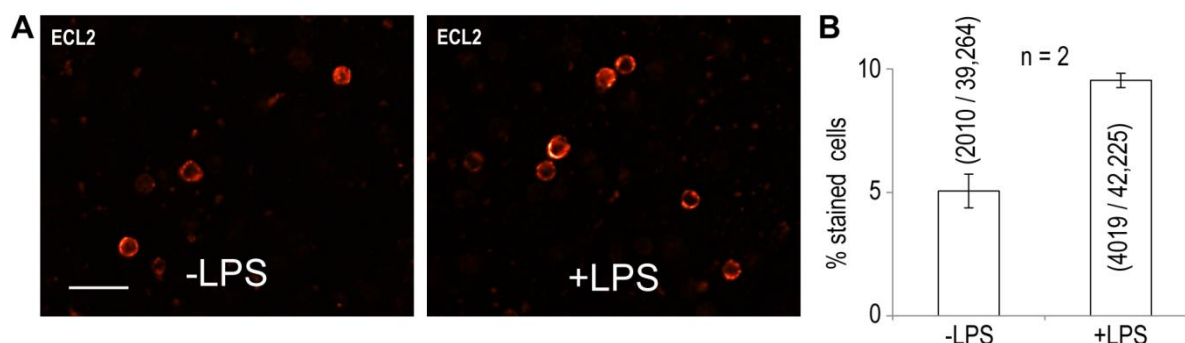


Figure 25. **Fpr3 protein levels rise with increasing mRNA levels upon LPS stimulation.** **A**, representative immunostainings for Fpr3 in unstimulated (left) and LPS stimulated (right) bone marrow cells from C57Bl/6NCrl mice. **B**, quantification for stainings on both conditions. Scale bar, 20 μ m. Bar chart shows mean increase of Fpr3-expressing cells upon LPS stimulation from two independent experiments carried out as triplicates. Numbers in parentheses denote positive versus total cells. Error bars, S.D.

Taken together, these results prove mRNA expression for murine and human *Fpr3* in neutrophil granulocytes and the presence of murine Fpr3 protein in this cell type. They also demonstrate upregulation of murine *Fpr3* mRNA expression upon LPS-stimulation.

3.3 Strain-Specific Variants of Murine Fpr3

Two previous studies (Gao *et al.*, 1998; Wang and Ye, 2002) reported divergent sequences for murine *Fpr3* between BALB/c and 129/S6 mice, with a main difference of four amino acids missing in the fourth transmembrane region. Data from these reports suggest strain-specific variants of the receptor that could result in altering expression patterns. The experiments described thus far were performed in C57Bl/6NCrl mice. To investigate potential altering expression patterns of *Fpr3*, some of the previously described experiments were also performed in other mouse strains. In line with published data, I received varying staining patterns for Fpr3 in different mouse strains, indicating diverging expression patterns for the receptor in different mouse strains. However, initial examinations on this issue lacked a systematic approach.

3.3.1 Fpr3 Protein Expression Occurs in a Strain-Specific Manner

To test the hypothesis of murine Fpr3 variations present in different mouse strains which possibly lead to strain-specific variations in the Fpr3 expression pattern, I performed a systematic expression and genotype analysis of *Fpr3* in five mouse strains and combined these results with sequence data from 32 laboratory and nine wild-derived strains. First, 129X1/Sv mice were analyzed via immunohistochemistry using ECL2 and ECL1 (Figure 26).

Remarkably, 129X1/Sv mice showed no Fpr3 expression in leukocytes, whereas C57/Bl6NCrl mice showed Fpr3 expression as before (Figure 26A). Fpr3 expression was also examined in vomeronasal cells of the two mouse strains to prove the result obtained in leukocytes. In vomeronasal cells from 129X1/Sv mice, Fpr3 was not detected, whereas examinations in C57/Bl6NCrl mice resembled the already shown results. In these experiments, ECL2 and ECL1 were used (Figure 26B), and the obtained result was highly reproducible in multiple animals ($n = 9$).

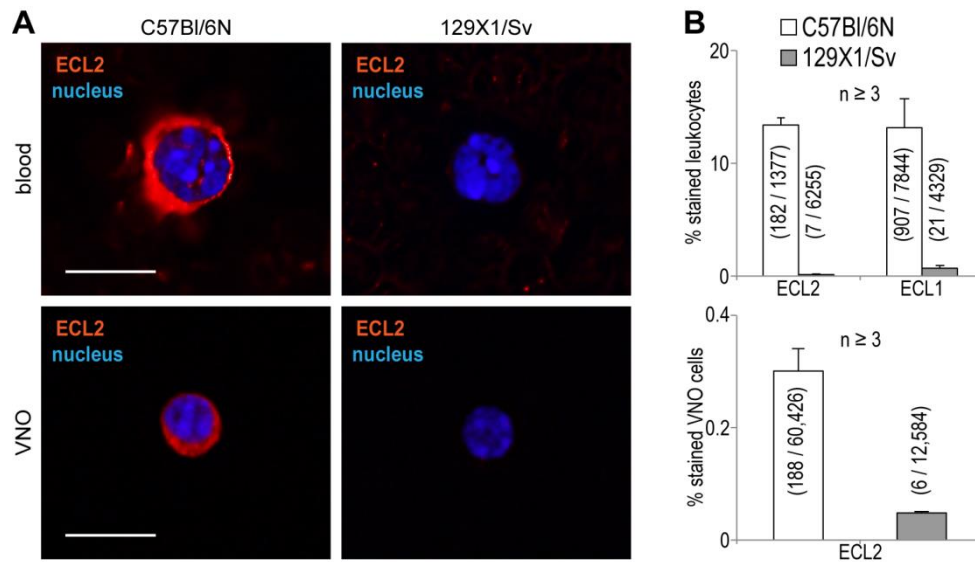


Figure 26. **Strain-specific loss of Fpr3 expression in mice.** **A**, representative immunostainings of Fpr3 expression in leukocytes and vomeronasal cells of C57Bl/6NCrI mice (left) *versus* 129X1/Sv mice (right). Fpr3 is only detectable in cells from C57Bl/6NCrI mice. Scale bars, 10 μ m. **B**, quantification of Fpr3 expression in leukocytes (upper panel) and vomeronasal cells (lower panel). Bar charts show average percentage of stained cells from at least three independent experiments. Numbers in parentheses denote positive *versus* total cells. Error bars, S.D.

To investigate this in more detail, additional immunostainings in leukocytes from C57Bl/6NCrI, 129X1/Sv, BALB/cJ, FVB/N, and NZB/Ola mice were performed. Fpr3 protein expression was observed in NZB/Ola and C57Bl/6NCrI mice. By contrast, BALB/cJ, FVB/N, and 129X1/Sv mice showed no Fpr3 expression. However, *Fpr3* mRNA expression from the VNO by the production and detection of cDNA in all negatively tested strains was still detectable. Possibly, variations in the *Fpr3* gene alter the Fpr3 protein structure and thus prevent its detection by the antibodies. Therefore, I amplified and sequenced *Fpr3* from genomic DNA of C57Bl/6NCrI and 129X1/Sv mice and compared the results (Figure 27).

This analysis indeed revealed two distinct *Fpr3* variants: the *Fpr3* sequence from C57Bl/6NCrI mice perfectly matched the annotated NCBI reference sequence NM_008042.2, whereas the *Fpr3* sequence from 129X1/Sv mice showed a 12 nucleotide *in-frame* deletion (Figure 27A). This deletion comprised the nucleotides 424 to 435 of the coding region and resulted in the loss of alanine142, arginine143, asparagine144, and valine145 but left the open reading frame intact. For a clear discrimination, the version carrying the 12 nucleotide deletion was called *Fpr3* $\Delta_{424-435}$ and the full-length version was called *Fpr3*_{wt}.

Next, examinations on *Fpr3* in BALB/cJ, FVB/N, and NZB/Ola mice revealed a clear correlation between specific gene variants and the presence or absence of Fpr3 antibody staining (Figure 27B). *Fpr3* $\Delta_{424-435}$ was present in the genome of 129X1/Sv, BALB/cJ, and

FVB/N mice that had no detectable Fpr3 protein whereas C57Bl/6NCrl and NZB/Ola, in which Fpr3 protein was readily detectable, carried the *Fpr3_{wt}* gene. To obtain a more comprehensive view of the distribution of both *Fpr3* variants in different inbred strains, the Mouse Genomes Project Database was consulted. The analyses revealed the occurrence of *Fpr3_{wt}* in C57, C58, I, KK NOD, NZB, NZW, and ST mice, whereas 129S, 129P, AKR, A, BALB, BUB, C3H, CBA, DBA, FVB, LP, NZO, RF, and SEA all carried the *Fpr3 $\Delta_{424-435}$* variant.

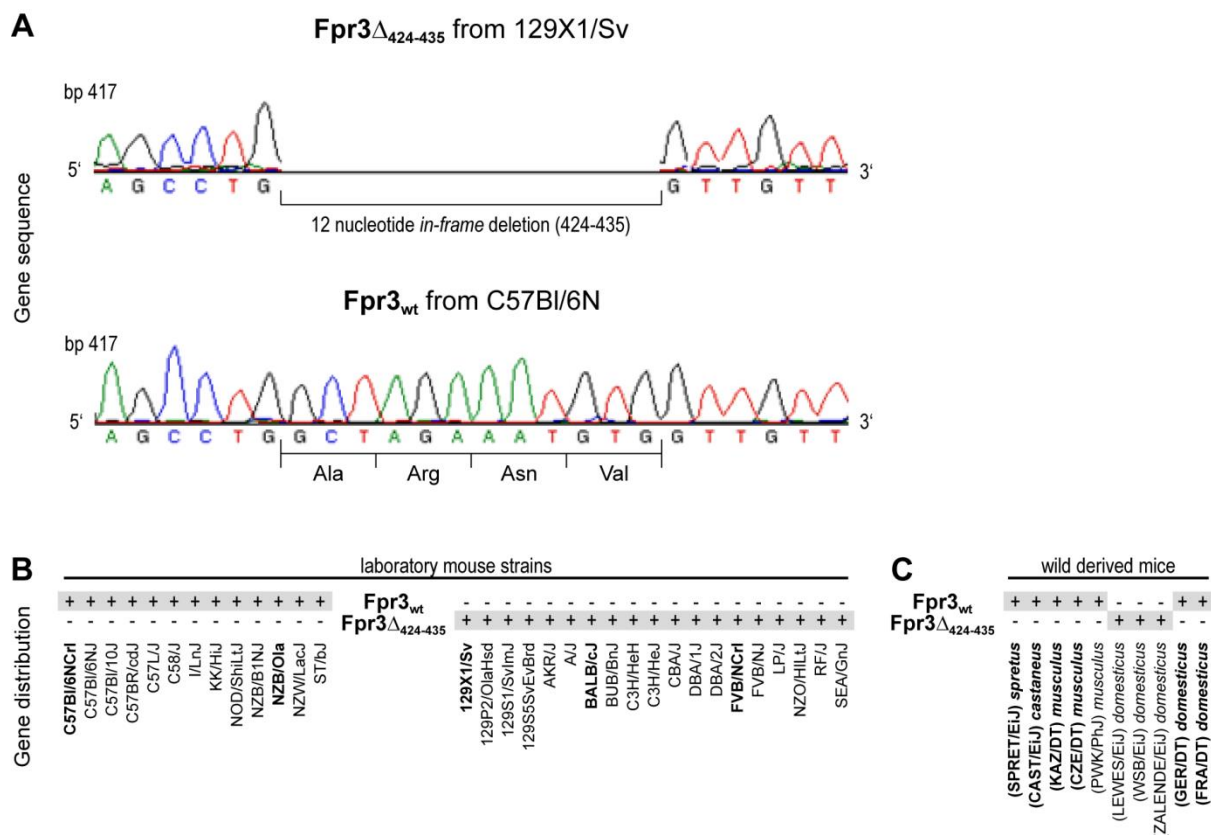


Figure 27. Sequence and distribution of the 12 nucleotide *in-frame* deletion in *Fpr3 $\Delta_{424-435}$* . **A**, genotyping of Fpr3 in 129X1/Sv and C57Bl/6NCrl mice revealed two receptor variants *Fpr3_{wt}* and *Fpr3 $\Delta_{424-435}$* . A 12 nucleotide *in-frame* deletion from base pair 424 to 435 was observed in 129X1/Sv mice resulting in a loss of an Alanine, Arginine, Asparagine, and Valine at the end of the second intracellular loop. Identical results were obtained from three individuals of each strain. **B**, distribution of both *Fpr3* gene variants in different laboratory mouse strains. Gray shading denotes the genomically encoded variants. Bold letters annotate in house sequenced strains. All other data were obtained from the Mouse Genome Project (<https://www.sanger.ac.uk>; release REL-1505). **C**, distribution of both *Fpr3* gene variants in wild-derived mouse strains from different subspecies and geographical origins. *Mus musculus castaneus* was from Thailand (CAST/EiJ). *M. m. domesticus* were from Germany (GER/DT), France (FRA/DT), the United States of America (LEWES/EiJ, WSB/EiJ), and Switzerland (ZALNDE/EiJ). *M. m. musculus* were from Kazakhstan (KAZ/DT) and Czech Republic (CZE/DT, PWK/PhJ), *M. m. spretus* was from Spain (SPRET/EiJ).

Because of this high frequency of both variants in laboratory mice, I asked about the possible origin of the two *Fpr3* variants. The development of a receptor variant could have emerged under natural conditions or may have been a consequence of breeding conditions. Therefore, I was interested in determining whether both variants could be found in wild mouse strains and thus looked at the frequency of both *Fpr3* variants in wild-derived animals. Most laboratory mouse strains are crossbreedings from three *Mus musculus* subspecies: *M. m. castaneus*, *M. m. domesticus*, and *M. m. musculus*. Hence, their genomes depict mosaics of the genomes of these three ancestor strains. To elucidate which of these ancestors carried the *Fpr3* $\Delta_{424-435}$ variant, the *Fpr3* sequence of wild-derived *Mus musculus* strains was investigated (Figure 27C). The genomes of wild-derived mouse strains, unlike that of laboratory inbred strains, mainly mimic the genome of only one ancestor strain.

My panel of six genomic DNAs covered samples of *M. m. castaneus*, *M. m. domesticus*, *M. m. musculus*, and an additional *M. m. spretus* sample. The samples were collected from different locations on the three continents North America, Europe, and Asia. CAST/EiJ was the only representative of *M. m. castaneus* originated in Thailand. GER/DT and FRA/DT representing *M. m. domesticus* were from Germany and France, respectively. The wild-derived strains representing *M. m. musculus*, KAZ/DT and CZE/DT, were from Kazakhstan and the Czech Republic. SPRET/EiJ, representing *M. m. spretus*, originated in Spain. The analysis of these DNA samples by direct sequencing of PCR products showed that they all carried *Fpr3*_{wt}. Additional data mining in the Mouse Genomes Project Database indicated three *M. m. domesticus* lines, LEWES/EiJ, WSB/EiJ, and ZALLENDE/EiJ from the United States of America and Switzerland, respectively, that carried the *Fpr3* $\Delta_{424-435}$ variant. Thus, *Fpr3* $\Delta_{424-435}$ was most likely introduced into inbred mouse lines through breeding with *M. m. domesticus* mice that accidentally carried *Fpr3* $\Delta_{424-435}$.

3.3.2 Loss of *Fpr3* $\Delta_{424-435}$ Function Due to Diminished Receptor Expression

The deletion in *Fpr3* $\Delta_{424-435}$ leads to a loss of only four amino acids in the second intracellular loop but leaves the open reading frame intact (see chapter 3.3.1). The presence of *Fpr3* mRNA in the absence of a detectable protein strongly argues for structural alterations in *Fpr3* $\Delta_{424-435}$. I thus hypothesized that these alterations may affect the receptor function. To test this, I used an established *in vitro* calcium imaging assay (Bufe *et al.*, 2012) (Figure 28).

First calcium imaging in HEK cells transiently transfected with either *Fpr3* $\Delta_{424-435}$ or *Fpr3*_{wt} were performed and calcium responses to 30 μ M W-peptide were recorded. This substance was chosen for initial comparative functional experiments on *Fpr3* because it is a

well-characterized Fpr agonist (Bufe *et al.*, 2012; Bufo *et al.*, 2015). 37% (177/475) of *Fpr3_{wt}* transfected cells were robustly activated by W-peptide. However, none of the analyzed 686 cells transfected with *Fpr3 Δ ₄₂₄₋₄₃₅* responded to this stimulus (Figure 28). This dramatic result was unexpected as the deletion left the open reading frame intact.

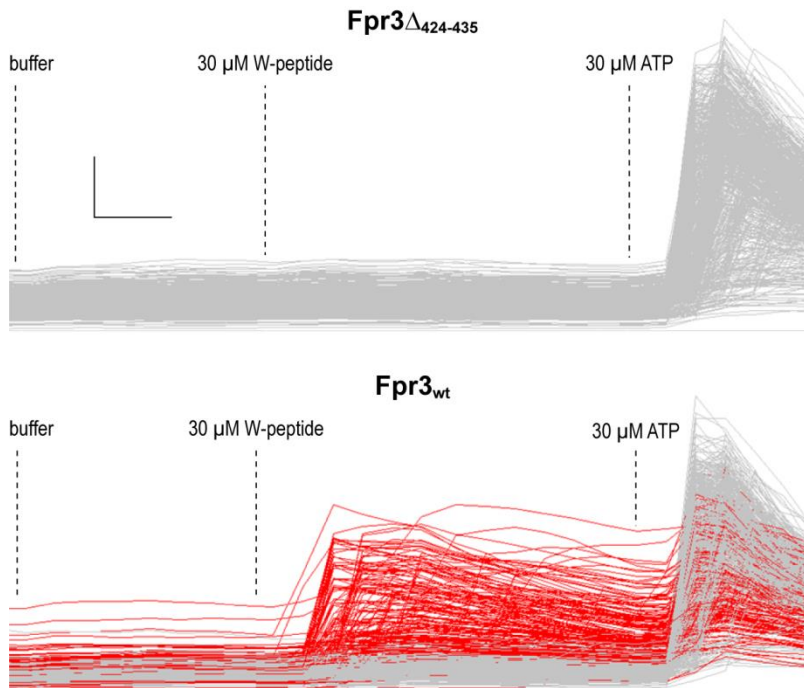


Figure 28. **Fpr3 Δ ₄₂₄₋₄₃₅ does not respond to the synthetic Fpr3 agonist W-peptide.** Single cell calcium imaging of HEK293T cells transfected with Fpr3 Δ ₄₂₄₋₄₃₅ or Fpr3_{wt} upon W-peptide stimulation. Each trace represents an individual cell. Left: Fpr3 Δ ₄₂₄₋₄₃₅ transfected cells. None of 686 cells responded to 30 μ M W-peptide. Right: Fpr3_{wt} transfected cells. 177 of 475 cells (red) responded to 30 μ M W-peptide. Buffer was used to exclude mechanical activation; 30 μ M ATP that activates endogenous receptors was used as positive control for cell viability. Scale bars, vertical 0.5 340 nm/380 nm, horizontal 10 s.

I wondered whether this lack of function for *Fpr3 Δ ₄₂₄₋₄₃₅* was specific for W-peptide, or if it also occurred with other ligands that activated Fpr3. To answer this question, I tested three bacterial signal peptide fragments – *Salmonella*-SP24, *Psychromonas*-SP6, and *Hydrogenobacter*-SP16 – that were recently identified as naturally occurring Fpr3 activators (Bufe *et al.*, 2015) and the synthetic M-peptide, which exhibits high sequence divergence to W-peptide (Figure 29). *Fpr3 Δ ₄₂₄₋₄₃₅* transfected cells were neither activated by M-peptide nor any of the three sequence divergent bacterial signal peptides. By contrast, 26.0% \pm 4.3% *Fpr3_{wt}* transfected cells were activated by M-peptide and 30.0% \pm 1.5%, 27.6% \pm 3.8%, and 9.8% \pm 2.4% of the cells were activated by the bacterial signal peptides, respectively. Thus, I concluded that the lack of Fpr3 Δ ₄₂₄₋₄₃₅ function was not dependent on the substance, but rather constitutes a general effect.

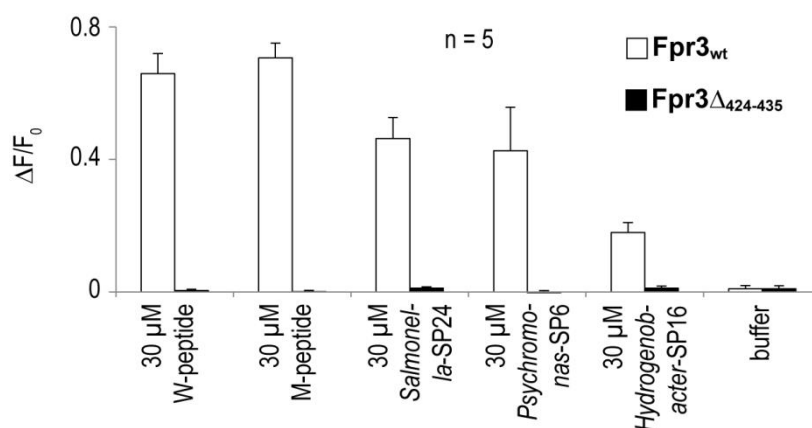


Figure 29. **Fpr3_{Δ424-435} does not respond to natural Fpr3 activators.** Mean calcium responses of HEK293T cells transfected with Fpr3_{wt} or Fpr3_{Δ424-435} to various agonists. Buffer was used as negative control. Bars denote average percentage of responding cells from five independent experiments, measured in duplicates. Error bars, S.D.

3.3.3 Lack of *Fpr3*_{Δ424-435} Expression in HEK Cells

The absence of specific Fpr3 staining in VNO cells and leukocytes from mice carrying the *Fpr3*_{Δ424-435} gene may have been caused by diminished or no expression of the Fpr3 protein. Therefore, the degree of protein expression by both *Fpr3* variants was assessed by ECL1 and ECL2 immunostaining on HEK cells. Representative immunohistochemistry images showed clear staining for Fpr3_{wt} with both antibodies (Figure 30). Supporting the results obtained in vomeronasal and immune cells, Fpr3_{Δ424-435} was not detected with either antibody. ECL2 stained 11.2% ± 1.7% of the *Fpr3*_{wt} and 0.3% ± 0.2% of the *Fpr3*_{Δ424-435} transfected cells, whereas ECL1 stained 11.6% ± 2.7% and 0.4% ± 0.5%, respectively.

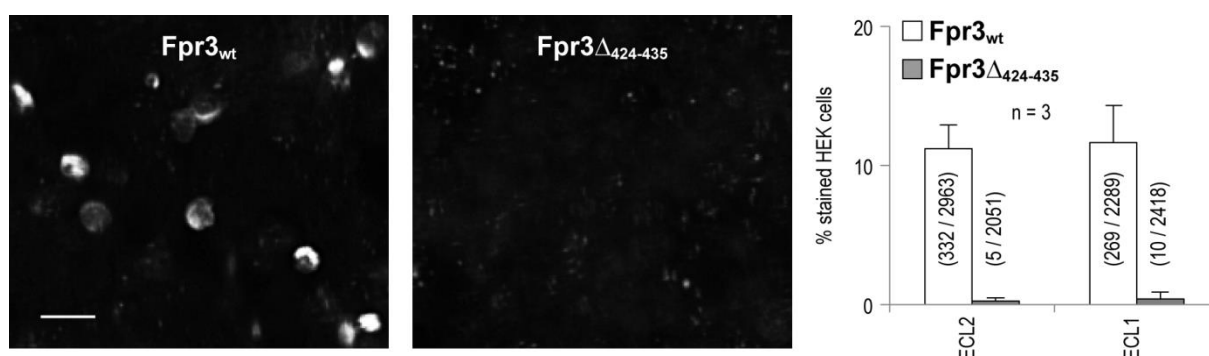


Figure 30. **Expression of Fpr3_{Δ424-435} and Fpr3_{wt} in HEK293T cells.** Immunostainings of HEK293T cells expressing Fpr3_{wt} (left) or Fpr3_{Δ424-435} (middle) and their quantification (right). Only Fpr3_{wt} was detectable. The bar chart shows the average percentage of stained cells from three independent experiments. Numbers in parentheses denote positive versus total cells. Error bars, S.D. Scale bar, 20 μm.

The lack of specific Fpr3_{Δ424-435} staining observed in the overexpressing system closely resembled the lack of Fpr3_{Δ424-435} protein in VSNs and leukocytes (see chapter 3.3.1). The lack of staining by two independent antibodies that recognize different parts of the receptor

strongly suggests degradation of the $Fpr3\Delta_{424-435}$ variant in HEK cells. However, technical issues could also produce such results. To distinguish between these possibilities, I subcloned *Fpr3* into a novel vector to create an $Fpr3\Delta_{424-435}$ fusion protein exhibiting specific N- and C-terminal epitopes. This strategy permitted independent detection of the receptor sites using two different antibodies specific for these epitopes. N-terminal rhodopsin-epitope (Rho) and C-terminal herpes simplex virus-epitope (HSV) tags were attached to $Fpr3\Delta_{424-435}$ and named the Rho- $Fpr3\Delta_{424-435}$ -HSV fusion protein. Three independent copies were produced, sequenced, and tested to exclude any possible corruption in the vector (Figure 31).

The N-terminal Rho-tag showed pronounced staining of the transiently transfected cells. Rho- $Fpr3_{wt}$ stained $33.71\% \pm 5.79\%$ of the cells, and Rho- $Fpr3\Delta_{424-435}$ -HSV stained $9.65\% \pm 2.54\%$ of the cells, representing a three-fold reduction of expression. The extent of receptor expression was examined with the C-terminal HSV-tag. The positive control was T2R16-HSV transfected cells, in which $30.23\% \pm 2.67\%$ of the cells were stained. Rho- $Fpr3\Delta_{424-435}$ -HSV showed complete loss of staining with the HSV antibody for all three of its copies.

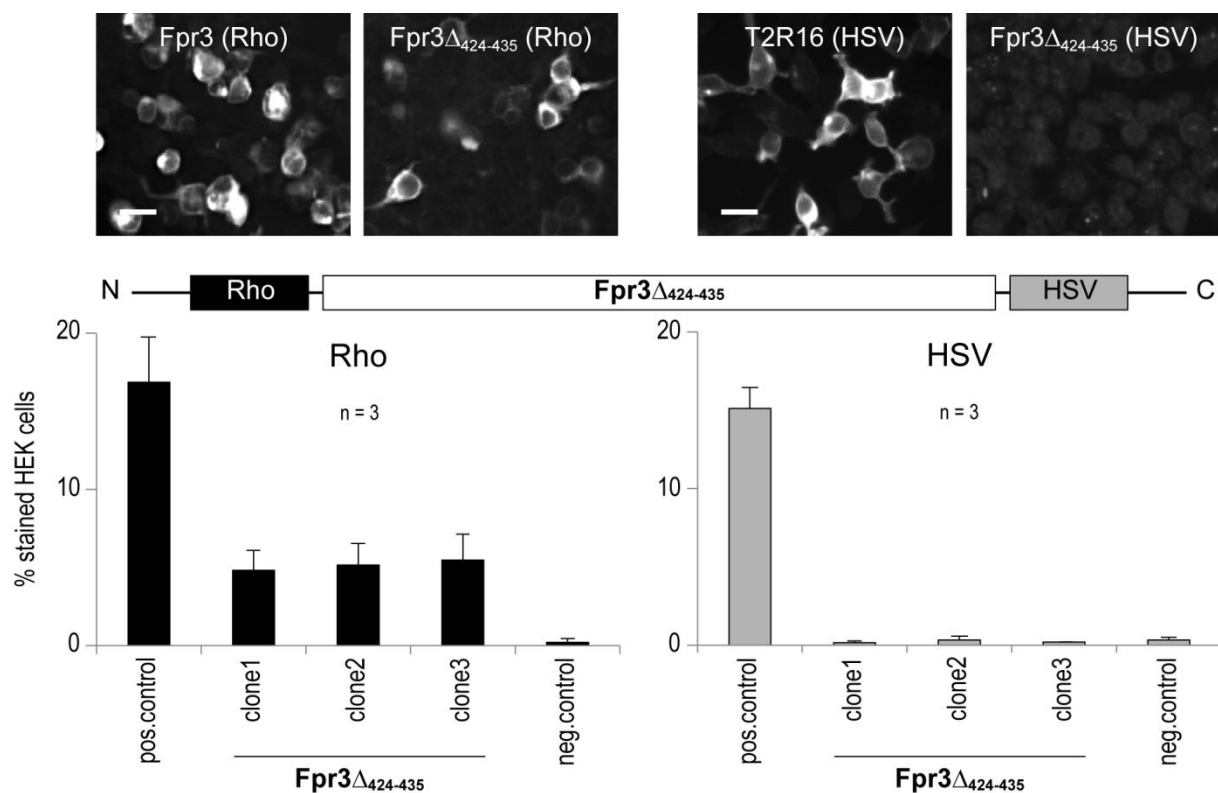


Figure 31. **$Fpr3\Delta_{424-435}$ exhibits truncated expression in HEK293T cells.** Immunostainings of HEK293T cells transfected with an independent plasmid copy of Rho- $Fpr3\Delta_{424-435}$ -HSV that is a fusion protein of $Fpr3\Delta_{424-435}$ with an N-terminal Rhodopsin-epitope (Rho) and a C-terminal herpes simplex virus-epitope (HSV). left: quantification of stainings with an anti Rho antibody. Right: quantification of stainings with an anti HSV antibody. Bars show average percentage of stained cells from three independent experiments. As controls

Rho-Fpr3_{wt}, a fusion protein of Fpr3_{wt} with an N-terminal Rho-epitope, and T2R16-HSV, a fusion protein of T2R16 with a C-terminal HSV-epitope, were used. *Error bars, S.D.*

Taken together, these experiments strongly argue that structural alterations in Fpr3 $\Delta_{424-435}$ resulted in production of an unstable protein in HEK cells, which was C-terminally truncated and subsequently degraded. This mechanism is likely to be responsible for degradation of Fpr3 $\Delta_{424-435}$ in mouse VSNs and leukocytes.

3.3.4 Fpr3 $\Delta_{424-435}$ is Non-Functional in the Vomeronasal Organ

My previous findings showed strain-specific Fpr3 expression in two variants. The variant functional in HEK cells was called Fpr3_{wt}, and the non-functional variant was called Fpr3 $\Delta_{424-435}$. I was interested in determining whether these findings also affected the responses of VNO cells to Fpr3 agonists.

If Fpr3 $\Delta_{424-435}$ was non-functional *in vivo*, it should have affected the animal response and would therefore have influenced their infection susceptibility and all other potential functions and behaviors related to Fpr3. To test the functionality of both Fpr3 variants *in vivo*, calcium imaging experiments on whole-mount preparations of the sensory side of the VNOs from C57Bl/6NCrl and 129X1/Sv mice were performed with the potent Fpr3 activator *Salmonella*-SP24 in cooperation with Dr. Andreas Schmid (Figure 32). Dendritic endings on the sensory side contact the outside world and express different receptors, including Fprs (Dietschi *et al.*, 2013). Based on my previous results I hypothesized that signals would only be detectable in C57Bl/6NCrl mice expressing Fpr3_{wt}, whereas no signals would be detected in 129X1/Sv mice encoding Fpr3 $\Delta_{424-435}$.

First, the VNOs of C57Bl/6NCrl mice were tested with three consecutive applications of 1 μ M *Salmonella*-SP24. Several dendritic endings were robustly activated with each of the three signal peptide fragment applications (Figure 32A). In total, an area of $\sim 300,000 \mu\text{m}^2$ was analyzed in seven independent experiments. Of approximately 34,000 dendritic endings found in this area, 41 responded to repeated applications of the ligand (Figure 32B). A total of $0.12\% \pm 0.04\%$ cells responded, which corresponded well with the immunostaining results (see chapter 3.2.1).

Subsequently, VNOs of 129X1/Sv mice expressing Fpr3 $\Delta_{424-435}$ were tested. A total area of $\sim 100,000 \mu\text{m}^2$ was examined in four independent experiments (Figure 32B). None of the approximately 12,000 dendritic endings in 129X1/Sv mice responded to any of the repeated applications of 1 μ M *Salmonella*-SP24. These data show that VSNs in C57Bl/6NCrl mice,

expressing the functional *Fpr3*_{wt}, can be activated by an *Fpr3* activator, whereas cells in 129X1/Sv mice cannot. Taken together, these results demonstrate the novel discovery of two strain-specific *Fpr3* variants that are functionally distinct.

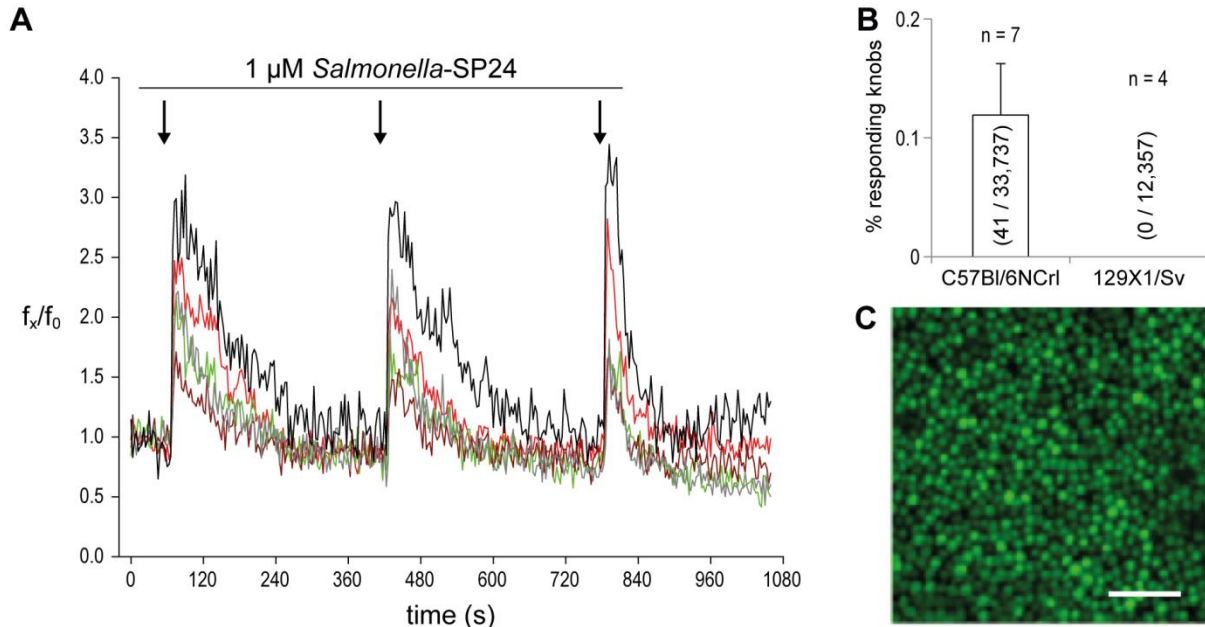


Figure 32. **Fpr3 agonists activate dendritic endings of VSNs.** Calcium imaging on individual dendritic knobs of a whole mount preparation of VNOs of C57Bl/6NCrI and 129X1/Sv mice upon stimulation with 1 μ M *Salmonella*-SP24. **A**, representative calcium traces of responding dendritic knobs. Each trace represents an individual knob of a C57Bl/6NCrI mouse that responds to each of three stimulations with the ligand, indicated by the arrows. Similar results were achieved over seven experiments. **B**, quantification of all measured dendritic knobs of both mouse strains. Bars represent the percentage of responding knobs upon stimulation. **C**, view on a section of the sensory side of the VNO. Dendritic knobs are depicted in green. Scale bar, 20 μ m. The results were kindly provided by Dr. Andreas Schmid, Department of Physiology, Saarland University. Subfigure **C** was adapted and modified from Oboti *et al.*, 2015.

3.4 Comparative Characterization of Murine and Human *Fpr3* Function

In this study, *Fpr3* was expressed in the VNO and the immune system of mice (see chapters 3.2.1 and 3.2.2). This expression pattern suggests an immune cell function for murine *Fpr3* and argues for a close relationship with immune Fprs. Mouse *Fpr1* has been suggested to be a human *FPR1* orthologue, whereas murine *Fpr2* has been suggested to be a human *FPR2* orthologue (Migeotte *et al.*, 2006; Önnheim *et al.*, 2008; Dahlgren *et al.*, 2016). Hence, I hypothesized that *Fpr3* of both species could occupy the same functional niche. However, the evolutionary relationship between murine and human *Fpr3* has not been clarified.

3.4.1 Orthology between Murine and Human *Fpr3* is not Assessable by Sequence Comparison

The amino acid sequence of murine *Fpr3* was compared to those of all human FPRs to investigate the evolutionary relationship between murine and human *Fpr3* (Figure 33A). A sequence alignment analysis revealed only modest similarity between *Fpr3* of both species. Murine *Fpr3* was 82% similar with human *FPR2*, followed by 74% with human *FPR3*, and 72% with human *FPR1*. This result resembled the receptor similarities of all murine and human immune receptors in the dendrogram (Figure 33B). Murine *Fpr3* was on the same branch with murine *Fpr2* and separated from murine *Fpr1* and human *FPR1*, which aligned on the second branch slightly nearer to human *FPR2* than to human *FPR3*. Meta-analyses comprised of 12 orthology prediction tools (see chapter 2.8.2.2) revealed that the relationship between mouse and human *Fpr3* was listed by only three of the tools, such as Compara, HGNC, and Panther, whereas *Fpr1* and *Fpr2* were annotated as human counterparts of *FPR1* and *FPR2* by 11 and nine consulted tools, respectively (Figure 33C). The other nine tools, such as HomoloGene, InParanoid, Isobase, OMA Browser, OrthoDB, OrthoMCL, PhylomeDB, Roundup, and TreeFam, did not list mouse and human *Fpr3* as orthologues. These results suggest that the orthology between murine and human *Fpr3* cannot be determined only by a sequence comparison. Thus, I next compared the functional properties of the two receptors.

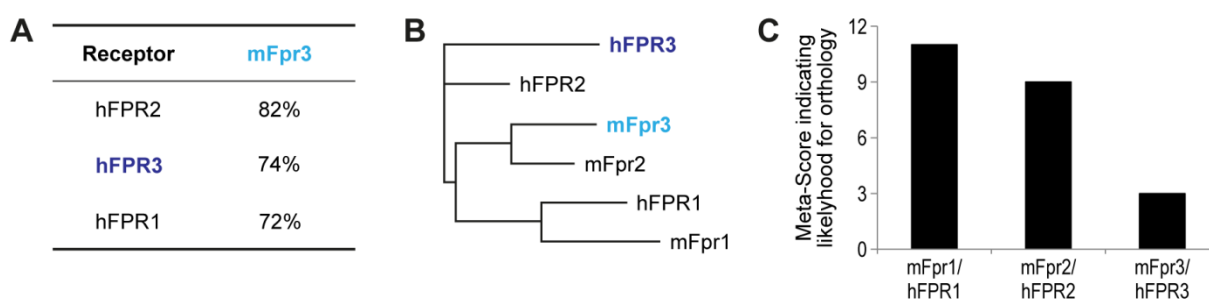


Figure 33. **Sequence relationship between murine *Fpr3* and human *Fprs*.** **A**, Comparison of amino acid sequence similarities between mouse *Fpr3* and all three human *Fprs*. **B**, Phylogenetic relationship between all mouse and human *Fprs*. **C**, integrative meta-analyses of the orthology of murine and human *Fprs* using the integrative search algorithm of DIOPT that combines orthology search results from 12 renowned ortholog prediction tools. The Meta-Score represents the number of individual tools listing murine and human *Fprs* as orthologs. Orthology between *Fpr3* of mouse and human is only listed by Compara, HGNC, and Panther. hFPR = human *Fpr*; mFpr = murine *Fpr*.

3.4.2 Murine and Human *Fpr3* Show Similar Functional Properties

To compare the function of murine and human *Fpr3* to each other and in the context of the *Fpr* families, I first studied the concentration dependent responses of human *FPR1*, *FPR2*, and

FPR3 with those of murine Fpr1, Fpr2, and Fpr3 to the synthetic compounds W-peptide (WKYMVm-NH₂) and L-M-peptide (MMHWAM-NH₂), and the bacterially derived signal peptide *Psychromonas*-SP6 (f-MLFYFS) (Figure 34). These peptides show a considerable structural variability because their amino acid composition differed in all positions. The closest resemblance in their structure is that they all contain a methionine with a chemical modification. But even these methionines are chemically divergent: W-peptide ends with an amidated methionine in D-conformation (m-NH₂), whereas the amidated methionine at the end of L-M-peptide has an L-conformation (M-NH₂), and the signal peptide *Psychromonas*-SP6 starts with a formylated L-methionine (f-M).

Concentrations-response curves revealed clear similarities in the responses of specific mouse and human FPR receptor pairs to the selected test substances (Figure 34). Murine and human Fpr1 showed identical agonist preferences. Both receptors preferred the bacterial signal peptide *Psychromonas*-SP6, over W-peptide and L-M-peptide. Their half maximal activation values (EC₅₀) for the different stimuli were also closely related. For *Psychromonas*-SP6 the EC₅₀ were 0.15 nM and 0.048 nM respectively, for W-peptide 2.2 nM and 0.99 nM and for L-M-peptide 360 nM and 89.6 nM. The high similarity in the responses of murine and human Fpr1 to all three stimuli fits well to the concept of an identical function for both receptors in both species. Murine and human Fpr2 also displayed clear similarities. Both receptors showed similar EC₅₀ values for W-peptide and L-M-peptide and preferred W-peptide over the two other agonists (Figure 34). Only their EC₅₀ for L-M-peptide differed by approximately 50-fold. Interestingly, the responses of murine and human Fpr3 also correlated (Figure 34). First, I observed that both receptors were drastically less sensitive than Fpr1 and Fpr2 and usually responded in the high nanomolar to micromolar range. The W-peptide responses are a prime example for this behavior. The EC₅₀ of murine Fpr1, Fpr2 and human FPR1, FPR2 were 0.99 ± 0.23 nM, 0.36 ± 0.24 nM, 2.20 ± 2.12 nM, and 0.26 ± 0.19 nM, respectively, whereas the corresponding values of murine Fpr3 and human FPR3 were 676 ± 174 nM and 6117 ± 618 nM, respectively. A general lower sensitivity of murine and human Fpr3 was also visible for L-M-peptide and *Psychromonas*-SP6. Moreover, the maximal signal amplitudes of Fpr3 of both species to all tested stimuli were clearly reduced in comparison to the responses of Fpr1 and Fpr2 (Figure 34). These observations argue for functional similarities between murine Fpr3 and human FPR3.

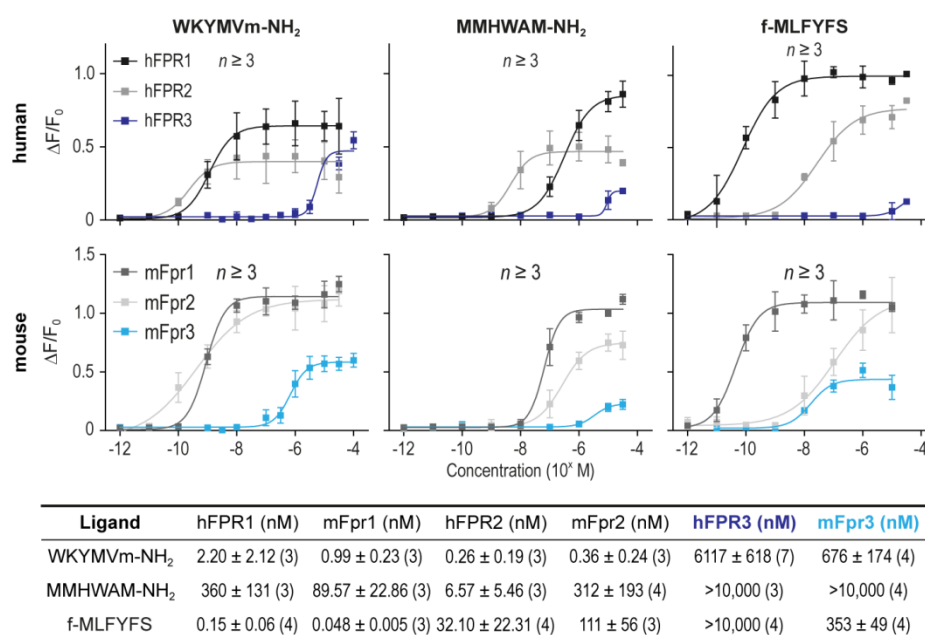


Figure 34. **Murine and human Fpr3 show related agonist responses.** Concentration-responses of HEK293T cells expressing mouse (lower panel) and human (upper panel) Fpr1, Fpr2, and Fpr3 upon stimulation with four sequence divergent Fpr activators. EC₅₀ values from all six receptors for the tested peptides are listed under the concentration-response curves. The number of experiments (*n*) is indicated above the curves. hFPR = human Fpr; mFpr = murine Fpr. Error bars, S.D.

3.4.3 Murine and Human Fpr3 are More Selective than Fpr1 and Fpr2

To further determine the degree of similarity between the agonist spectra of mouse and human Fpr3, I next compared their responses to a larger set of stimuli (Figure 35A). It is well-established that Fprs can respond to formylated bacterial and mitochondrial peptides with extraordinary sensitivity, which suggests these compounds being the prime activators of Fprs (Schiffmann *et al.*, 1975; Le *et al.*, 2001a; Tiffany *et al.*, 2001; Harada *et al.*, 2004; Rabiet *et al.*, 2005; He *et al.*, 2013). Therefore, I focused on these agonist families. A panel of 23 compounds that varied significantly in structure, sequence and length was tested (Figure 35B). It contained 12 different formylated mitochondrial peptides (three of human and nine of murine origin), seven formylated bacterial peptides, and four other typical peptide activators of FPRs. All compounds were first tested at 10 μ M to 30 μ M on the six receptors murine Fpr1, Fpr2, Fpr3 and human FPR1, FPR2, FPR3. The results show that Fpr1 and Fpr2 of mouse and human are capable of detecting a broad variety of structurally divergent peptides of mitochondrial or bacterial origin, while murine and human Fpr3 are far more selective.

Clear parallels between responses of distinct mouse and human receptor pairs were revealed (Figure 35A). Murine and human Fpr1 showed the most homogeneous activation pattern. Both receptors were strongly activated by all 23 test compounds and their response

amplitudes were always similar to those of W-peptide. Murine and human Fpr2 also displayed related responses. Both receptors were activated by 22 of the 23 substances. In contrast to the homogeneous signal amplitudes of Fpr1 the responses of Fpr2 to a few compounds were clearly diminished. This effect was most pronounced for mATP6 and mND4L. For human FPR2 the signals to mATP6 and mND4L were reduced by 79% and 81%, respectively. Murine Fpr2 showed a similar reduction to mND4L and no signal to mATP6. In addition, mouse Fpr2 also showed responses that were more than 60% reduced to mCytb, mND6, mND5, mND3, mND2, and hND4 which were not visible for human FPR2.

Interestingly, clear similarities between murine and human Fpr3 were also observable. Both receptors showed a specific response pattern that was clearly distinguishable from that of Fpr1 and Fpr2 of both species. Both receptors responded to a far smaller set of compounds than their family members. Human FPR3 was only activated by 14 of the 23 tested substances – *Staphylococcus*-SP22, *Staphylococcus*-SP22-FuLe, *Salmonella*-SP24, *Psychromonas*-SP6, *Hydrogenobacter*-SP16, hND6, D-M-peptide, W-peptide, f-MIVILY, mND2, mND4, mND4L, mCOIII, and Ac2-26. Murine Fpr3 was even only activated by nine substances – *Staphylococcus*-SP22, *Staphylococcus*-SP22-FuLe, *Salmonella*-SP24, *Psychromonas*-SP6, *Hydrogenobacter*-SP16, hND6, M-peptide, W-peptide and f-MIVILY. The observation that human FPR3 was only activated by 14 compounds and murine Fpr3 even responded to only nine test substances argues for a higher selectivity of both receptors than that of Fpr1 and Fpr2. It is to mention that all activators of murine Fpr3 were also activators of human FPR3 what results in an overlap of the receptors' ligand spectra by at least 64%. The fact that all mouse Fpr3 agonists overlapped to 100% with those of human FPR3 strongly support the hypothesis that murine and human Fpr3 fulfill similar roles in the immune systems of mouse and human. However, the fact that human FPR3 is activated by five additional test compounds (Ac2-26, mND2, mND4, mND4L, and mCOIII) illustrates species-specific adaptations in the sensitivity and selectivity of both receptors.

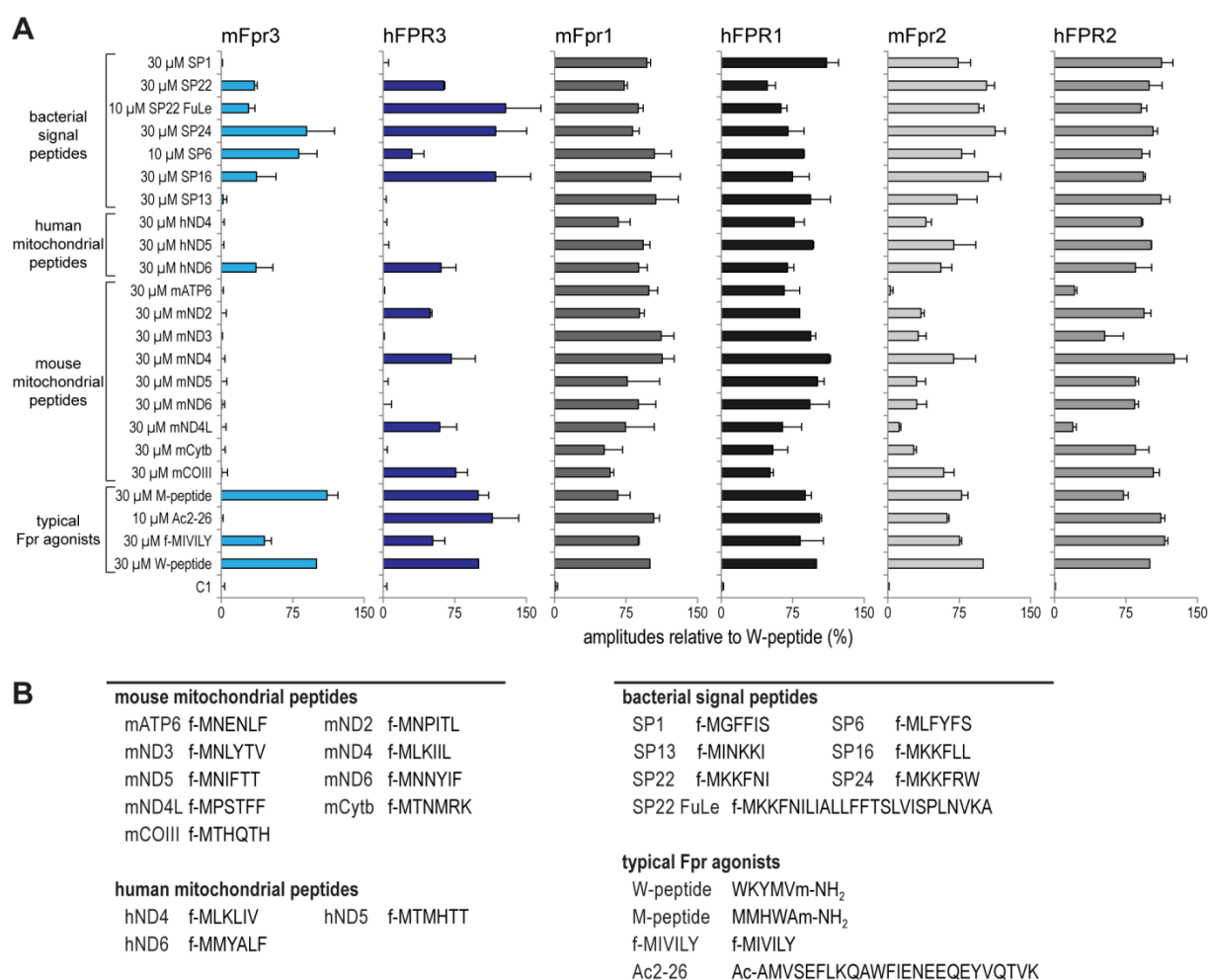


Figure 35. Mouse and human Fpr3 display similar agonist selectivity. **A**, Comparison of the calcium responses of HEK293T cells transfected with either Fpr1, Fpr2, or Fpr3 of mouse or human to high agonist concentrations. All compounds were applied at 10 μ M to 30 μ M. Buffer application was used as negative control to render mechanical stimulation visible. To account for receptor specific variations in the maximal obtainable signal amplitude each response was normalized to the response to 30 μ M W-peptide, a pan agonist for murine and human Fpr1, Fpr2 and Fpr3. Bars denote mean signals from three to eight independent experiments, carried out as duplicates. *Error bars*, S.D. **B**, the stimulus selection comprises six bacterial signal peptides, three human (h) and ten mouse (m) mitochondrial peptides, and four other typical FPR activators that strongly differ in their structure, sequence, and length. hFPR = human Fpr; mFpr = murine Fpr.

3.4.4 Specification of Fpr3 Function in Mouse and Human

To assess the amount of species-specific alterations in more detail, I next compared the concentration responses of both receptors to four common activators: the human mitochondrial peptide hND6, the bacterial signal peptide *Psychromonas*-SP6 and to the D- and L-stereoisomers of the synthetic M-peptide (Figure 36). The responses of murine and human Fpr3 to hND6 and L-M-peptide were quite similar, whereas the receptors displayed clear differences in the responses to D-M-peptide and *Psychromonas*-SP6. The EC₅₀ of Fpr3 for D-M-peptide and *Psychromonas*-SP6 were 933 ± 432 nM and 347 ± 49 nM, respectively. Human FPR3 showed an EC₅₀ value of more than 10,000 nM for both substances. Thus,

murine Fpr3 is at least 10-fold more sensitive for D-M-peptide and even 28-fold more sensitive for *Psychromonas*-SP6. I also noticed that the maximal signal amplitude of murine Fpr3 to L-M-peptide and hND6 were approximately 50% smaller than those to D-M-peptide and *Psychromonas*-SP6, although the receptor signals clearly reached saturation for all four compounds. This provided the possibility for partial activation of murine Fpr3 through both compounds.

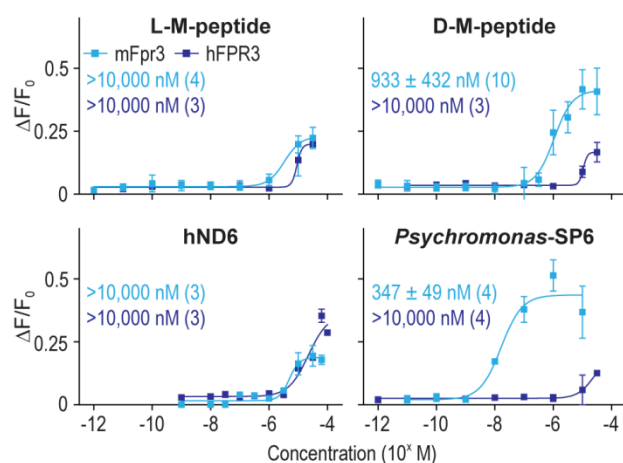


Figure 36. Mouse and human Fpr3 differ in their agonist sensitivity. Concentration-responses of murine and human Fpr3 upon activation by four structurally divergent peptides reveal a differential sensitivity. Number of experiments (*n*) is indicated in parentheses. hFPR = human Fpr; mFpr = murine Fpr. Error bars, S.D.

To examine whether this was true or if the differences in the signal amplitude were caused by non-saturated responses, I next compared the signal amplitudes to selected agonists at 30 μ M and 60 μ M concentrations (Figure 37). If the responses were not in saturation one would expect an increase of the signal amplitude at the higher concentration. In case that the compounds were partial agonists, higher concentrations should not have altered the signal size. For these tests four common activators of Fpr3 of both species (hND6, *Staphylococcus*-SP22, *Psychromonas*-SP6, and *Hydrogenobacter*-SP16), two peptides that were selective activators of human FPR3 (mND2 and mND4L), and two controls that did not activate murine or human Fpr3 (mATP6 and *Clostridium*-SP13) were chosen based on the results obtained in previous experiments (Figure 34). No significant differences in the signal amplitudes of murine and human Fpr3 to 30 μ M and 60 μ M stimulus concentrations were observed. hND6, *Staphylococcus*-SP22, *Psychromonas*-SP6, and *Hydrogenobacter*-SP16 activated murine Fpr3 at both concentrations but showed no increase in signal size (Figure 37). Responses of human FPR3 to hND6, mND2, mND4L, *Psychromonas*-SP6, *Hydrogenobacter*-SP16, and *Staphylococcus*-SP22 also induced no significant alterations. Additionally, all tested compounds that did not activate one of the receptors at 30 μ M also

evoked no responses at 60 μM . This demonstrates that the receptor responses were in saturation at 30 μM .

Next, I obtained clear evidence for partial agonists of murine Fpr3. Although the results indicate sufficient concentrations to monitor the maximal signal amplitude, some of the signals were much smaller than those obtained for W-peptide. For murine Fpr3 only the signal size of *Psychromonas*-SP6 was comparable to that of W-peptide. The signal amplitudes of hND6, *Hydrogenobacter*-SP16, and *Staphylococcus*-SP22 were reduced by 74%, 65%, and 61% respectively, providing clear evidence that these three stimuli are indeed partial agonists of murine Fpr3. By contrast, nearly all of the identified agonists for human FPR3 were full activators. The signals of this receptor to hND6, mND2, mND4L, *Hydrogenobacter*-SP16, and *Staphylococcus*-SP22 were similar to those obtained with W-peptide (Figure 37). Only the response to *Psychromonas*-SP6 was reduced by 79%. Thus, it seemed that Fpr3 was more selective in terms of signal amplitude.

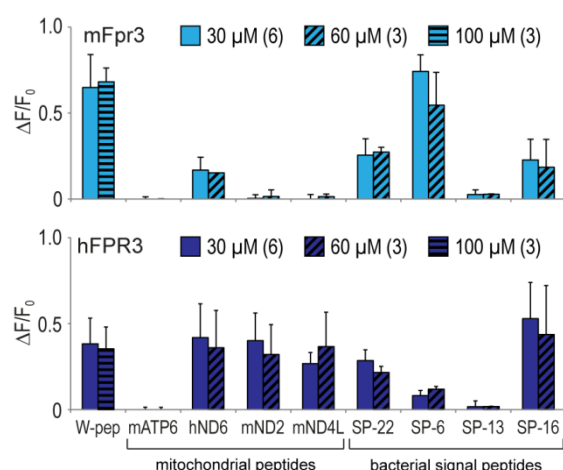


Figure 37. **Calcium responses of murine and human Fpr3 saturate at 30 μM ligand concentration.** Calcium responses of cells transfected with murine (light blue, upper panel) or human (dark blue, lower panel) Fpr3 upon stimulation with 30 μM (filled bars) and 60 μM (shaded bars) of the indicated Fpr3 agonist. All eight activators showed no significant differences between both concentrations, demonstrating that signal saturation was reached at 30 μM . Bars denote mean signal amplitudes from three independent experiments, carried out as duplicates. Number of experiments (n) is indicated in parentheses. hFPR = human Fpr; mFpr = murine Fpr. Error bars, S.D.

3.4.5 Ligand Preferences of Murine and Human Fpr3 Differ Partially

To assess to what extent variations in the ligand structure affect the responses of murine and human Fpr3, I next tested both receptors with a number of closely related chemical derivatives of the same agonist. Bernd Bufe and colleagues recently reported varying importance of individual amino acid residues of W-peptide for the interaction with murine Fpr3 (Bufe *et al.*, 2012) and human FPR3 (Bufe *et al.*, 2015). W-peptide is a common activator of mouse and human Fpr3 that robustly activates both receptors (Figure 34). Thus, I reasoned that structural derivatives of W-peptide may be well-suited to reveal differences in the agonist preferences.

Previous studies already demonstrated the exclusive importance of the amidated methionine at the C-terminus of W-peptide and the three following residues for the interaction between W-peptide and the receptor (Bufe *et al.*, 2012, Bufo *et al.*, 2015). Therefore, I focused on systematic tests of these four residues with a panel of 24 test compounds (Figure 38). In each peptide an individual amino acid of W-peptide was replaced by a non-polar, polar, aromatic or charged substitution. My results showed that alterations of the C-terminal D-methionine (m) affected the responses of murine and human Fpr3 in a similar manner (Figure 38). At this position, charged or polar residues, such as glutamate (e), lysine (k) or glutamine (q) totally abolished the responses of both receptors. Replacement by hydrophobic residues, such as alanine (a), cysteine (c), isoleucine (i), and ornithine (o) or amino acids in L-conformation led to drastically reduced signals. Only the substitution of D-methionine by homocysteine (hcy) or isoleucine (i) were relatively well-tolerated. Thus, the methionine was of equal importance for the ligand recognition of both receptors. Alterations at the second last residue showed little effects on the receptor responses (Figure 38), suggesting low importance for the interaction between W-peptide and the receptors at this position. Replacement of the third last residue by other amino acids was well-tolerated by murine Fpr3, whereas all responses of human FPR3 were diminished. The substitution of the hydrophobic methionine (M) by charged glutamate (E) led to the strongest difference. It totally abolished the response of human FPR3, whereas the response of murine Fpr3 was only diminished by 43% (Figure 38). The most pronounced differences between murine Fpr3 and human FPR3 were seen for substitutions at the fourth last position (Figure 38). Interestingly most replacements of this residue by another amino acid were well-tolerated by murine Fpr3. In sharp contrast, nearly all substitutions totally abolished the response of human FPR3. This receptor tolerated only the relatively conserved exchange of tryptophan (W) by phenylalanine (F), both of which are aromatic amino acids. However, even in this case a marked reduction in the signal amplitude was recognized. This indicates differences in the response of murine and human Fpr3 to agonists are primarily that are caused by variable preference of both receptors of the fourth residue after the chemical modification. Furthermore, both receptors show comparable signal amplitudes to the majority of the W-peptide derivatives. In summary, the test with W-peptide derivatives revealed definite similarities in the structural preferences of murine and human Fpr3.

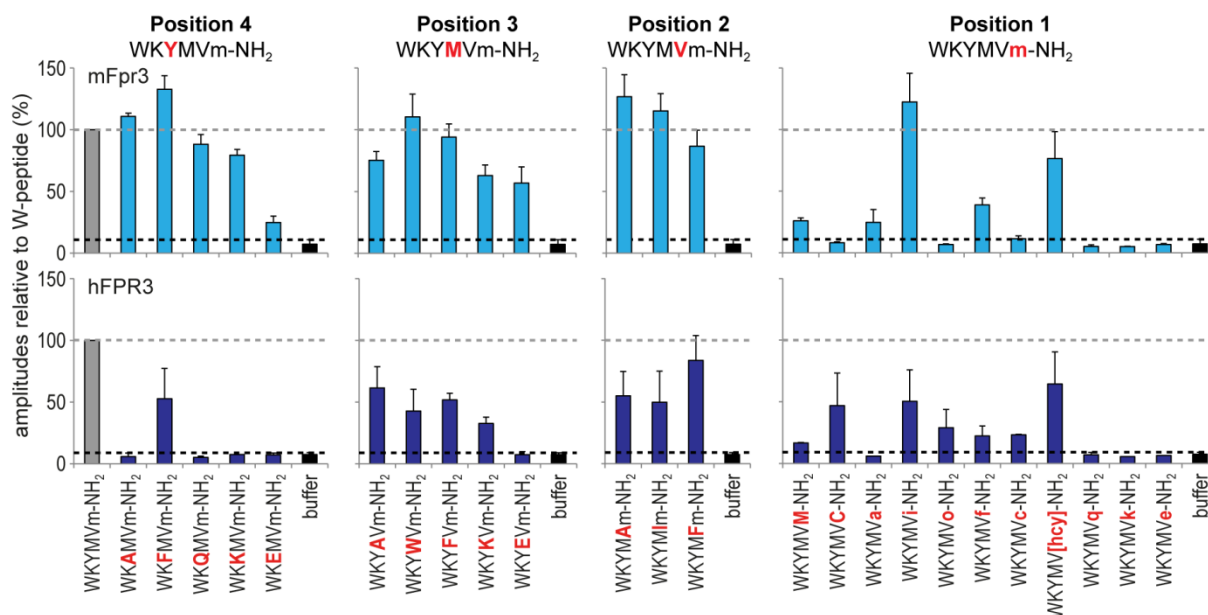


Figure 38. **The ligand recognition of murine and human Fpr3 partially differs.** Calcium responses of HEK293T cells transiently transfected with either Fpr3 of mouse (light blue, upper panel) or human (dark blue, lower panel) to W-peptide derivatives (10 μ M) with systematically exchanged amino acid residues at position 1, 2, 3, and 4 (counted from the amidated C-terminus). Buffer application (black bar and dotted line) was used as negative control. To account for receptor specific variations in the maximal obtainable signal amplitude the responses were normalized to 30 μ M W-peptide (gray bar and dotted line). Bars denote signal amplitudes of responding cells from four independent experiments. The lead structure of W-peptide is shown in black letters. Modifications in the peptide structure are labeled in red. Peptide sequences are shown in one-letter amino acid code. L-isomers are given in capital letters, whereas D-isomers are displayed in lowercase letters. -NH₂ = amidated C-terminus. hFPR = human Fpr; mFpr = murine Fpr. *Error bars*, S.D.

4 DISCUSSION

This thesis provides new insight into the expression and function of murine Fpr3 in the vomeronasal and immune systems and reports the existence of natural knockout strains for this receptor.

Two murine *Fpr3* variants, *Fpr3_{wt}* and *Fpr3 Δ ₄₂₄₋₄₃₅*, which differed by 12 nucleotides were discovered during this study. *Fpr3_{wt}* constituted the annotated receptor, whereas *Fpr3 Δ ₄₂₄₋₄₃₅* encoded an *in-frame* deletion from nucleotides 424–435. Immunocytochemistry revealed that the deletion left the open reading frame intact, but the mouse strains encoding *Fpr3 Δ ₄₂₄₋₄₃₅* did not express the Fpr3 protein. *In vitro* calcium imaging and immunofluorescence analyses demonstrated that the lack of four amino acids lead to an unstable, truncated, and non-functional receptor protein. Moreover, comprehensive genotyping analyses and a database search revealed at least 13 mouse strains expressing *Fpr3_{wt}* and at least 19 other strains encoding *Fpr3 Δ ₄₂₄₋₄₃₅*; thus establishing various natural *Fpr3* knockout mouse strains. Sequencing and genomic haplotype analyses attributed the origin of *Fpr3 Δ ₄₂₄₋₄₃₅* to the subspecies *Mus musculus domesticus*. The discovery of a multitude of natural *Fpr3* knockout mouse strains will be valuable to study murine Fpr3 function in the context of various genetic backgrounds.

Murine Fpr3 showed significant sequence overlap with human FPR3. Both receptors have been reported to detect bacterial peptides. Thus, they are assumed to fulfill related biological roles. However, the two receptors differed in their expression patterns, which challenge the concept of congruent function. The function and receptor expression of murine and human Fpr3 were examined in the vomeronasal organ and immune system to better understand their roles. *In vitro* calcium imaging experiments showed that the functional properties of the receptors were similar. Ligand screening revealed overlapping agonist response patterns in which the agonists were mainly of bacterial origin. Two anti-Fpr3 antibodies were generated and validated to analyze the occurrence of the murine Fpr3 protein and examine receptor expression. Immunocytochemistry combined with RT-PCR and *in situ* hybridization revealed murine Fpr3 expression in a subset of vomeronasal sensory neurons, mature neutrophil granulocytes, and bone marrow cells, whereas RT-PCR demonstrated the presence of human *FPR3* RNA in neutrophil granulocytes. Moreover, expression of the murine Fpr3 protein was upregulated in immune cells upon stimulation with a bacterial endotoxin (lipopolysaccharide). Taken together, my results provide clear evidence for a common biological function of murine and human Fpr3 and support their role as bacterial sensors in immune defense.

4.1 Fpr3 of Mouse and Human are Functional Orthologs

Identification of human orthologs in model organisms, such as the house mouse *mus musculus*, is of paramount importance for insight into human biology (Dolan *et al.*, 2015). Orthologs are genes in different species that evolved from a common ancestral gene by speciation (Fitch, 1970; Fitch, 2000; Fang *et al.*, 2010). Such genes can be identified by two criteria – a high sequence homology and the same biological function (Tatusov *et al.*, 1997; Fang *et al.*, 2010). I compared the sequence and function of murine and human *Fpr3*, to investigate to what degree both receptors fit these criteria.

4.1.1 Genetic Evidence for the Orthology between Fpr3 of Mouse and Human

Isabelle Migeotte and colleagues recently reported a shared gene locus with conserved synteny in the genomic arrangement for *Fpr3* of both species, as described earlier (see chapter 1.3.4) (Migeotte *et al.*, 2006). They illustrated that murine and human *Fpr3* are located on chromosomal regions 17A3.2 and 19q13.3, respectively, where they are both the third protein coding gene within the *Fpr* gene cluster. However, due to the *Fpr* gene cluster expansion in rodents (Figure 5C), flanking regions of murine *Fpr3* that comprise the pseudogenes $\psi Fpr-rs2$ (*Fpr-rs8*) and $\psi Fpr-rs3$ (*Fpr-rs5*) challenge the syntenic arrangement of murine and human *Fpr3* (Gao *et al.*, 1998; Wang and Ye, 2002). It is conceivable that all three of these genes evolved parallel to the human *FPR3* gene. However, the nucleotide sequences of $\psi Fpr-rs2$ and $\psi Fpr-rs3$ are both more homologous to *Fpr2* than to *Fpr3* (Gao *et al.*, 1998; Tiffany *et al.*, 2011) which suggests evolution alongside this receptor. Furthermore, the two pseudogenes include premature stop codons (Migeotte *et al.*, 2006) and thus do not have open reading frames. Hence, the *Fpr3* gene encodes the only intact GPCR of these three genes. These observations consider *Fpr3* to be the only mouse receptor qualified as ortholog of human *FPR3*.

To examine this hypothesis, I compared the amino acid sequences of murine and human *Fpr3*, and aligned them with those of *Fpr1* and *Fpr2* of both species (Figure 33A, B). Surprisingly, by sharing 82% similarity, mouse *Fpr3* rather resembled human *FPR2* than human *FPR3* that was 74% similar with murine *Fpr3*. This finding is consistent with other studies (Takano *et al.*, 1997; Gao *et al.*, 1998; Rabiet *et al.*, 2011) and challenges orthology between murine and human *Fpr3*.

In line with these observations, meta-analyses comprised of 12 orthology prediction tools listed orthology for murine and human *Fpr3* in only three of these tools (Figure 33C), underpinning the notion that their orthology is unclear. However, a recent study that examined

the adaptive evolution of *Fprs* in mammals reported that *Fpr3* evolved under completely different conditions than *Fpr1* and *Fpr2* (Muto *et al.*, 2015). With examinations of site- and lineage-specific selection patterns, combined with 3D homology modeling analyses, the authors indicated strong positive selection for the *Fpr1* and *Fpr2* genes during evolution. By contrast, selective pressure in the *Fpr3* lineage was more relaxed (Muto *et al.*, 2015). This argues for common evolution of murine and human *Fpr3* and provides a possible explanation for their orthology despite not sharing the highest sequence similarity amongst *Fprs*.

4.1.2 Fpr3 of Mouse and Human Share Functional Similarities

The same biological role is a criterion for orthology (Remm *et al.*, 2001; Fang *et al.*, 2010), as mentioned before (see chapter 0). Thus, I compared the function of murine and human Fpr3. Examining the biological role of Fpr3 has been difficult in the past due to the lack of identified activators. Recent studies identified several synthetic, bacterial, and endogenous host peptides as activators of mouse and human Fpr3 (Harada *et al.*, 2004; Ernst *et al.*, 2004; Migeotte *et al.*, 2005; Bufe *et al.*, 2012, Bufe *et al.*, 2015). This enabled me to assess functional orthology between murine and human Fpr3.

In heterologous calcium imaging experiments both receptors responded to overlapping subsets of Fpr agonists from different origins. Murine and human Fpr3 responded to nine common ligands, thus overlapping by at least 64% (Figure 35). This is consistent with a study that compared the receptors' responses to 21 bacterial signal peptide fragments (Bufe *et al.*, 2015) and provides first evidence for a similar function of both receptors.

Five of the nine shared ligands for murine and human Fpr3 were bacterial signal peptides. By contrast, endogenous host stimuli, such as mitochondrial peptides, were no prominent agonists of murine and human Fpr3. Both receptors responded to only one of three human mitochondrial peptides. Murine Fpr3 even lacked activation through any tested mitochondrial peptide of the mouse. This finding is consistent with reports that described detection of bacterial peptides by murine and human Fpr3 (Betten *et al.*, 2001; de Paulis *et al.*, 2004; Bufe *et al.*, 2015). These data suggest prime roles for murine and human Fpr3 in bacterial detection, while they are less important in endogenous host stimuli detection.

Response characteristics of Fpr3 differed drastically from those of Fpr1 and Fpr2 which are promiscuous receptors (Migeotte *et al.*, 2006; Fu *et al.*, 2006). In my screening, these receptors responded to nearly all of the 23 tested ligands (Figure 35). By contrast, Fpr3 of both species detected only a small sub-fraction of the tested ligands. Thus, Fpr3 was much more narrowly tuned than the other *Fpr* family members. Concentration-response curves

revealed also differing sensitivity and maximal signal amplitudes for Fpr3 towards Fpr1 and Fpr2 (Figure 34). To all tested substances – W-peptide, M-peptide, the bacterial signal peptide *Psychromonas*-SP6, and the mitochondrial peptide hND6 – Fpr3 exhibited ~3-fold to ~30-fold lower sensitivity than Fpr1 and Fpr2 of both species. Additionally, signal amplitudes of Fpr3 reached only ~20% to ~50% of those of Fpr1 and Fpr2. Drastically lower sensitivity of Fpr3 to bacterial signal peptides has been described before (Bufe *et al.*, 2015). While Fpr1 and Fpr2 were activated by many substances in the nanomolar range, Fpr3 was activated only in the micromolar range. A more specialized ligand spectrum argues for a specific niche of Fpr3 within the murine and human *Fpr* families. This could characterize Fpr3 as a receptor providing information about high concentrations of external stimuli.

A speculated function of Fpr3 in the literature is that of a decoy receptor. These receptors bind ligands to inhibit binding to their destined receptor. Thereby, they exhibit minimal plasma membrane expression but undergo rapid constitutive recycling to bind extracellular ligands and internalize them for degradation. In this process they do not transduce signals (Rabiet *et al.*, 2011). Several recent studies support the idea of Fpr3 being a decoy receptor, based on a relative insensitivity to common Fpr2 ligands and high basal levels of receptor phosphorylation and internalization (Migeotte *et al.*, 2005; Rabiet *et al.*, 2011; He *et al.*, 2013; Dorward *et al.*, 2015). These reports suggest regulation of the function of other formylated peptide receptors through Fpr3. However, Fpr3 showed sensitivity in the micromolar range to most tested ligands that is at least 1,000-fold lower than sensitivities of Fpr1 and Fpr2 in the nanomolar range (Figure 34). With such inferior sensitivity, Fpr3 could not hinder ligands from binding to Fpr1 or Fpr2. Thus, my data argue against decoy activity mediated by Fpr3.

4.1.3 Adaptations of Murine Fpr3 for a Function in Olfaction

Murine Fpr3 was initially discovered in the VNO (Liberles *et al.*, 2009; Rivière *et al.*, 2009), whereas no evidence exists for human FPR3 expression in the olfactory system (Liman and Innan, 2003; Zhang and Webb, 2003). Thus, it is likely that, despite functional orthology between murine and human Fpr3, murine Fpr3 developed specific adaptations to requirements in olfaction. To examine this, I compared the function of murine and human Fpr3 in more detail. Indeed, concentration-response curves supported the hypothesis of functional adaptations by revealing sensitivity differences between murine and human Fpr3 to two of four tested ligands (Figure 36). Thus, although both receptors detected the same ligands, they showed partial differing ligand tunings.

Investigations on responses of both receptors to single amino acid variations in W-peptide – a potent common ligand – were made to assess the degree of these subtle functional differences. Screening of 24 W-peptide derivatives (see chapter 2.1.1) revealed differing response patterns for murine and human Fpr3 (see chapter 3.4.5). Residue exchanges at the fourth last position of W-peptide showed the most distinct difference in the responses of the two receptors. The other three exchanged amino acid positions showed no or only minor differences between receptor responses (Figure 38). This finding indicates a possible adaptation of murine Fpr3 to a function in the VNO. However, it also shows that the functional differences between murine and human Fpr3 are very subtle. It is conceivable that these slight tuning differences indicate a trend in the evolution of both receptors that will become more pronounced in the future. Thus, murine Fpr3 function might adapt to requirements in olfaction, whereas human FPR3 might become more specialized for its function in the immune system.

4.2 Murine Fpr3 is Expressed in Multiple Tissues

Controversial reports about the expression pattern of murine Fpr3 exist, as described earlier (see chapter 1.3.3) (Gao *et al.*, 1998; Lee *et al.*, 2004; Southgate *et al.*, 2008; Rivière *et al.*, 2009; Chiu *et al.*, 2013). To clarify if murine Fpr3 is expressed in immune cells, I examined the occurrence of receptor protein in different organs with immunocytochemistry techniques. To this end I generated and characterized two Fpr3-specific antibodies, ECL1 and ECL2 (see chapter 3.1).

4.2.1 Fpr3 Protein is Expressed in the Vomeronasal Organ

Specificity of an antibody is a general issue in immunocytochemistry. Thus, a number of methods were used to assure the quality of the newly generated antibodies. Epitope mapping (Figure 13) and heterologous immunocytochemistry experiments, in which murine Fpr3 was stained exclusively (Figure 14), provided substantial *in vitro* evidence for the specificity of both antibodies. Subsequent comparative tests identified ECL2 as the more sensitive antibody that also produced slightly less background (Figure 15). Thus, this antibody was primarily used for further experiments in native cells. The VNO provided perfect testing conditions to assess the quality of the antibody, because of consistent reports on *Fpr3* expression in the literature (Liberles *et al.*, 2009; Rivière *et al.*, 2009) and a challenging amount of target cells (0.3% to 0.7%) (Rivière *et al.*, 2009; Stempel *et al.*, 2016). In agreement with previous reports

(Liberles *et al.*, 2009; Rivière *et al.*, 2009), Fpr3 was detected in a small subpopulation of ~0.3% VSNs with immunocytochemistry, RT-PCR, and *in situ* hybridization techniques (Figures 16, 17). This amount of cells is consistent with a study that recognized *Fpr3* mRNA in 0.7% of the cells in VNO slices (Rivière *et al.*, 2009). Verification of staining specificity was realized by successfully blocking the epitope specific binding site with the peptide that was used for antibody generation (Figure 17). These results confirmed the high quality of my used antibody for immunocytochemistry experiments in native cells.

Next, the molecular characteristics of the cells expressing Fpr3 protein in the VNO were examined (Figure 18). The studies that discovered *Fpr3* in the VNO reported coexpression of the receptor in VSNs with $G\alpha_o$ and a lack of coexpression with $G\alpha_{i2}$ (Liberles *et al.*, 2009; Rivière *et al.*, 2009), markers for VSNs of the basal and the apical expression zone, respectively (Halpern *et al.*, 1995; Berghard and Buck, 1996; Herrada and Dulac, 1997; Matsunami and Buck, 1997). Furthermore, tests using a pan *V2ra* *in situ* probe detecting 17 of the altogether 122 type 2 vomeronasal receptors indicated a lack of *Vmn2r* expression in *Fpr3*-positive VSNs (Liberles *et al.*, 2009). My findings, using colabeling immunocytochemistry techniques were fully consistent with these reports (Liberles *et al.*, 2009; Rivière *et al.*, 2009). The majority of Fpr3-positive cells colocalized with $G\alpha_o$. Furthermore, neither significant coexpression of Fpr3 with Phosphodiesterase 4A (PDE4A), which labels $G\alpha_{i2}$ -positive VSNs (Lau and Cherry, 2000; Leinders-Zufall *et al.*, 2004), nor with type 2 vomeronasal receptors, were detected. These results confirmed the previous findings which showed that Fpr3 in the VNO is exclusively expressed in VSNs of the basal expression zone and does not coexpress with type 2 vomeronasal receptors on the protein level (Liberles *et al.*, 2009; Rivière *et al.*, 2009). Fpr3 was also colabeled with OMP, which is expressed in all mature VSNs, to examine if the dissociated cells expressing Fpr3 were VSNs (Margolis, 1982). Indeed, ~60% of the Fpr3-expressing cells in the dissociated cell preparation coexpressed Fpr3 with OMP (Figure 18) and thus were identified as VSNs. Surprisingly, another ~40% of the Fpr3-positive cells lacked colocalization with any VSN-specific marker and thus provide clear evidence for the existence of a second Fpr3-expressing cell type in my dissociated cell preparation.

Colocalization immunocytochemistry experiments with different immune cell markers were performed to examine the second cell type in my preparation (Figure 19). The lymphocyte antigen 6G (Ly6G) is only present in neutrophil granulocytes (Fleming *et al.*, 1993; Lai *et al.*, 1998), whereas the cluster of differentiation molecule (CD45R) can be found in all other immune cells (Ballas and Rasmussen, 1993; Rolink *et al.*, 1996; Lai *et al.*, 1998).

Colabeling ECL2 with Ly6G identified these cells as neutrophil granulocytes. Consistent with this finding, colabeling with CD45R was negative (Figure 19). Ly6G expression and the lack of CD45R expression argue that these cells were neutrophil granulocytes. Neutrophils are leukocytes that are released from the bone marrow into the peripheral blood after maturation (Bekkering and Torensma, 2013). Thus, they were likely introduced into my preparation through blood contamination.

4.2.2 Fpr3 Protein is Expressed in Immune Cells

Careful examination of Fpr3 expression in cells that were directly isolated from blood was performed to confirm the receptor's occurrence in murine leukocytes. With both newly generated Fpr3 antibodies, ECL1 and ECL2, Fpr3 expression in a subpopulation of ~13% of the nucleated cells was detected (Figure 20). This amount of cells correlates well with the reported strain-dependent neutrophil granulocyte count of ~9% to ~18% in mouse blood (Gowen and Calhoun, 1943). Additional investigation on nucleus morphology of stained cells substantiated the evidence for Fpr3 expression in neutrophil granulocytes. Nuclei of Fpr3-expressing cells all had a structure including nuclear lobes and connecting segments, the typical shape of nuclei of mature neutrophil granulocytes (Campbell *et al.*, 1995; Sanchez and Wangh, 1999; Carvalho *et al.*, 2015); whereas all non-stained cells had other nucleus shapes (Figure 39). Fpr3 protein expression in neutrophil granulocytes was confirmed by subsequent colabeling of the receptor with the neutrophil marker Ly6G. *Fpr3* expression in leukocytes was also proven on the RNA level with RT-PCR experiments (Figure 23). Interestingly, Fpr3 protein production increased after LPS exposure (Figure 25). Taken together, these results clearly demonstrate the presence of murine Fpr3 in neutrophil granulocytes.

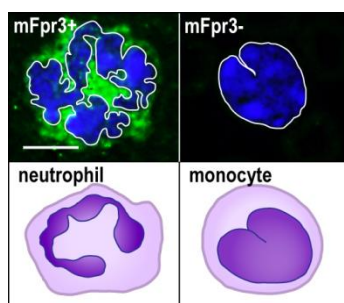


Figure 39. Fpr3-positive leukocytes contain polymorphonuclear nuclei. Comparison of nuclear morphologies for Fpr3 positive and negative leukocytes. Fpr3 was stained with the antibody ECL1 (green), for nuclear staining Hoechst33342 (blue) was used. Fpr3-positive cell (upper left) showing a clearly multi-lobed nucleus, typical for neutrophil granulocytes (lower left). Fpr3-negative cell (upper right) showing a horseshoe-shaped nucleus, typical for monocytes (lower right). mFpr = murine Fpr. Scale bar, 5 μ m.

Fpr3 expression in leukocytes has been discussed controversially in the past. One early report detected low amounts of *Fpr3* RNA in murine leukocytes (Gao *et al.*, 1998). However, several subsequent studies failed to confirm this result despite the use of sensitive techniques,

such as RT-PCR (Lee *et al.*, 2004; Southgate *et al.*, 2008; Rivière *et al.*, 2009; Chiu *et al.*, 2013). Detection of RNA from neutrophil granulocytes is much more difficult than from other leukocytes because RNA amounts in neutrophil granulocytes are 10-fold to 20-fold lower than in other leukocytes, such as monocytes (Cassatella, 1999). Consistent with the majority of reports, my attempts failed to detect *Fpr3* from neutrophil granulocyte RNA without LPS stimulation (Figure 22). In immune cells expression of selected genes is elevated after contact with a pathogen (Guha and Mackman, 2001; Heumann and Roger, 2002). One important pathogen factor for this is LPS (Cui *et al.*, 2002; Iribarren *et al.*, 2003). In neutrophil granulocytes, LPS-induced expression for *Fpr1* has been observed earlier (Mandal *et al.*, 2005). Thus, it is conceivable that *Fpr3* is also upregulated after LPS stimulation in this cell type. Utilizing this RNA elevation mechanism, I could now establish *Fpr3* joining the ranks of upregulated genes upon LPS exposure in neutrophils (Figure 23). This finding resolves the controversy about *Fpr3* expression in mouse leukocytes and strongly supports the involvement of *Fpr3* in immune defense.

Of note, occurrence of murine and human *Fpr3* in the same type of immune cells would provide further evidence for a similar biological function of both receptors in the immune systems of mouse and human. However, current literature gives no evidence for a common expression of murine and human *Fpr3* in neutrophil granulocytes. RNA of human *FPR3* has been detected in monocytes using northern blot analysis (Durstin *et al.*, 1994) and in immature and mature dendritic cells via RT-PCR, immunocytochemistry, and internalization experiments (Yang *et al.*, 2002; Migeotte *et al.*, 2005). However, expression of human *FPR3* in neutrophil granulocytes is poorly examined. To clarify *FPR3* expression in human neutrophil granulocytes, I isolated neutrophils from peripheral blood, stimulated the cells with LPS, and extracted their total RNA. RT-PCR showed a band for human *FPR3* with specific primers besides the already well-examined *FPR1* and *FPR2* (Figure 24). Consecutive sequencing confirmed the amplification products as human *FPR1*, *FPR2*, and *FPR3*. This pilot study shows that human *FPR3* is likely expressed in human neutrophils.

4.3 Strain-Specific *Fpr3* Variants

During the course of my studies, I made a puzzling observation: *Fpr3* protein was not detectable by immunocytochemistry in dissociated VNO cells or immune cells of 129X1/Sv, BALB/cJ, and FVB/N mice but in C57Bl/6NCrl and NZB/Ola mice (Figure 26). However, the presence of *Fpr3* mRNA in those cell types of all tested mouse strains was clearly proven

(see chapter 3.3.1). Subsequent genotyping of the *Fpr3* gene from Fpr3-positive and -negative strains revealed a clear correlation between antibody staining patterns and the presence or absence of a 12 nucleotide *in-frame* deletion in *Fpr3* (Figure 27).

4.3.1 Two Functionally Distinct Fpr3 Variants Exist in Mice

The deletion results in a loss of four amino acids in the second intracellular loop. The Fpr3 variant comprising the deletion was called *Fpr3* $\Delta_{424-435}$, the variant without the deletion, *Fpr3*_{wt}. *Fpr3*_{wt} and *Fpr3* $\Delta_{424-435}$ were compared with calcium imaging to evaluate if the structural alteration in the Fpr3 variants would affect the receptor function (see chapter 3.3.2). The relatively small change of four amino acids at an intracellular site argues for modest effects on the receptor function. However, initial heterologous experiments in HEK cells revealed drastic functional differences between the two Fpr3 variants. *Fpr3* $\Delta_{424-435}$ transfected HEK cells responded to none of the applied potent Fpr3 activators, while those transfected with *Fpr3*_{wt} clearly responded to all of them (Figures 28, 29). These results provide clear evidence for a complete loss of receptor function for the *Fpr3* $\Delta_{424-435}$ variant. A lack of receptor function should have been also observable in mice, whereby mice carrying *Fpr3* $\Delta_{424-435}$ should have displayed a lack of function and mice expressing *Fpr3*_{wt} should have shown intact receptor function. To examine this hypothesis, the response of vomeronasal sensory neurons of C57Bl6/NCrl and 129X1/Sv mice was tested (Figure 32). When applying the bacterial signal peptide fragment *Salmonella*-SP24, a specific subset of sensory knobs from C57Bl6/NCrl mice that express *Fpr3*_{wt} were activated, while knobs from 129X1/Sv mice that carry *Fpr3* $\Delta_{424-435}$ showed no responses. These results are consistent with a lack of receptor function in animals expressing *Fpr3* $\Delta_{424-435}$ caused by lack of four amino acids. Thus I conclude that *Fpr3* $\Delta_{424-435}$ is a non-functional Fpr3 variant, whereas *Fpr3*_{wt} is a fully functional receptor variant. I further conclude that mice carrying *Fpr3* $\Delta_{424-435}$ lack Fpr3 function in general and thus provide functional knockout animals for *Fpr3*. Due to the lack of Fpr3 function, these mice likely suffer from impaired functions in the organs that express the receptor – the VNO and the immune system. However, the precise role of Fpr3 is not yet unraveled what makes it difficult to assess the kind of effect caused by the deletion. Moreover, my results demonstrate the detection of a pathogen-associated ligand by the VNO through Fpr3 arguing for an involvement of the intact receptor in vomeronasal pathogen-detection (see chapter 1.1).

4.3.2 Truncation of Fpr3 $\Delta_{424-435}$ Protein Causes a Lack of Receptor Function

Because of the relatively small change of four amino acids, I initially expected both Fpr3 variants, Fpr3_{wt} and Fpr3 $\Delta_{424-435}$, to be functional. However, although the open reading frame remained intact, Fpr3 $\Delta_{424-435}$ lacked complete receptor function. Surprisingly, mRNA expression for both receptor variants was clearly demonstrated (see chapter 3.3.1) but receptor protein was only detectable for Fpr3_{wt} (Figure 30). Thorough examination of Fpr3 $\Delta_{424-435}$ expression was performed to investigate the lack of receptor protein (see chapter 3.3.3).

Fpr3 $\Delta_{424-435}$ was not detectable in immunocytochemistry experiments using the newly generated antibodies, ECL1 and ECL2, in both HEK and dissociated VNO cells (Figures 26, 30). This argues that the 12 nucleotide *in-frame* deletion in Fpr3 $\Delta_{424-435}$ causes no or extremely diminished protein expression. An alternative explanation would be an altered protein structure that masks all antibody binding sites.

I generated a fusion-protein with an N-terminal Rho-tag and a C-terminal HSV-tag to evaluate if receptor protein was expressed at least partially (see chapter 2.3.11). Experiments with the resulting *Rho-Fpr3 $\Delta_{424-435}$ -HSV* construct revealed a clear but diminished staining for the Rho-tag antibody that bound N-terminally (Figure 31). Together with a lack of staining using the C-terminally binding HSV-tag antibody, the results indicate a truncated expression of Fpr3 $\Delta_{424-435}$ protein. The expressed protein included an N-terminus and discontinued somewhere before the C-terminus. I did not determine the exact extent to which the receptor was truncated but the lack of cellular staining with ECL1, which recognizes an epitope localized in front of the *in-frame* deletion (Figure 13), argues for a very short protein or severe misfolding of the resulting protein. The strongly reduced staining using the Rho-tag antibody argues for inefficient receptor synthesis or transport. Misfolded, damaged, and truncated proteins are prone to degradation via the ubiquitin-proteasome system (Goldberg, 2003; Bhattacharyya *et al.*, 2014). This quality control system rapidly eliminates those proteins, as demonstrated early by the degradation of abnormally folded globin (Goldberg and Dice, 1974; Etlinger and Goldberg, 1976; Klemes *et al.*, 1981; Sherman and Goldberg, 2001). Thus, reduced staining with the Rho-tag antibody is likely due to degradation of the truncated or misfolded receptor protein. However, the exact reason for the truncation and diminished protein amount has to be addressed in future experiments.

4.3.3 Distribution of the Fpr3 Variants Amongst Laboratory Mice

Genotyping combined with database analyses of the *Fpr3* nucleotide sequence in different mouse strains revealed an astonishing number of mouse lines carrying the non-functional

Fpr3 $\Delta_{424-435}$ variant. Thus far, I identified 19 different strains encoding the *Fpr3* $\Delta_{424-435}$ variant. The functional *Fpr3*_{wt} variant was present in 13 examined mouse strains. Surprisingly, the heredity transmission patterns of both receptor variants were inconsistent (Figure 40). The patterns show that *Fpr3*_{wt} and *Fpr3* $\Delta_{424-435}$ were present in numerous laboratory mouse lines that originated either in Europe, North America, or Asia. Data from genetic analyses (Figures 27, 40) implied multiple places of origin for the *Fpr3* $\Delta_{424-435}$ variant. This finding argues for an independent emergence of *Fpr3* $\Delta_{424-435}$ in several founder mice.

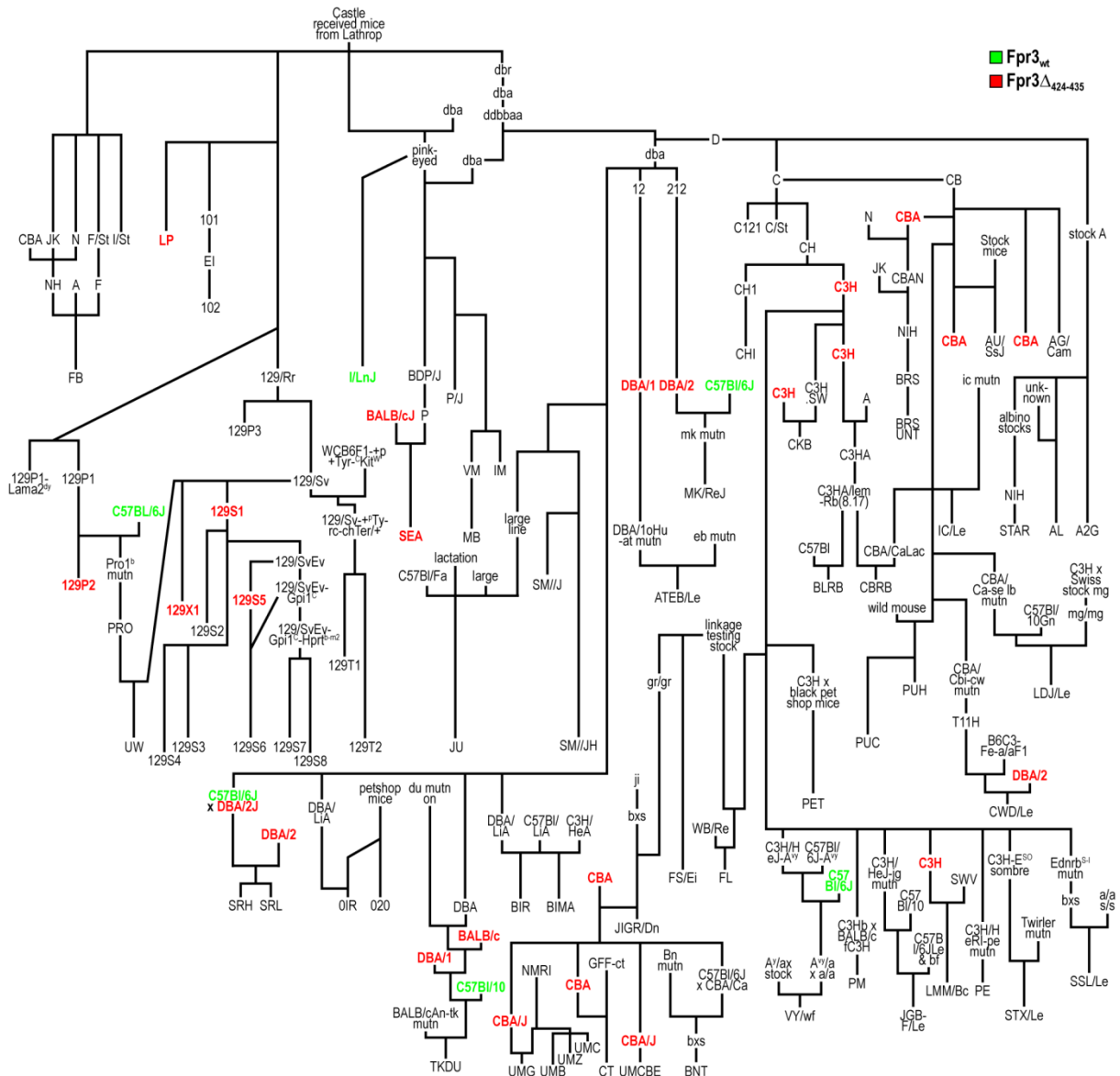


Figure 40. **Distribution of the *Fpr3* variants in the laboratory mouse genealogy using the example of Castle's mice.** Distribution of strains expressing *Fpr3*_{wt} (green) and *Fpr3* $\Delta_{424-435}$ (red) is inconsistent with any heredity transmission pattern. Strains of the same origin cluster, such as 129-related strains, seem to express the same variant. This argues for individual emergence of the *Fpr3* $\Delta_{424-435}$ variant and subsequent heredity. Strains not examined for their expressed variant are written in black letters. Figure after Beck *et al.*, 2000.

One possible explanation for the inconsistent appearance of *Fpr3* $\Delta_{424-435}$ is occasional breeding with mice carrying this receptor variant. Gene refreshing by crosses with maximum genetic diversity to the foundation stocks is often performed between laboratory and wild living mice of common genetic background to prevent genetic drift in mouse breeding (Beck *et al.*, 2000; Lambert, 2009). However, more laboratory strains expressing the non-functional *Fpr3* $\Delta_{424-435}$ variant rather than the functional *Fpr3*_{wt} variant were identified (Figure 27). Although the distribution of *Fpr3* $\Delta_{424-435}$ in the laboratory mouse genealogy is wide and scattered (Figure 40), cluster-like heredity was partly observed. For instance, all examined 129-related mice expressed *Fpr3* $\Delta_{424-435}$. This argues for individual emergence of the *Fpr3* $\Delta_{424-435}$ variant and subsequent heredity. In this scenario the non-functional variant may have provided evolutionary benefits under breeding conditions. The loss of Fpr3 receptor function could have led to a positive selection of mice encoding *Fpr3* $\Delta_{424-435}$ during the breeding process by a phenotype that was favorable under laboratory conditions.

Mice can distinguish between healthy and infected individuals and avoid company of infected conspecifics dependent on a functioning VNO (Boillat *et al.*, 2015). Laboratory mice may even stop breeding when in an unhealthy state (Lambert, 2009). My data from expression and functional experiments (see chapters 3.2 and 3.4) argue for the involvement of Fpr3 function in vomeronasal pathogen-detection. Thus, loss of Fpr3 function could have resulted in greater acceptance of non-suitable mating partners, food, bedding, and other breeding performance factors (see chapter 1.1). In line with this, several mouse strains, such as NFR/N mice, have become resistant to different types of stress, making them “high breeders” in most types of environmental conditions (Liljander *et al.*, 2006). For these strains it is not examined which variant of Fpr3 they encode. However, mouse strains expressing the functional *Fpr3*_{wt}, such as C57Bl-related mice, normally produce lower numbers of litters and are often denoted as “moderate breeders” (Liljander *et al.*, 2006). Mice experiencing less stress, *e. g.* through the lack of contact with sick conspecifics, produce more offspring. Thus, mice with an inhibited detection ability of stress factors through the lack of Fpr3 function could feature a better breeding phenotype in the laboratory breeding process. This argues for *Fpr3* being a gene critical for reproduction in mice alongside already identified genes, such as *Fecq1*, *Fecq2*, and *Ori* (Kirkpatrick *et al.*, 1998; Spearow and Barkley, 1999; Peripato *et al.*, 2002; Peripato *et al.*, 2004; Rocha *et al.*, 2004; Everett *et al.*, 2004).

4.3.4 *Fpr3* Variants Originated in Wild Living Mice

One possible reason for the high frequency of the non-functional *Fpr3* $\Delta_{424-435}$ variant in laboratory mice was a frequent occurrence of *Fpr3* $\Delta_{424-435}$ in many wild-type mice. Mice of the species *Mus musculus* are believed to have originated in the north of the Indian subcontinent. From there they spread throughout the world probably 0.5 million years ago (Yonekawa *et al.*, 1981; Boursot *et al.*, 1993). Different colonization paths led to different local subspecies, such as *Mus musculus castaneus* in Southeast Asia, *M. m. domesticus* in Western Europe and the Mediterranean basin, and *M. m. musculus* in Central Europe and North China (Boursot *et al.*, 1993). The genomes of most laboratory mouse strains comprise a mixed genetic background derived from these three subspecies (Beck *et al.*, 2000).

Hence, I examined several wild-derived mouse strains that represent one of the individual subspecies *M. m. castaneus*, *M. m. domesticus*, and *M. m. musculus*, respectively. Nearly all examined wild-derived mouse strains carried the *Fpr3*_{wt} gene (Figure 27). However, *Fpr3* $\Delta_{424-435}$ was present in three substrains of *M. m. domesticus* – LEWES/EiJ, WSB/EiJ, ZALENDE/EiJ – whereas two other substrains of *M. m. domesticus* – GER/DT, FRA/DT – carried the *Fpr3*_{wt} variant. This result provides first evidence that strains from the subspecies *M. m. domesticus* are the original source of *Fpr3* $\Delta_{424-435}$ in laboratory mouse strains.

The genomes of many laboratory strains derived of only a few ancestral wild living strains with limited haplotype diversity (Tucker *et al.*, 1992; Beck *et al.*, 2000; Yang *et al.*, 2011). In line with this, their genomes comprise mosaic patterns of different *mus musculus* subspecies (Bonhomme *et al.*, 1987). Thus it is still possible that the *Fpr3* $\Delta_{424-435}$ gene emerged in different subspecies. A haplotype analysis of the *Fpr3* gene in mouse strains carrying one of the two variants with the Mouse Phylogeny Viewer were performed to clarify the origin of *Fpr3* $\Delta_{424-435}$ (see chapter 2.8.2.5; Table 13; Appendix). This analysis gives information about from which founder mouse a defined gene locus in different laboratory mouse strains emerged (Yang *et al.*, 2011). Most strains of either variant received their *Fpr3* gene from *M. m. domesticus*. Only three other tested strains carrying *Fpr3*_{wt} – C57BR/cdJ, C57L/J, C58/J – showed a *M. m. musculus* heredity. Intriguingly, all tested strains in which the non-functional *Fpr3* $\Delta_{424-435}$ variant was found, obtained their *Fpr3* gene from a *M. m. domesticus* ancestor. This finding shows that the *Fpr3* $\Delta_{424-435}$ variant undoubtedly originated from the subspecies *M. m. domesticus*.

Different strains representing *M. m. domesticus* from different geographic regions were investigated for their encoded *Fpr3* variant to determine which *M. m. domesticus* strain introduced *Fpr3* $\Delta_{424-435}$ into laboratory mice. Distribution of *Fpr3* $\Delta_{424-435}$ in wild-type

M. m. domesticus was highly unusual because it could not be retraced to a clear geographic origin. One strain from Switzerland and two others from North America carried *Fpr3* $\Delta_{424-435}$ whereas two other lines from Germany and France carried *Fpr3*_{wt} (Figure 27). I expected that the non-functional *Fpr3* $\Delta_{424-435}$ was a rare incidence. However, the occurrence of *Fpr3* $\Delta_{424-435}$ in at least three wild living strains from geographically separated regions argues for multiple independent origins of *Fpr3* $\Delta_{424-435}$ under natural conditions.

Surprisingly, database analyses revealed that a wild-derived strain representing *M. m. molossinus*, which is believed to have solely originated from *M. m. castaneus* and *M. m. musculus* in Japan (Boursot *et al.*, 1993; Beck *et al.*, 2000; Yang *et al.*, 2011) also expresses *Fpr3* $\Delta_{424-435}$ despite a geographic barrier that should prevent a cross-breeding with *M. m. domesticus* mice from North America or Europe.

4.4 Outlook

The functional orthology of murine Fpr3 to human FPR3 and upregulation of the receptor protein after stimulation with lipopolysaccharide in immune cells suggest a role for murine Fpr3 in the immune system and thus in pathogen detection. Furthermore, as bacterial signal peptides were detected by Fpr3-expressing vomeronasal sensory neurons, the receptor may be involved in pathogen detection by the vomeronasal organ. These findings pave the way for further investigations into the biological role of murine Fpr3.

The discovery of a multitude of natural *Fpr3* knockout mouse strains provides a valuable tool to study murine Fpr3 function in the context of various genetic backgrounds. Thereby, comparative analyses of functional *Fpr3*_{wt} and non-functional *Fpr3* $\Delta_{424-435}$ in native tissues will provide crucial information about the biological role of murine Fpr3.

To gain a deeper understanding of the biological role of Fpr3 in the immune system, calcium imaging experiments and assays including chemotaxis or release of reactive oxygen species could be performed with neutrophil granulocytes. However, no exclusive ligand for murine Fpr3 has been identified. Thus, identifying an exclusive Fpr3 ligand is an important step to shed light on the biological role of the receptor in the immune system. Moreover, neutrophil granulocytes express functionally promiscuous Fpr1 and Fpr2, which detect all known Fpr3 ligands with higher sensitivity than Fpr3. Thus, and because of the lack of reliable blockers for murine Fpr1 and Fpr2, definite answers about Fpr3 function in neutrophil granulocytes await the availability of such tools.

Fpr3 was not coexpressed with any other Fpr or other type of vomeronasal receptor in the vomeronasal organ (Liberles *et al.*, 2009; Rivière *et al.*, 2009). Thus, a detailed examination on the role of murine Fpr3 in the vomeronasal organ is possible. The main issue when investigating Fpr3 function in the vomeronasal organ is the small proportion of cells (0.3%) that express the receptor. This study introduced tools to unambiguously identify Fpr3-expressing cells. In cooperation with Dr. Andreas Schmid, I determined that mouse strains carrying *Fpr3* $\Delta_{424-435}$ had a functional *Fpr3* knockout phenotype in the vomeronasal organ. Thus, Fpr3 function could be investigated by comparatively examining vomeronasal cells in strains expressing either Fpr3_{wt} or Fpr3 $\Delta_{424-435}$ with calcium imaging. To verify the functional data, Fpr3 expression in responding cells could be demonstrated by immunocytochemistry *post-hoc* using the newly generated ECL1 and ECL2 antibodies. In this context, the most interesting question is whether Fpr3 is actually involved in pathogen detection by the olfactory system. To this end, calcium imaging of vomeronasal cells and pathogen-related compounds in combination with a behavioral aversion assay (Boillat *et al.*, 2015) could be performed. Thereafter, olfactory-based compounds would be of interest to evaluate adaptations of the receptor to the olfactory system.

A comparison of the behavior of mice carrying either *Fpr3*_{wt} or *Fpr3* $\Delta_{424-435}$ would provide insight into the involvement of Fpr3 in general social behaviors mediated by the vomeronasal organ, such as aggressive or sexual behavior. However, based on the different genetic backgrounds of the mice, the results must be checked with *Fpr3* knockout mice from the same genetic background.

This thesis reports the functional orthology of murine *Fpr3* to human *FPR3*. Further studies should examine genes orthologous with murine *Fpr3* in other species. Interesting questions include which functions of orthologous *Fpr3* genes are conserved and if specific roles are associated with an olfactory phenotype. *Fpr3* genes have been predicted in numerous apes and monkeys and the rat (NCBI data), but definite confirmation of receptor proteins remains to be shown. Thus, the first step to further evaluate *Fpr3* orthology between species is to identify *Fpr3* genes in more species. I speculate that *Fpr3* genes will be identified in various rodents in the future. It would be interesting to compare Fpr3 function in animals with an intact vomeronasal organ to those without. To this end, functional measurements *in vitro* and in native tissues could be used as presented in this study.

5 LITERATURE

1. Altenhoff AM, Škunca N, Glover N, Train CM, Sueki A, Piližota I, Gori K, Tomiczek B, Müller S, Redestig H, Gonnet GH, Dessimoz C (2015) The OMA orthology database in 2015: function predictions, better plant support, syteny view and other improvements. *Nucleic Acids Res* 43: D240-249
2. Altizer S, Nunn CL, Thrall PH, Gittleman JL, Antonovics J, Cunningham AA, Dobson AP, Ezenwa V, Jones KE, Pedersen AB, Poss M, Pulliam JRC (2003) Social organization and parasite risk in mammals: Integrating theory and empirical studies. *Annu Rev Ecol Evol S* 34: 517-547
3. Alvarez V, Coto E, Setién F, López-Larrea C (1994) A physical map of two clusters containing the genes for six proinflammatory receptors. *Immunogenetics* 40: 100-103
4. Apfelbach R, Blanchard CD, Blanchard RJ, Hayes RA, McGregor IS (2005) The effects of predator odors in mammalian prey species: a review of field and laboratory studies. *Neurosci Biobehav Rev* 29: 1123-1144
5. Bae GH, Lee HY, Jung YS, Shim JW, Kim SD, Baek SH, Kwon JY, Park JS, Bae YS (2012) Identification of novel peptides that stimulate human neutrophils. *Exp Mol Med* 44: 130-137
6. Ballas ZK, Rasmussen W (1993) Lymphokine-activated killer cells. VII. IL-4 induces an NK1.1+CD8 alpha+beta- TCR-alpha beta B220+ lymphokine-activated killer subset. *J Immunol* 150: 17-30
7. Bao L, Gerard NP, Eddy RL, Jr., Shows TB, Gerard C (1992) Mapping of genes for the human C5a receptor (C5AR), human FMLP receptor (FPR), and two FMLP receptor homologue orphan receptors (FPRH1, FPRH2) to chromosome 19. *Genomics* 13: 437-440
8. Beck JA, Lloyd S, Hafezparast M, Lennon-Pierce M, Eppig JT, Festing MF, Fisher EM (2000) Genealogies of mouse inbred strains. *Nat Genet* 24: 23-25
9. Becker EL, Forouhar FA, Grunnet ML, Boulay F, Tardif M, Bormann BJ, Sodja D, Ye RD, Woska JR, Jr., Murphy PM (1998) Broad immunocytochemical localization of the formylpeptide receptor in human organs, tissues, and cells. *Cell Tissue Res* 292: 129-135
10. Bekkering S, Torensma R (2013) Another look at the life of a neutrophil. *World J Hematol* 2 44-58
11. Bellringer JF, Pratt HP, Keverne EB (1980) Involvement of the vomeronasal organ and prolactin in pheromonal induction of delayed implantation in mice. *J Reprod Fertil* 59: 223-228
12. Belluscio L, Koentges G, Axel R, Dulac C (1999) A map of pheromone receptor activation in the mammalian brain. *Cell* 97: 209-220
13. Bennett JP, Hirth KP, Fuchs E, Sarvas M, Warren GB (1980) The bacterial factors which stimulate neutrophils may be derived from procaryote signal peptides. *FEBS Lett* 116: 57-61
14. Berghard A, Buck LB (1996) Sensory transduction in vomeronasal neurons: evidence for G alpha o, G alpha i2, and adenylyl cyclase II as major components of a pheromone signaling cascade. *J Neurosci* 16: 909-918
15. Betten Å, Bylund J, Christophe T, Boulay F, Romero A, Hellstrand K, Dahlgren C (2001) A proinflammatory peptide from *Helicobacter pylori* activates monocytes to induce lymphocyte dysfunction and apoptosis. *J Clin Invest* 108: 1221-1228
16. Bhattacharyya S, Yu H, Mim C, Matouschek A (2014) Regulated protein turnover: snapshots of the proteasome in action. *Nat Rev Mol Cell Biol* 15: 122-133
17. Bloes DA, Kretschmer D, Peschel A (2015) Enemy attraction: bacterial agonists for leukocyte chemotaxis receptors. *Nat Rev Microbiol* 13: 95-104
18. Boehm T, Zufall F (2006) MHC peptides and the sensory evaluation of genotype. *Trends Neurosci* 29: 100-107

19. Boillat M, Challet L, Rossier D, Kan C, Carleton A, Rodriguez I (2015) The vomeronasal system mediates sick conspecific avoidance. *Curr Biol* 25: 251-255
20. Bonhomme F, Guenet JL, Dod B, Moriwaki K, Bulfield G (1987) The polyphyletic origin of laboratory inbred mice and their rate of evolution. *Biol J Linn Soc* 30: 51-58
21. Boschhat C, Pélofi C, Randin O, Roppolo D, Lüscher C, Broillet MC, Rodriguez I (2002) Pheromone detection mediated by a V1r vomeronasal receptor. *Nat Neurosci* 5: 1261-1262
22. Boulay F, Tardif M, Bouchon L, Vignais P (1990) The human N-formylpeptide receptor. Characterization of two cDNA isolates and evidence for a new subfamily of G-protein-coupled receptors. *Biochemistry* 29: 11123-11133
23. Boursot P, Auffray J-C, Britton-Davidian J, Bonhomme F (1993) The evolution of house mice. *Annu Rev Ecol Syst* 24: 119-152
24. Boxio R, Bossenmeyer-Pourie C, Steinckwich N, Dournon C, Nüsse O (2004) Mouse bone marrow contains large numbers of functionally competent neutrophils. *J Leukocyte Biol* 75: 604-611
25. Brennan PA, Zufall F (2006) Pheromonal communication in vertebrates. *Nature* 444: 308-315
26. Brennan PA (2009) Outstanding issues surrounding vomeronasal mechanisms of pregnancy block and individual recognition in mice. *Behav Brain Res* 200: 287-294
27. Broman I (1920) Das Organon vomero-nasale Jacobsoni — ein Wassergeruchsorgan! *Brain Structure and Function* 58: 137-191
28. Brouette-Lahlou I, Godinot F, Vernet-Maury E (1999) The mother rat's vomeronasal organ is involved in detection of dodecyl propionate, the pup's preputial gland pheromone. *Physiol Behav* 66: 427-436
29. Bruce HM (1959) An exteroceptive block to pregnancy in the mouse. *Nature* 184: 105
30. Bufo B, Schumann T, Zufall F (2012) Formyl peptide receptors from immune and vomeronasal system exhibit distinct agonist properties. *J Biol Chem* 287: 33644-33655
31. Bufo B, Schumann T, Kappl R, Bogeski I, Kummerow C, Podgórska M, Smola S, Hoth M, Zufall F (2015) Recognition of bacterial signal peptides by mammalian formyl peptide receptors: a new mechanism for sensing pathogens. *J Biol Chem* 290: 7369-7387
32. Bufo B, Zufall F (2016) The sensing of bacteria: emerging principles for the detection of signal sequences by formyl peptide receptors. *Biomol Concepts* 7: 205-214
33. Bylund J, Michael G, Winther W, Önnheim K, Dahlgren C, Forsman H (2014) Turning chemoattractant receptors on and off with conventional ligands and allosteric modulators: recent advances in formyl peptide receptor signaling and regulation. *Inflamm Cell Signal* 1
34. Campbell MS, Lovell MA, Gorbsky GJ (1995) Stability of nuclear segments in human neutrophils and evidence against a role for microfilaments or microtubules in their genesis during differentiation of HL60 myelocytes. *J Leukoc Biol* 58: 659-666
35. Carvalho LO, Aquino EN, Neves AC, Fontes W (2015) The neutrophil nucleus and its role in neutrophilic function. *J Cell Biochem* 116: 1831-1836
36. Cassatella MA (1999) Neutrophil-derived proteins: selling cytokines by the pound. *Adv Immunol* 73: 369-509
37. Chamero P, Marton TF, Logan DW, Flanagan K, Cruz JR, Saghatelian A, Cravatt BF, Stowers L (2007) Identification of protein pheromones that promote aggressive behaviour. *Nature* 450: 899-902
38. Chamero P, Katsoulidou V, Hendrix P, Bufo B, Roberts R, Matsunami H, Abramowitz J, Birnbaumer L, Zufall F, Leinders-Zufall T (2011) G protein G(alpha)o is essential for vomeronasal function and aggressive behavior in mice. *Proc Natl Acad Sci U S A* 108: 12898-12903

39. Chamero P, Leinders-Zufall T, Zufall F (2012) From genes to social communication: molecular sensing by the vomeronasal organ. *Trends Neurosci* 35: 597-606
40. Cheetham SA, Thom MD, Jury F, Ollier WE, Beynon RJ, Hurst JL (2007) The genetic basis of individual-recognition signals in the mouse. *Curr Biol* 17: 1771-1777
41. Chiu IM, Heesters BA, Ghasemlou N, Von Hehn CA, Zhao F, Tran J, Wainger B, Strominger A, Muralidharan S, Horswill AR, Bubeck Wardenburg J, Hwang SW, Carroll MC, Woolf CJ (2013) Bacteria activate sensory neurons that modulate pain and inflammation. *Nature* 501: 52-57
42. Church DM, Goodstadt L, Hillier LW, Zody MC, Goldstein S, She X, Bult CJ, Agarwala R, Cherry JL, DiCuccio M, Hlavina W, Kapustin Y, Meric P, Maglott D, Birtle Z, Marques AC, Graves T, Zhou S, Teague B, Potamowski K, Churas C, Place M, Herschleb J, Runnheim R, Forrest D, Amos-Landgraf J, Schwartz DC, Cheng Z, Lindblad-Toh K, Eichler EE, Ponting CP (2009) Lineage-specific biology revealed by a finished genome assembly of the mouse. *PLoS Biol* 7: e1000112
43. Cowley JJ, Wise DR (1972) Some effects of mouse urine on neonatal growth and reproduction. *Anim Behav* 20: 499-506
44. Cui YH, Le Y, Gong W, Proost P, Van Damme J, Murphy WJ, Wang JM (2002) Bacterial lipopolysaccharide selectively up-regulates the function of the chemotactic peptide receptor formyl peptide receptor 2 in murine microglial cells. *J Immunol* 168: 434-442
45. Czapiga M, Gao JL, Kirk A, Lekstrom-Himes J (2005) Human platelets exhibit chemotaxis using functional N-formyl peptide receptors. *Exp Hematol* 33: 73-84
46. Dahlgren C, Gabl M, Holdfeldt A, Winther M, Forsman H (2016) Basic characteristics of the neutrophil receptors that recognize formylated peptides, a danger-associated molecular pattern generated by bacteria and mitochondria. *Biochem Pharmacol* 114: 22-39
47. Dantzer R, O'Connor JC, Freund GG, Johnson RW, Kelley KW (2008) From inflammation to sickness and depression: when the immune system subjugates the brain. *Nat Rev Neurosci* 9: 46-56
48. de Paulis A, Montuori N, Prevete N, Fiorentino I, Rossi FW, Visconte V, Rossi G, Marone G, Ragno P (2004) Urokinase induces basophil chemotaxis through a urokinase receptor epitope that is an endogenous ligand for formyl peptide receptor-like 1 and -like 2. *J Immunol* 173: 5739-5748
49. Del Punta K, Puche A, Adams NC, Rodriguez I, Mombaerts P (2002a) A divergent pattern of sensory axonal projections is rendered convergent by second-order neurons in the accessory olfactory bulb. *Neuron* 35: 1057-1066
50. Del Punta K, Leinders-Zufall T, Rodriguez I, Jukam D, Wysocki CJ, Ogawa S, Zufall F, Mombaerts P (2002b) Deficient pheromone responses in mice lacking a cluster of vomeronasal receptor genes. *Nature* 419: 70-74
51. DeLuca TF, Wu IH, Pu J, Monaghan T, Peshkin L, Singh S, Wall DP (2006) Roundup: a multi-genome repository of orthologs and evolutionary distances. *Bioinformatics* 22: 2044-2046
52. DeLuca TF, Cui J, Jung JY, St Gabriel KC, Wall DP (2012) Roundup 2.0: enabling comparative genomics for over 1800 genomes. *Bioinformatics* 28: 715-716
53. Dey S, Matsunami H (2011) Calreticulin chaperones regulate functional expression of vomeronasal type 2 pheromone receptors. *Proc Natl Acad Sci U S A* 108: 16651-16656
54. Dietschi Q, Assens A, Challet L, Carleton A, Rodriguez I (2013) Convergence of FPR-rs3-expressing neurons in the mouse accessory olfactory bulb. *Mol Cell Neurosci* 56: 140-147
55. Dolan ME, Baldarelli RM, Bello SM, Ni L, McAndrews MS, Bult CJ, Kadin JA, Richardson JE, Ringwald M, Eppig JT, Blake JA (2015) Orthology for comparative genomics in the mouse genome database. *Mamm Genome* 26: 305-313

56. Dorward DA, Lucas CD, Chapman GB, Haslett C, Dhaliwal K, Rossi AG (2015) The role of formylated peptides and formyl peptide receptor 1 in governing neutrophil function during acute inflammation. *Am J Pathol* 185: 1172-1184
57. Døving KB, Trotier D (1998) Structure and function of the vomeronasal organ. *J Exp Biol* 201: 2913-2925
58. Dulac C, Axel R (1995) A novel family of genes encoding putative pheromone receptors in mammals. *Cell* 83: 195-206
59. Dulac C, Torello AT (2003) Molecular detection of pheromone signals in mammals: from genes to behaviour. *Nat Rev Neurosci* 4: 551-562
60. Durstin M, Gao JL, Tiffany HL, McDermott D, Murphy PM (1994) Differential expression of members of the N-formylpeptide receptor gene cluster in human phagocytes. *Biochem Biophys Res Commun* 201: 174-179
61. Edwards JC, Barnard CJ (1987) The Effects of *Trichinella* Infection on Intersexual Interactions between Mice. *Animal Behaviour* 35: 533-540
62. Ehman KD, Scott ME (2001) Urinary odour preferences of MHC congenic female mice, *Mus domesticus*: implications for kin recognition and detection of parasitized males. *Animal Behaviour* 62: 781-789
63. Ehman KD, Scott ME (2002) Female mice mate preferentially with non-parasitized males. *Parasitology* 125: 461-466
64. Ernst S, Lange C, Wilbers A, Goebeler V, Gerke V, Rescher U (2004) An annexin 1 N-terminal peptide activates leukocytes by triggering different members of the formyl peptide receptor family. *J Immunol* 172: 7669-7676
65. Etlinger JD, Goldberg AL (1977) A soluble ATP-dependent proteolytic system responsible for the degradation of abnormal proteins in reticulocytes. *Proc Natl Acad Sci U S A* 74: 54-58
66. Everett CA, Auchincloss CA, Kaufman MH, Abbott CM, West JD (2004) Genetic influences on ovulation of primary oocytes in LT/Sv strain mice. *Reproduction* 128: 565-571
67. Fang G, Bhardwaj N, Robilotto R, Gerstein MB (2010) Getting started in gene orthology and functional analysis. *PLoS Comput Biol* 6: e1000703
68. Ferrero DM, Lemon JK, Fluegge D, Pashkovski SL, Korzan WJ, Datta SR, Spehr M, Fendt M, Liberles SD (2011) Detection and avoidance of a carnivore odor by prey. *Proc Natl Acad Sci U S A* 108: 11235-11240
69. Ferrero DM, Moeller LM, Osakada T, Horio N, Li Q, Roy DS, Cichy A, Spehr M, Touhara K, Liberles SD (2013) A juvenile mouse pheromone inhibits sexual behaviour through the vomeronasal system. *Nature* 502: 368-371
70. Fitch WM (1970) Distinguishing homologous from analogous proteins. *Syst Zool* 19: 99-113
71. Fitch WM (2000) Homology a personal view on some of the problems. *Trends Genet* 16: 227-231
72. Fleming TJ, Fleming ML, Malek TR (1993) Selective expression of Ly-6G on myeloid lineage cells in mouse bone marrow. RB6-8C5 mAb to granulocyte-differentiation antigen (Gr-1) detects members of the Ly-6 family. *J Immunol* 151: 2399-2408
73. Fu H, Karlsson J, Bylund J, Movitz C, Karlsson A, Dahlgren C (2006) Ligand recognition and activation of formyl peptide receptors in neutrophils. *J Leukoc Biol* 79: 247-256
74. Gao JL, Chen H, Filie JD, Kozak CA, Murphy PM (1998) Differential expansion of the N-formylpeptide receptor gene cluster in human and mouse. *Genomics* 51: 270-276

75. Goldberg AL, Dice JF (1974) Intracellular protein degradation in mammalian and bacterial cells. *Annu Rev Biochem* 43: 835-869
76. Goldberg AL (2003) Protein degradation and protection against misfolded or damaged proteins. *Nature* 426: 895-899
77. Gourbal BEF, Gabrion C (2004) A study of mate choice in mice with experimental *Taenia crassiceps* cysticercosis: can males choose? *Can J Zool* 82: 635-643
78. Gowen JW, Calhoun ML (1943) On the Physical Basis for Genetic Resistance to Mouse Typhoid, *Salmonella Typhimurium*. *Proc Natl Acad Sci U S A* 29: 144-149
79. Gripentrog JM, Miettinen HM (2008) Formyl peptide receptor-mediated ERK1/2 activation occurs through G(i) and is not dependent on beta-arrestin1/2. *Cell Signal* 20: 424-431
80. Guha M, Mackman N (2001) LPS induction of gene expression in human monocytes. *Cell Signal* 13: 85-94
81. Haga S, Hattori T, Sato T, Sato K, Matsuda S, Kobayakawa R, Sakano H, Yoshihara Y, Kikusui T, Touhara K (2010) The male mouse pheromone ESP1 enhances female sexual receptive behaviour through a specific vomeronasal receptor. *Nature* 466: 118-122
82. Haga-Yamanaka S, Ma L, He J, Qiu Q, Lavis LD, Looger LL, Yu CR (2014) Integrated action of pheromone signals in promoting courtship behavior in male mice. *Elife* 3: e03025
83. Haga-Yamanaka S, Ma L, Yu CR (2015) Tuning properties and dynamic range of type 1 vomeronasal receptors. *Front Neurosci* 9: 244
84. Halpern M (1987) The organization and function of the vomeronasal system. *Annu Rev Neurosci* 10: 325-362
85. Halpern M, Shapiro LS, Jia C (1995) Differential localization of G proteins in the opossum vomeronasal system. *Brain Res* 677: 157-161
86. Halpern M, Martínez-Marcos A (2003) Structure and function of the vomeronasal system: an update. *Prog Neurobiol* 70: 245-318
87. Hamilton WD, Zuk M (1982) Heritable true fitness and bright birds: a role for parasites? *Science* 218: 384-387
88. Harada M, Habata Y, Hosoya M, Nishi K, Fujii R, Kobayashi M, Hinuma S (2004) N-Formylated humanin activates both formyl peptide receptor-like 1 and 2. *Biochem Biophys Res Commun* 324: 255-261
89. Hartt JK, Barish G, Murphy PM, Gao JL (1999) N-formylpeptides induce two distinct concentration optima for mouse neutrophil chemotaxis by differential interaction with two N-formylpeptide receptor (FPR) subtypes. Molecular characterization of FPR2, a second mouse neutrophil FPR. *J Exp Med* 190: 741-747
90. He HQ, Liao D, Wang ZG, Wang ZL, Zhou HC, Wang MW, Ye RD (2013) Functional characterization of three mouse formyl peptide receptors. *Mol Pharmacol* 83: 389-398
91. Herrada G, Dulac C (1997) A novel family of putative pheromone receptors in mammals with a topographically organized and sexually dimorphic distribution. *Cell* 90: 763-773
92. Heumann D, Roger T (2002) Initial responses to endotoxins and Gram-negative bacteria. *Clin Chim Acta* 323: 59-72
93. Holland SM (2013) Chronic granulomatous disease. *Hematol Oncol Clin North Am* 27: 89-99, viii
94. Hurst JL, Payne CE, Nevison CM, Marie AD, Humphries RE, Robertson DH, Cavaggioni A, Beynon RJ (2001) Individual recognition in mice mediated by major urinary proteins. *Nature* 414: 631-634

95. Iribarren P, Cui YH, Le Y, Ying G, Zhang X, Gong W, Wang JM (2003) IL-4 down-regulates lipopolysaccharide-induced formyl peptide receptor 2 in murine microglial cells by inhibiting the activation of mitogen-activated protein kinases. *J Immunol* 171: 5482-5488
96. Ishii T, Hirota J, Mombaerts P (2003) Combinatorial coexpression of neural and immune multigene families in mouse vomeronasal sensory neurons. *Curr Biol* 13: 394-400
97. Ishii T, Mombaerts P (2008) Expression of nonclassical class I major histocompatibility genes defines a tripartite organization of the mouse vomeronasal system. *J Neurosci* 28: 2332-2341
98. Isogai Y, Si S, Pont-Lezica L, Tan T, Kapoor V, Murthy VN, Dulac C (2011) Molecular organization of vomeronasal chemoreception. *Nature* 478: 241-245
99. Jacobson L (1813) Anatomisk Beskrivelse over et nyt Organ i Huusdyrenes Næse. Veterinær=Selskapets Skrifter [in Danish]: 209–246
100. Jemiolo B, Xie TM, Novotny M (1991) Socio-sexual olfactory preference in female mice: attractiveness of synthetic chemosignals. *Physiol Behav* 50: 1119-1122
101. Jemiolo B, Novotny M (1994) Inhibition of sexual maturation in juvenile female and male mice by a chemosignal of female origin. *Physiol Behav* 55: 519-522
102. Jia C, Halpern M (1996) Subclasses of vomeronasal receptor neurons: differential expression of G proteins (Gi alpha 2 and G(o alpha)) and segregated projections to the accessory olfactory bulb. *Brain Res* 719: 117-128
103. Karlson P, Lüscher M (1959) 'Pheromones': a new term for a class of biologically active substances. *Nature* 183: 55-56
104. Kaur AW, Ackels T, Kuo TH, Cichy A, Dey S, Hays C, Kateri M, Logan DW, Marton TF, Spehr M, Stowers L (2014) Murine pheromone proteins constitute a context-dependent combinatorial code governing multiple social behaviors. *Cell* 157: 676-688
105. Kavaliers M, Colwell DD (1993) Aversive responses of female mice to the odors of parasitized males - neuromodulatory mechanisms and implications for mate choice. *Ethology* 95: 202-212
106. Kavaliers M, Colwell DD (1995) Odors of parasitized males induce aversive responses in female mice. *Animal Behaviour* 50: 1161-1169
107. Kavaliers M, Colwell DD, Ossenkopp KP, Perrot-Sinal TS (1997) Altered responses to female odors in parasitized male mice: Neuromodulatory mechanisms and relations to female choice. *Behav Ecol Sociobiol* 40: 373-384
108. Kavaliers M, Colwell DD, Choleris E (1998) Analgesic responses of male mice exposed to the odors of parasitized females: effects of male sexual experience and infection status. *Behav Neurosci* 112: 1001-1011
109. Kavaliers M, Colwell DD, Choleris E (2000) Parasites and behaviour: an ethopharmacological perspective. *Parasitol Today* 16: 464-468
110. Kavaliers M, Colwell DD, Braun WJ, Choleris E (2003a) Brief exposure to the odour of a parasitized male alters the subsequent mate odour responses of female mice. *Animal Behaviour* 65: 59-68
111. Kavaliers M, Fudge MA, Colwell DD, Choleris E (2003b) Aversive and avoidance responses of female mice to the odors of males infected with an ectoparasite and the effects of prior familiarity. *Behav Ecol Sociobiol* 54: 423-430
112. Kavaliers M, Choleris E, Agmo A, Pfaff DW (2004) Olfactory-mediated parasite recognition and avoidance: linking genes to behavior. *Horm Behav* 46: 272-283
113. Kavaliers M, Choleris E, Pfaff DW (2005) Recognition and avoidance of the odors of parasitized conspecifics and predators: differential genomic correlates. *Neurosci Biobehav Rev* 29: 1347-1359

114. Keller M, Douhard Q, Baum MJ, Bakker J (2006) Destruction of the main olfactory epithelium reduces female sexual behavior and olfactory investigation in female mice. *Chem Senses* 31: 315-323
115. Kelliher KR, Spehr M, Li XH, Zufall F, Leinders-Zufall T (2006) Pheromonal recognition memory induced by TRPC2-independent vomeronasal sensing. *Eur J Neurosci* 23: 3385-3390
116. Kimoto H, Haga S, Sato K, Touhara K (2005) Sex-specific peptides from exocrine glands stimulate mouse vomeronasal sensory neurons. *Nature* 437: 898-901
117. Kimoto H, Sato K, Nodari F, Haga S, Holy TE, Touhara K (2007) Sex- and strain-specific expression and vomeronasal activity of mouse ESP family peptides. *Curr Biol* 17: 1879-1884
118. Kirkpatrick BW, Mengelt A, Schulman N, Martin IC (1998) Identification of quantitative trait loci for prolificacy and growth in mice. *Mamm Genome* 9: 97-102
119. Klemes Y, Etlinger JD, Goldberg AL (1981) Properties of abnormal proteins degraded rapidly in reticulocytes. Intracellular aggregation of the globin molecules prior to hydrolysis. *J Biol Chem* 256: 8436-8444
120. Kobayakawa K, Kobayakawa R, Matsumoto H, Oka Y, Imai T, Ikawa M, Okabe M, Ikeda T, Itohara S, Kikusui T, Mori K, Sakano H (2007) Innate versus learned odour processing in the mouse olfactory bulb. *Nature* 450: 503-508
121. Lacy M, Jones J, Whittemore SR, Haviland DL, Wetsel RA, Barnum SR (1995) Expression of the receptors for the C5a anaphylatoxin, interleukin-8 and FMLP by human astrocytes and microglia. *J Neuroimmunol* 61: 71-78
122. Lai L, Alaverdi N, Maltais L, Morse HC, 3rd (1998) Mouse cell surface antigens: nomenclature and immunophenotyping. *J Immunol* 160: 3861-3868
123. Lambert R (2009) Breeding Strategies for Maintaining Colonies of Laboratory Mice. In: Lambert R (ed) *A Jackson Laboratory Resource Manual*. The Jackson Laboratory
124. Lau YE, Cherry JA (2000) Distribution of PDE4A and G(o) alpha immunoreactivity in the accessory olfactory system of the mouse. *Neuroreport* 11: 27-32
125. Le Y, Jiang S, Hu J, Gong W, Su S, Dunlop NM, Shen W, Li B, Ming Wang J (2000) N36, a synthetic N-terminal heptad repeat domain of the HIV-1 envelope protein gp41, is an activator of human phagocytes. *Clin Immunol* 96: 236-242
126. Le Y, Gong W, Tiffany HL, Tumanov A, Nedospasov S, Shen W, Dunlop NM, Gao JL, Murphy PM, Oppenheim JJ, Wang JM (2001a) Amyloid (beta)42 activates a G-protein-coupled chemoattractant receptor, FPR-like-1. *J Neurosci* 21: RC123
127. Le Y, Oppenheim JJ, Wang JM (2001b) Pleiotropic roles of formyl peptide receptors. *Cytokine Growth Factor Rev* 12: 91-105
128. Lee HY, Kang HK, Jo EJ, Kim JI, Lee YN, Lee SH, Park YM, Ryu SH, Kwak JY, Bae YS (2004) Trp-Lys-Tyr-Met-Val-Met stimulates phagocytosis via phospho-lipase D-dependent signaling in mouse dendritic cells. *Exp Mol Med* 36: 135-144
129. Lehmann T (1993) Ectoparasites: direct impact on host fitness. *Parasitol Today* 9: 8-13
130. Leinders-Zufall T, Lane AP, Puche AC, Ma W, Novotny MV, Shipley MT, Zufall F (2000) Ultrasensitive pheromone detection by mammalian vomeronasal neurons. *Nature* 405: 792-796
131. Leinders-Zufall T, Brennan P, Widmayer P, S PC, Maul-Pavicic A, Jäger M, Li XH, Breer H, Zufall F, Boehm T (2004) MHC class I peptides as chemosensory signals in the vomeronasal organ. *Science* 306: 1033-1037
132. Leinders-Zufall T, Ishii T, Mombaerts P, Zufall F, Boehm T (2009) Structural requirements for the activation of vomeronasal sensory neurons by MHC peptides. *Nat Neurosci* 12: 1551-1558

133. Leinders-Zufall T, Ishii T, Chamero P, Hendrix P, Oboti L, Schmid A, Kircher S, Pyrski M, Akiyoshi S, Khan M, Vaes E, Zufall F, Mombaerts P (2014) A family of nonclassical class I MHC genes contributes to ultrasensitive chemodetection by mouse vomeronasal sensory neurons. *J Neurosci* 34: 5121-5133
134. Leybold BG, Yu CR, Leinders-Zufall T, Kim MM, Zufall F, Axel R (2002) Altered sexual and social behaviors in *trp2* mutant mice. *Proc Natl Acad Sci U S A* 99: 6376-6381
135. Li Q, Korzan WJ, Ferrero DM, Chang RB, Roy DS, Buchi M, Lemon JK, Kaur AW, Stowers L, Fendt M, Liberles SD (2013) Synchronous evolution of an odor biosynthesis pathway and behavioral response. *Curr Biol* 23: 11-20
136. Liao CS, Lu K, Baym M, Singh R, Berger B (2009) IsoRankN: spectral methods for global alignment of multiple protein networks. *Bioinformatics* 25: i253-258
137. Liberles SD, Horowitz LF, Kuang D, Contos JJ, Wilson KL, Siltberg-Liberles J, Liberles DA, Buck LB (2009) Formyl peptide receptors are candidate chemosensory receptors in the vomeronasal organ. *Proc Natl Acad Sci U S A* 106: 9842-9847
138. Liberles SD (2014) Mammalian pheromones. *Annu Rev Physiol* 76: 151-175
139. Liljander M, Sällström MA, Andersson S, Wernhoff P, Andersson Å, Holmdahl R, Mattsson R (2006) Identification of genetic regions of importance for reproductive performance in female mice. *Genetics* 173: 901-909
140. Liman ER, Innan H (2003) Relaxed selective pressure on an essential component of pheromone transduction in primate evolution. *Proc Natl Acad Sci U S A* 100: 3328-3332
141. Lin W, Arellano J, Slotnick B, Restrepo D (2004) Odors detected by mice deficient in cyclic nucleotide-gated channel subunit A2 stimulate the main olfactory system. *J Neurosci* 24: 3703-3710
142. Loconto J, Papes F, Chang E, Stowers L, Jones EP, Takada T, Kumánovics A, Fischer Lindahl K, Dulac C (2003) Functional expression of murine V2R pheromone receptors involves selective association with the M10 and M1 families of MHC class Ib molecules. *Cell* 112: 607-618
143. Lomas DE, Keverne EB (1982) Role of the vomeronasal organ and prolactin in the acceleration of puberty in female mice. *J Reprod Fertil* 66: 101-107
144. Ma M (2007) Encoding olfactory signals via multiple chemosensory systems. *Crit Rev Biochem Mol Biol* 42: 463-480
145. Mandal P, Novotny M, Hamilton TA (2005) Lipopolysaccharide induces formyl peptide receptor 1 gene expression in macrophages and neutrophils via transcriptional and posttranscriptional mechanisms. *J Immunol* 175: 6085-6091
146. Margolis FL (1982) Olfactory marker protein (OMP). *Scand J Immunol Suppl* 9: 181-199
147. Martini S, Silvotti L, Shirazi A, Ryba NJ, Tirindelli R (2001) Co-expression of putative pheromone receptors in the sensory neurons of the vomeronasal organ. *J Neurosci* 21: 843-848
148. Matsunami H, Buck LB (1997) A multigene family encoding a diverse array of putative pheromone receptors in mammals. *Cell* 90: 775-784
149. Migeotte I, Riboldi E, Franssen JD, Grégoire F, Loison C, Wittamer V, Detheux M, Robberecht P, Costagliola S, Vassart G, Sozzani S, Parmentier M, Communi D (2005) Identification and characterization of an endogenous chemotactic ligand specific for FPRL2. *J Exp Med* 201: 83-93
150. Migeotte I, Communi D, Parmentier M (2006) Formyl peptide receptors: a promiscuous subfamily of G protein-coupled receptors controlling immune responses. *Cytokine Growth Factor Rev* 17: 501-519
151. Montani G, Tonelli S, Sanghez V, Ferrari PF, Palanza P, Zimmer A, Tirindelli R (2013) Aggressive behaviour and physiological responses to pheromones are strongly impaired in mice deficient for the olfactory G-protein -subunit G8. *J Physiol* 591: 3949-3962

152. Mora OA, Cabrera MM (1997) The pheromonal restoration of cyclic activity in young estrogenized persistent estrus female rats is a vomeronasal effect. *Life Sci* 60: 493-498
153. Munger SD, Leinders-Zufall T, Zufall F (2009) Subsystem organization of the mammalian sense of smell. *Annu Rev Physiol* 71: 115-140
154. Murphy PM, Özçelik T, Kenney RT, Tiffany HL, McDermott D, Francke U (1992) A structural homologue of the N-formyl peptide receptor. Characterization and chromosome mapping of a peptide chemoattractant receptor family. *J Biol Chem* 267: 7637-7643
155. Muto Y, Guindon S, Umemura T, Kōhidai L, Ueda H (2015) Adaptive evolution of formyl peptide receptors in mammals. *J Mol Evol* 80: 130-141
156. Novotny M, Jemiolo B, Harvey S, Wiesler D, Marchlewska-Koj A (1986) Adrenal-mediated endogenous metabolites inhibit puberty in female mice. *Science* 231: 722-725
157. Numan M, Fleming AS, Levy F (2006) Maternal behavior. In: Neill J (ed) In Knobil and Neill's *Physiology of Reproduction*. ELSEVIER Academic Press, St. Louis, pp 1921-1993
158. Oboti L, Pérez-Gómez A, Keller M, Jacobi E, Birnbaumer L, Leinders-Zufall T, Zufall F, Chamero P (2014) A wide range of pheromone-stimulated sexual and reproductive behaviors in female mice depend on G protein Galphao. *BMC Biol* 12: 31
159. Oboti L, Ibarra-Soria X, Pérez-Gómez A, Schmid A, Pyrski M, Paschek N, Kircher S, Logan DW, Leinders-Zufall T, Zufall F, Chamero P (2015) Pregnancy and estrogen enhance neural progenitor-cell proliferation in the vomeronasal sensory epithelium. *BMC Biol* 13: 104
160. Önnheim K, Bylund J, Boulay F, Dahlgren C, Forsman H (2008) Tumour necrosis factor (TNF)-alpha primes murine neutrophils when triggered via formyl peptide receptor-related sequence 2, the murine orthologue of human formyl peptide receptor-like 1, through a process involving the type I TNF receptor and subcellular granule mobilization. *Immunology* 125: 591-600
161. Panaro MA, Cianciulli A, Lisi S, Sisto M, Acquafredda A, Mitolo V (2007) Formyl peptide receptor expression in birds. *Immunopharmacol Immunotoxicol* 29: 1-16
162. Pantages E, Dulac C (2000) A novel family of candidate pheromone receptors in mammals. *Neuron* 28: 835-845
163. Papes F, Logan DW, Stowers L (2010) The vomeronasal organ mediates interspecies defensive behaviors through detection of protein pheromone homologs. *Cell* 141: 692-703
164. Park D, Singh R, Baym M, Liao CS, Berger B (2011) IsoBase: a database of functionally related proteins across PPI networks. *Nucleic Acids Res* 39: D295-300
165. Parker H, Winterbourn CC (2013) Reactive oxidants and myeloperoxidase and their involvement in neutrophil extracellular traps. *Front Immunol* 3: 424
166. Penn D, Potts W (1998) How do major histocompatibility complex genes influence odor and mating preferences? *Adv Immunol* 69: 411-436
167. Penn D, Schneider G, White K, Slev P, Potts W (1998) Influenza infection neutralizes the attractiveness of male odour to female mice (*Mus musculus*). *Ethology* 104: 685-694
168. Perez HD, Holmes R, Kelly E, McClary J, Chou Q, Andrews WH (1992) Cloning of the gene coding for a human receptor for formyl peptides - characterization of a promoter region and evidence for polymorphic expression. *Biochemistry* 31: 11595-11599
169. Pérez-Gómez A, Stein B, Leinders-Zufall T, Chamero P (2014) Signaling mechanisms and behavioral function of the mouse basal vomeronasal neuroepithelium. *Front Neuroanat* 8: 135

170. Pérez-Gómez A, Bleyemehl K, Stein B, Pyrski M, Birnbaumer L, Munger SD, Leinders-Zufall T, Zufall F, Chamero P (2015) Innate predator odor aversion driven by parallel olfactory subsystems that converge in the ventromedial hypothalamus. *Curr Biol* 25: 1340-1346
171. Peripato AC, De Brito RA, Vaughn TT, Pletscher LS, Mاتيoli SR, Cheverud JM (2002) Quantitative trait loci for maternal performance for offspring survival in mice. *Genetics* 162: 1341-1353
172. Peripato AC, De Brito RA, Mاتيoli SR, Pletscher LS, Vaughn TT, Cheverud JM (2004) Epistasis affecting litter size in mice. *J Evol Biol* 17: 593-602
173. Rabiet MJ, Huet E, Boulay F (2005) Human mitochondria-derived N-formylated peptides are novel agonists equally active on FPR and FPRL1, while *Listeria monocytogenes*-derived peptides preferentially activate FPR. *Eur J Immunol* 35: 2486-2495
174. Rabiet MJ, Macari L, Dahlgren C, Boulay F (2011) N-formyl peptide receptor 3 (FPR3) departs from the homologous FPR2/ALX receptor with regard to the major processes governing chemoattractant receptor regulation, expression at the cell surface, and phosphorylation. *J Biol Chem* 286: 26718-26731
175. Raisman G (1972) An experimental study of the projection of the amygdala to the accessory olfactory bulb and its relationship to the concept of a dual olfactory system. *Exp Brain Res* 14: 395-408
176. Remm M, Storm CE, Sonnhammer EL (2001) Automatic clustering of orthologs and in-paralogs from pairwise species comparisons. *J Mol Biol* 314: 1041-1052
177. Restrepo D, Lin W, Salcedo E, Yamazaki K, Beauchamp G (2006) Odortypes and MHC peptides: Complementary chemosignals of MHC haplotype? *Trends Neurosci* 29: 604-609
178. Reynolds J, Keverne EB (1979) The accessory olfactory system and its role in the pheromonally mediated suppression of oestrus in grouped mice. *J Reprod Fertil* 57: 31-35
179. Rivière S, Challet L, Fluegge D, Spehr M, Rodriguez I (2009) Formyl peptide receptor-like proteins are a novel family of vomeronasal chemosensors. *Nature* 459: 574-577
180. Roberts SA, Simpson DM, Armstrong SD, Davidson AJ, Robertson DH, McLean L, Beynon RJ, Hurst JL (2010) Darcin: a male pheromone that stimulates female memory and sexual attraction to an individual male's odour. *BMC Biol* 8: 75
181. Roberts SA, Davidson AJ, McLean L, Beynon RJ, Hurst JL (2012) Pheromonal induction of spatial learning in mice. *Science* 338: 1462-1465
182. Rocha JL, Eisen EJ, Siewerdt F, Van Vleck LD, Pomp D (2004) A large-sample QTL study in mice: III. Reproduction. *Mamm Genome* 15: 878-886
183. Rodriguez I, Feinstein P, Mombaerts P (1999) Variable patterns of axonal projections of sensory neurons in the mouse vomeronasal system. *Cell* 97: 199-208
184. Rolink A, ten Boekel E, Melchers F, Fearon DT, Krop I, Andersson J (1996) A subpopulation of B220+ cells in murine bone marrow does not express CD19 and contains natural killer cell progenitors. *J Exp Med* 183: 187-194
185. Roppolo D, Ribaud V, Jungo VP, Lüscher C, Rodriguez I (2006) Projection of the Gruneberg ganglion to the mouse olfactory bulb. *Eur J Neurosci* 23: 2887-2894
186. Rünneburger K, Breer H, Boekhoff I (2002) Selective G protein beta gamma-subunit compositions mediate phospholipase C activation in the vomeronasal organ. *Eur J Cell Biol* 81: 539-547
187. Ryba NJ, Tirindelli R (1997) A new multigene family of putative pheromone receptors. *Neuron* 19: 371-379
188. Sanchez JA, Wanh LJ (1999) New insights into the mechanisms of nuclear segmentation in human neutrophils. *J Cell Biochem* 73: 1-10

189. Sánchez-Criado JE, Gallego A (1979) Male induced precocious-puberty in the female rat - role of the vomeronasal system. *Acta Endocrinol-Cop* 91: 255-255
190. Sánchez-Criado JE (1982) Involvement of the vomeronasal system in the reproductive physiology of the rat. In: Breipohl W (ed) *Olfaction and Endocrine Regulation*. IRL Press Limited, London, pp 209–217
191. Scalia F, Winans SS (1975) The differential projections of the olfactory bulb and accessory olfactory bulb in mammals. *J Comp Neurol* 161: 31-55
192. Schiffmann E, Corcoran BA, Wahl SM (1975) N-formylmethionyl peptides as chemoattractants for leucocytes. *Proc Natl Acad Sci U S A* 72: 1059-1062
193. Sherborne AL, Thom MD, Paterson S, Jury F, Ollier WE, Stockley P, Beynon RJ, Hurst JL (2007) The genetic basis of inbreeding avoidance in house mice. *Curr Biol* 17: 2061-2066
194. Sherman MY, Goldberg AL (2001) Cellular defenses against unfolded proteins: a cell biologist thinks about neurodegenerative diseases. *Neuron* 29: 15-32
195. Singh R, Xu J, Berger B (2008) Global alignment of multiple protein interaction networks with application to functional orthology detection. *Proc Natl Acad Sci U S A* 105: 12763-12768
196. Southgate EL, He RL, Gao JL, Murphy PM, Nanamori M, Ye RD (2008) Identification of formyl peptides from *Listeria monocytogenes* and *Staphylococcus aureus* as potent chemoattractants for mouse neutrophils. *J Immunol* 181: 1429-1437
197. Spearow JL, Barkley M (1999) Genetic control of hormone-induced ovulation rate in mice. *Biol Reprod* 61: 851-856
198. Spehr M, Spehr J, Ukhanov K, Kelliher KR, Leinders-Zufall T, Zufall F (2006a) Parallel processing of social signals by the mammalian main and accessory olfactory systems. *Cell Mol Life Sci* 63: 1476-1484
199. Spehr M, Kelliher KR, Li XH, Boehm T, Leinders-Zufall T, Zufall F (2006b) Essential role of the main olfactory system in social recognition of major histocompatibility complex peptide ligands. *J Neurosci* 26: 1961-1970
200. Stempel H, Jung M, Pérez-Gómez A, Leinders-Zufall T, Zufall F, Bufe B (2016) Strain-specific loss of formyl peptide receptor 3 in the murine vomeronasal and immune systems. *J Biol Chem* 291: 9762-9775
201. Stowers L, Holy TE, Meister M, Dulac C, Koentges G (2002) Loss of sex discrimination and male-male aggression in mice deficient for TRP2. *Science* 295: 1493-1500
202. Sturm T, Leinders-Zufall T, Maček B, Walzer M, Jung S, Pömmerl B, Stevanović S, Zufall F, Overath P, Rammensee HG (2013) Mouse urinary peptides provide a molecular basis for genotype discrimination by nasal sensory neurons. *Nat Commun* 4: 1616
203. Su SB, Gong WH, Gao JL, Shen WP, Grimm MC, Deng X, Murphy PM, Oppenheim JJ, Wang JM (1999a) T20/DP178, an ectodomain peptide of human immunodeficiency virus type 1 gp41, is an activator of human phagocyte N-formyl peptide receptor. *Blood* 93: 3885-3892
204. Su SB, Gao J, Gong W, Dunlop NM, Murphy PM, Oppenheim JJ, Wang JM (1999b) T21/DP107, a synthetic leucine zipper-like domain of the HIV-1 envelope gp41, attracts and activates human phagocytes by using G-protein-coupled formyl peptide receptors. *J Immunol* 162: 5924-5930
205. Takano T, Fiore S, Maddox JF, Brady HR, Petasis NA, Serhan CN (1997) Aspirin-triggered 15-epi-lipoxin A4 (LXA4) and LXA4 stable analogues are potent inhibitors of acute inflammation: evidence for anti-inflammatory receptors. *J Exp Med* 185: 1693-1704
206. Tatusov RL, Koonin EV, Lipman DJ (1997) A genomic perspective on protein families. *Science* 278: 631-637

207. Tiffany HL, Lavigne MC, Cui YH, Wang JM, Leto TL, Gao JL, Murphy PM (2001) Amyloid-beta induces chemotaxis and oxidant stress by acting at formylpeptide receptor 2, a G protein-coupled receptor expressed in phagocytes and brain. *J Biol Chem* 276: 23645-23652
208. Tiffany HL, Gao JL, Roffe E, Sechler JM, Murphy PM (2011) Characterization of Fpr-rs8, an atypical member of the mouse formyl peptide receptor gene family. *J Innate Immun* 3: 519-529
209. Tirindelli R, Dibattista M, Pifferi S, Menini A (2009) From pheromones to behavior. *Physiol Rev* 89: 921-956
210. Tucker PK, Lee BK, Lundrigan BL, Eicher EM (1992) Geographic origin of the Y chromosomes in "old" inbred strains of mice. *Mamm Genome* 3: 254-261
211. VanCompernelle SE, Clark KL, Rummel KA, Todd SC (2003) Expression and function of formyl peptide receptors on human fibroblast cells. *J Immunol* 171: 2050-2056
212. Vandenberg JG (1969) Male odor accelerates female sexual maturation in mice. *Endocrinology* 84: 658-660
213. Vandenberg JG (1973) Acceleration and inhibition of puberty in female mice by pheromones. *J Reprod Fertil Suppl* 19: 411-419
214. Wahid FN, Robinson M, Behnke JM (1989) Immunological relationships during primary infection with *Heligmosomoides polygyrus* (*Nematospiroides dubius*): expulsion of adult worms from fast responder syngeneic and hybrid strains of mice. *Parasitology* 98 Pt 3: 459-469
215. Wang ZG, Ye RD (2002) Characterization of two new members of the formyl peptide receptor gene family from 129S6 mice. *Gene* 299: 57-63
216. Wang R, Braughton KR, Kretschmer D, Bach TH, Queck SY, Li M, Kennedy AD, Dorward DW, Klebanoff SJ, Peschel A, DeLeo FR, Otto M (2007) Identification of novel cytolytic peptides as key virulence determinants for community-associated MRSA. *Nat Med* 13: 1510-1514
217. Whitten WK (1956) Modification of the oestrous cycle of the mouse by external stimuli associated with the male. *J Endocrinol* 13: 399-404
218. Winans SS, Scalia F (1970) Amygdaloid nucleus: new afferent input from the vomeronasal organ. *Science* 170: 330-332
219. Xu F, Schaefer M, Kida I, Schafer J, Liu N, Rothman DL, Hyder F, Restrepo D, Shepherd GM (2005) Simultaneous activation of mouse main and accessory olfactory bulbs by odors or pheromones. *J Comp Neurol* 489: 491-500
220. Yang D, Chen Q, Schmidt AP, Anderson GM, Wang JM, Wooters J, Oppenheim JJ, Chertov O (2000) LL-37, the neutrophil granule- and epithelial cell-derived cathelicidin, utilizes formyl peptide receptor-like 1 (FPRL1) as a receptor to chemoattract human peripheral blood neutrophils, monocytes, and T cells. *J Exp Med* 192: 1069-1074
221. Yang D, Chen Q, Le Y, Wang JM, Oppenheim JJ (2001) Differential regulation of formyl peptide receptor-like 1 expression during the differentiation of monocytes to dendritic cells and macrophages. *J Immunol* 166: 4092-4098
222. Yang D, Chen Q, Gertz B, He R, Phulsuksombati M, Ye RD, Oppenheim JJ (2002) Human dendritic cells express functional formyl peptide receptor-like-2 (FPRL2) throughout maturation. *J Leukoc Biol* 72: 598-607
223. Yang H, Wang JR, Didion JP, Buus RJ, Bell TA, Welsh CE, Bonhomme F, Yu AH, Nachman MW, Pialek J, Tucker P, Boursot P, McMillan L, Churchill GA, de Villena FP (2011) Subspecific origin and haplotype diversity in the laboratory mouse. *Nat Genet* 43: 648-655
224. Ye RD, Cavanagh SL, Quehenberger O, Prossnitz ER, Cochrane CG (1992) Isolation of a cDNA that encodes a novel granulocyte N-formyl peptide receptor. *Biochem Biophys Res Commun* 184: 582-589

225. Ye RD, Boulay F (1997) Structure and function of leukocyte chemoattractant receptors. *Adv Pharmacol* 39: 221-289
226. Ye RD, Boulay F, Wang JM, Dahlgren C, Gerard C, Parmentier M, Serhan CN, Murphy PM (2009) International Union of Basic and Clinical Pharmacology. LXXIII. Nomenclature for the formyl peptide receptor (FPR) family. *Pharmacol Rev* 61: 119-161
227. Yonekawa H, Moriwaki K, Gotoh O, Hayashi JI, Watanabe J, Miyashita N, Petras ML, Tagashira Y (1981) Evolutionary relationships among five subspecies of *Mus musculus* based on restriction enzyme cleavage patterns of mitochondrial DNA. *Genetics* 98: 801-816
228. Young JM, Trask BJ (2007) V2R gene families degenerated in primates, dog and cow, but expanded in opossum. *Trends Genet* 23: 212-215
229. Zhang J, Webb DM (2003) Evolutionary deterioration of the vomeronasal pheromone transduction pathway in catarrhine primates. *Proc Natl Acad Sci U S A* 100: 8337-8341
230. Zhang X, Firestein S (2007) Comparative genomics of odorant and pheromone receptor genes in rodents. *Genomics* 89: 441-450
231. Ziesmann J, Ma W, Novotny MV, Zufall F, Leinders-Zufall T (2002) Combinatorial pheromone coding visualized in the mouse main olfactory epithelium. *Chem Senses*: 664
232. Zufall F (2005) The TRPC2 ion channel and pheromone sensing in the accessory olfactory system. *Naunyn Schmiedebergs Arch Pharmacol* 371: 245-250
233. Zufall F, Ukhonov K, Lucas P, Liman ER, Leinders-Zufall T (2005) Neurobiology of TRPC2: from gene to behavior. *Pflugers Arch* 451: 61-71
234. Zufall F, Leinders-Zufall T (2007) Mammalian pheromone sensing. *Curr Opin Neurobiol* 17: 483-489

Appendix

Table 10. Peptide spot array epitopes

Peptide#	Amino Acid#	Peptide Sequence
1	1 to 15	M-E-T-N-Y-S-I-P-L-N-G-S-D-V-V
2	6 to 20	S-I-P-L-N-G-S-D-V-V-I-Y-D-S-T
3	11 to 25	G-S-D-V-V-I-Y-D-S-T-I-S-R-V-L
4	16 to 30	I-Y-D-S-T-I-S-R-V-L-W-I-L-S-M
5	21 to 35	I-S-R-V-L-W-I-L-S-M-V-V-V-S-I
6	26 to 40	W-I-L-S-M-V-V-V-S-I-T-F-F-L-G
7	31 to 45	V-V-V-S-I-T-F-F-L-G-V-L-G-N-G
8	36 to 50	T-F-F-L-G-V-L-G-N-G-L-V-I-W-V
9	41 to 55	V-L-G-N-G-L-V-I-W-V-A-G-F-R-M
10	46 to 60	L-V-I-W-V-A-G-F-R-M-P-H-T-V-T
11	51 to 65	A-G-F-R-M-P-H-T-V-T-T-I-W-Y-L
12	56 to 70	P-H-T-V-T-T-I-W-Y-L-N-L-A-L-A
13	61 to 75	T-I-W-Y-L-N-L-A-L-A-D-F-S-F-T
14	66 to 80	N-L-A-L-A-D-F-S-F-T-A-T-L-P-F
15	71 to 85	D-F-S-F-T-A-T-L-P-F-L-L-V-E-M
16	76 to 90	A-T-L-P-F-L-L-E-V-M-A-M-K-E-K
17	81 to 95	L-L-V-E-M-A-M-K-E-K-W-P-F-G-W
18	86 to 100	A-M-K-E-K-W-P-F-G-W-F-L-C-K-L
19	91 to 105	W-P-F-G-W-F-L-C-K-L-V-H-I-A-V
20	96 to 110	F-L-C-K-L-V-H-I-A-V-D-V-N-L-F
21	101 to 115	V-H-I-A-V-D-V-N-L-F-G-S-V-F-L
22	106 to 120	D-V-N-L-F-G-S-V-F-L-I-A-V-I-A
23	111 to 125	G-S-V-F-L-I-A-V-I-A-L-D-R-C-I
24	116 to 130	I-A-V-I-A-L-D-R-C-I-C-V-L-H-P
25	121 to 135	L-D-R-C-I-C-V-L-H-P-V-W-A-Q-N
26	126 to 140	C-V-L-H-P-V-W-A-Q-N-H-R-T-V-S
27	131 to 145	V-W-A-Q-N-H-R-T-V-S-L-A-R-N-V
28	136 to 150	H-R-T-V-S-L-A-R-N-V-V-V-G-S-W
29	141 to 155	L-A-R-N-V-V-V-G-S-W-I-F-A-L-I
30	146 to 160	V-V-G-S-W-I-F-A-L-I-L-T-L-P-L
31	151 to 165	I-F-A-L-I-L-T-L-P-L-F-L-F-L-T
32	156 to 170	L-T-L-P-L-F-L-F-L-T-T-V-R-D-A
33	161 to 175	F-L-F-L-T-T-V-R-D-A-R-G-D-V-H
34	166 to 180	T-V-R-D-A-R-G-D-V-H-C-R-L-S-F
35	171 to 185	R-G-D-V-H-C-R-L-S-F-V-S-W-G-N
36	176 to 190	C-R-L-S-F-V-S-W-G-N-S-V-E-E-R
37	181 to 195	V-S-W-G-N-S-V-E-E-R-L-N-T-A-I
38	186 to 200	S-V-E-E-R-L-N-T-A-I-T-F-V-T-T
39	191 to 205	L-N-T-A-I-T-F-V-T-T-R-G-I-I-R
40	196 to 210	T-F-V-T-T-R-G-I-I-R-F-I-V-S-F
41	201 to 215	R-G-I-I-R-F-I-V-S-F-S-L-P-M-S
42	206 to 220	F-I-V-S-F-S-L-P-M-S-F-V-A-I-C
43	211 to 225	S-L-P-M-S-F-V-A-I-C-Y-G-L-I-T
44	216 to 230	F-V-A-I-C-Y-G-L-I-T-T-K-I-H-K
45	221 to 235	Y-G-L-I-T-T-K-I-H-K-K-A-F-V-N
46	226 to 240	T-K-I-H-K-K-A-F-V-N-S-S-R-P-F
47	231 to 245	K-A-F-V-N-S-S-R-P-F-R-V-L-T-G
48	236 to 250	S-S-R-P-F-R-V-L-T-G-V-V-A-S-F
49	241 to 255	R-V-L-T-G-V-V-A-S-F-F-I-C-W-F
50	246 to 260	V-V-A-S-F-F-I-C-W-F-P-F-Q-L-V
51	251 to 265	F-I-C-W-F-P-F-Q-L-V-A-L-L-G-T
52	256 to 270	P-F-Q-L-V-A-L-L-G-T-V-W-L-K-E
53	261 to 275	A-L-L-G-T-V-W-L-K-E-M-Q-F-S-G
54	266 to 280	V-W-L-K-E-M-Q-F-S-G-S-Y-K-I-I
55	271 to 285	M-Q-F-S-G-S-Y-K-I-I-G-R-L-V-N
56	276 to 290	S-Y-K-I-I-G-R-L-V-N-P-T-S-S-L
57	281 to 295	G-R-L-V-N-P-T-S-S-L-A-F-F-N-S
58	286 to 300	P-T-S-S-L-A-F-F-N-S-C-L-N-P-I
59	291 to 305	A-F-F-N-S-C-L-N-P-I-L-Y-V-F-M
60	296 to 310	C-L-N-P-I-L-Y-V-F-M-G-Q-D-F-Q
61	301 to 315	L-Y-V-F-M-G-Q-D-F-Q-E-R-L-I-H
62	306 to 320	G-Q-D-F-Q-E-R-L-I-H-S-L-S-S-R
63	311 to 325	E-R-L-I-H-S-L-S-S-R-L-Q-R-A-L
64	316 to 330	S-L-S-S-R-L-Q-R-A-L-S-E-D-S-G
65	321 to 335	L-Q-R-A-L-S-E-D-S-G-H-I-S-D-T
66	326 to 340	S-E-D-S-G-H-I-S-D-T-R-T-N-L-A
67	331 to 345	H-I-S-D-T-R-T-N-L-A-S-L-P-E-D
68	336 to 350	R-T-N-L-A-S-L-P-E-D-I-E-I-K-A
69	337 to 351	T-N-L-A-S-L-P-E-D-I-E-I-K-A-I

Table 11. Mouse genes containing the AMKEK motif

Gene#	Gene Name	Gene Synonyms	Locus	Amino Acids	UniProtKB Accession Number
1	Ccdc83	-/-	CCD83_MOUSE	305 aa	Q9D4V3.1
2	Fpr2	Fpr-rs2	FPR2_MOUSE	351 aa	O88536.1
3	Fpr3	Fpr-rs1; Lxa4r	FPRS1_MOUSE	351 aa	O08790.2
4	Map9	Asap; Mtap9	MAP9_MOUSE	646 aa	Q3TRR0.2
5	Skil	Skir; Sno	SKIL_MOUSE	675 aa	Q60665.2
6	Tsga10	-/-	TSG10_MOUSE	697 aa	Q6NY15.1
7	Lppr3	Kiaa4076; Prg2	LPPR3_MOUSE	716 aa	Q7TPB0.1
8	Elmo2	Kiaa1834	ELMO2_MOUSE	732 aa	Q8BHL5.1
9	Nup98	-/-	NUP98_MOUSE	1816 aa	Q6PFD9.2
10	Unc13c	-/-	UN13C_MOUSE	2210 aa	Q8K0T7.3
11	Tpr	-/-	TPR_MOUSE	2431 aa	F6ZDS4.1
12	Pcnt	Pcnt2	PCNT_MOUSE	2898 aa	P48725.2
13	Akap9	Kiaa0803	AKAP9_MOUSE	3797 aa	Q70FJ1.2
14	Dnah8	Dnahc8	DYH8_MOUSE	4731 aa	Q91XQ0.2
15	Fsip2	-/-	FSIP2_MOUSE	6995 aa	A2ARZ3.3
16	Dst	Bpag1; Macf2	DYST_MOUSE	7393 aa	Q91ZU6.2
17	Syne1	-/-	SYNE1_MOUSE	8799 aa	Q6ZWR6.2

Table 12. Mouse genes containing the LNTA motif

Gene#	Gene Name	Gene Synonyms	Locus	Amino Acids	UniProtKB Accession Number
1	Atoh7	Ath5	ATOH7_MOUSE	149 aa	Q9Z2E5.1
2	Ormdl1	-/-	ORML1_MOUSE	153 aa	Q921I0.1
3	Ucn3	-/-	UCN3_MOUSE	164 aa	Q924A4.1
4	Ptn	-/-	PTN_MOUSE	168 aa	P63089.1
5	Fam159a	-/-	F159A_MOUSE	189 aa	A2A9G7.1
6	Isoc2a	Isoc2	ISC2A_MOUSE	206 aa	P85094.1
7	Ropn11	Asp	ROP1L_MOUSE	230 aa	Q9EQ00.1
8	Tmem65	-/-	TMM65_MOUSE	234 aa	Q4VAE3.1
9	Bpifa2	Psp	BPIA2_MOUSE	235 aa	P07743.1
10	Pex11g	Pex11c	PX11C_MOUSE	241 aa	Q6P6M5.2
11	Drgx	Drg11; Prrx11	DRGX_MOUSE	263 aa	Q8BYH0.2
12	Mad21bp	Mad2lbp	MD2BP_MOUSE	276 aa	Q9DCX1.2
13	Elov17	-/-	ELOV7_MOUSE	281 aa	Q9D2Y9.1
14	Mbd3	-/-	MBD3_MOUSE	285 aa	Q9Z2D8.1
15	Ralyl	-/-	RALYL_MOUSE	293 aa	Q8BTF8.1
16	Raly	Merc	RALY_MOUSE	312 aa	Q64012.3
17	Ccdc160	-/-	CC160_MOUSE	323 aa	Q3UYG1.1
18	Cdk6	Cdkn6; Crk2	CDK6_MOUSE	326 aa	Q64261.2
19	Utf1	-/-	UTF1_MOUSE	339 aa	Q6J1H4.2
20	Gpr139	Gm495; Gprg1; Pgr3	GP139_MOUSE	345 aa	Q80UC8.2
21	Fkbpl	Ng7	FKBPL_MOUSE	347 aa	Q35450.1
22	Fpr2	Fpr-rs2	FPR2_MOUSE	351 aa	O88536.1
23	Fpr3	Fpr-rs1; Lxa4r	FPRS1_MOUSE	351 aa	O08790.2
24	Tefm	-/-	TEFM_MOUSE	364 aa	Q5SSK3.1
25	Tm6sf1	-/-	TM6S1_MOUSE	370 aa	P58749.2
26	Sox18	Sox-18	SOX18_MOUSE	377 aa	P43680.3
27	Stoml1	-/-	STML1_MOUSE	399 aa	Q8CI66.1
28	Ager	Rage	RAGE_MOUSE	403 aa	Q62151.1
29	Slc22a18	Impt1; Itm; Orct12; Tssc5	S22AI_MOUSE	406 aa	Q78KK3.2
30	Tmlhe	Tmlh	TMLH_MOUSE	421 aa	Q91ZE0.2
31	Pm20d2	Acy112; Gm424	P20D2_MOUSE	431 aa	A3KG59.1
32	Gcdh	-/-	GCDH_MOUSE	438 aa	Q60759.2
33	Midn	-/-	MIDN_MOUSE	465 aa	Q3TPJ7.1
34	Pnliprp2	Plrp2	LIPR2_MOUSE	468 aa	P17892.1
35	Gtf2a1l	Alf; Gtf2a1lf	TF2AY_MOUSE	468 aa	Q8R414.2
36	Amigo1	Ali2; Amigo; Kiaa1163	AMGO1_MOUSE	492 aa	Q80ZD8.1
37	Phf10	Baf45a	PHF10_MOUSE	497 aa	Q9D8M7.4

38	Celf2	Cugbp2; Napor	CELF2_MOUSE	508 aa	Q9Z0H4.1
39	Apex2	Ape2	APEX2_MOUSE	516 aa	Q68G58.1
40	Snx1	-/-	SNX1_MOUSE	522 aa	Q9WV80.1
41	Ppp3cb	Calnb	PP2BB_MOUSE	525 aa	P48453.2
42	Fgfr1	Fgfr5	FGRL1_MOUSE	529 aa	Q91V87.1
43	Ccdc176	Bbof1	BBOF1_MOUSE	533 aa	Q3V079.2
44	Nrbp1	Madm; Nrbp	NRBP_MOUSE	535 aa	Q99J45.1
45	Slc2a10	Glut10	GTR10_MOUSE	536 aa	Q8VHD6.1
46	Stam	Stam1	STAM1_MOUSE	548 aa	P70297.3
47	Tbx4	-/-	TBX4_MOUSE	552 aa	P70325.3
48	Msto1	-/-	MSTO1_MOUSE	556 aa	Q2YDW2.1
49	Flvcr1	Mfsd7b	FLVC1_MOUSE	560 aa	B2RXV4.1
50	Cdc6	-/-	CDC6_MOUSE	562 aa	O89033.2
51	Deaf1	-/-	DEAF1_MOUSE	566 aa	Q9Z1T5.1
52	Znf704	Gig1; Zfp704	ZN704_MOUSE	566 aa	Q9ERQ3.1
53	Cecr6	-/-	CECR6_MOUSE	572 aa	Q99MX7.1
54	Taf5l	Paf65b	TAF5L_MOUSE	589 aa	Q91WQ5.1
55	Rangap1	Fug1	RAGP1_MOUSE	589 aa	P46061.2
56	Klhl10	-/-	KLH10_MOUSE	608 aa	Q9D5V2.1
57	Hap1	-/-	HAP1_MOUSE	628 aa	O35668.1
58	Vps9d1	-/-	VP9D1_MOUSE	649 aa	Q8C190.1
59	Znf746	Zfp746	ZN746_MOUSE	652 aa	Q3U133.3
60	Mepce	Bcdin3; Bip1; D5Wsu46e	MEPCE_MOUSE	666 aa	Q8K3A9.2
61	Eri2	Exod1; Kiaa1504	ERI2_MOUSE	688 aa	Q5BKS4.1
62	Polh	Rad30a; Xpv	POLH_MOUSE	694 aa	Q9JJN0.1
63	Ddx4	Vasa	DDX4_MOUSE	702 aa	Q61496.2
64	Nln	-/-	NEUL_MOUSE	704 aa	Q91YP2.1
65	Gga3	Kiaa0154	GGA3_MOUSE	718 aa	Q8BMI3.2
66	Mtif2	-/-	IF2M_MOUSE	727 aa	Q91YJ5.2
67	Prox1	-/-	PROX1_MOUSE	737 aa	P48437.2
68	Cnot10	-/-	CNO10_MOUSE	744 aa	Q8BH15.1
69	Hectd2	-/-	HECD2_MOUSE	774 aa	Q8CDU6.2
70	Zw10	-/-	ZW10_MOUSE	779 aa	O54692.3
71	Sp4	-/-	SP4_MOUSE	782 aa	Q62445.2
72	Vps35	Mem3	VPS35_MOUSE	796 aa	Q9EQH3.1
73	Rapgef5	Gfr; Kiaa0277; Mrgef	RPGF5_MOUSE	814 aa	Q8C0Q9.2
74	Bicd1	-/-	BICD1_MOUSE	835 aa	Q8BR07.2
75	Kdm1a	Aof2; Kiaa0601; Lsd1	KDM1A_MOUSE	853 aa	Q6ZQ88.2
76	Ppp1r10	Cat53; Pnuts	PP1RA_MOUSE	888 aa	Q80W00.1
77	Actn1	-/-	ACTN1_MOUSE	892 aa	Q7TPR4.1
78	Ctnna3	Catna3	CTNA3_MOUSE	895 aa	Q65CL1.2
79	Actn3	-/-	ACTN3_MOUSE	900 aa	O88990.1
80	unknown	-/-	CA112_MOUSE	903 aa	Q3TQQ9.2
81	Mcm2	Bm28; Cdc11; Kiaa0030; Mcmd2	MCM2_MOUSE	904 aa	P97310.3
82	Magee1	-/-	MAGE1_MOUSE	918 aa	Q6PCZ4.1
83	Paxbp1	Gcfc; Gcfc1	PAXB1_MOUSE	919 aa	P58501.3
84	Tex11	-/-	TEX11_MOUSE	947 aa	Q14AT2.1
85	Piwi2	Mili	PIWL2_MOUSE	971 aa	Q8CDG1.2
86	Nfkb1	-/-	NFKB1_MOUSE	971 aa	P25799.2
87	Inpp5b	-/-	I5P2_MOUSE	993 aa	Q8K337.1
88	Dennd1a	-/-	DEN1A_MOUSE	1016 aa	Q8K382.2
89	Paxip1	Ptip	PAXI1_MOUSE	1056 aa	Q6NZQ4.1
90	Hip1r	-/-	HIP1R_MOUSE	1068 aa	Q9JKY5.2
91	Rimbp2	Kiaa0318; Rbp2	RIMB2_MOUSE	1072 aa	Q80U40.3
92	Tmem132d	Molt	T132D_MOUSE	1097 aa	Q76HP3.1
93	Tmem132c	-/-	T132C_MOUSE	1099 aa	Q8CEF9.3
94	Pkp4	Armpr	PKP4_MOUSE	1190 aa	Q68FH0.1
95	Kcnh7	Erg3	KCNH7_MOUSE	1195 aa	Q9ER47.2
96	Egfr	-/-	EGFR_MOUSE	1210 aa	Q01279.1
97	Tdrd12	Ecat8; Repro23	TDR12_MOUSE	1215 aa	Q9CWU0.2
98	Evc2	Lbn	LBN_MOUSE	1220 aa	Q8K1G2.1
99	Gigyf2	Kiaa0642; Perq2; Tnrc15	PERQ2_MOUSE	1291 aa	Q6Y7W8.2
100	Disp2	Kiaa1742	DISP2_MOUSE	1345 aa	Q8CIP5.1

101	Adcy9	-/-	ADCY9_MOUSE	1353 aa	P51830.1
102	Cntnap1	Nrxn4	CNTP1_MOUSE	1385 aa	O54991.2
103	Atp10d	-/-	AT10D_MOUSE	1416 aa	Q8K2X1.2
104	Plb1	Plb	PLB1_MOUSE	1478 aa	Q3TTY0.2
105	Vprbp	Dcaf1; Kiaa0800	VPRBP_MOUSE	1506 aa	Q80TR8.4
106	Baz1a	Cbp146	BAZ1A_MOUSE	1555 aa	O88379.3
107	Adcy10	Sac; Sacy	ADCYA_MOUSE	1614 aa	Q8C0T9.2
108	C3	-/-	CO3_MOUSE	1663 aa	P01027.3
109	Helz	Kiaa0054	HELZ_MOUSE	1964 aa	Q6DFV5.2
110	Arfgef3	Big3; D10Bwg1379e; Kiaa1244	BIG3_MOUSE	2170 aa	Q3UGY8.1
111	Cacna1d	Cach3; Cacn4; Cacn11a2; Cchl1a2	CAC1D_MOUSE	2179 aa	Q99246.3
112	Cacna1e	Cach6; Cacn11a6; Cchra1	CAC1E_MOUSE	2272 aa	Q61290.1
113	Crebbp	Cbp	CBP_MOUSE	2441 aa	P45481.3
114	Atrx	Hp1bp2; Xnp	ATRX_MOUSE	2476 aa	Q61687.3
115	Helz2	-/-	HELZ2_MOUSE	2947 aa	E9QAM5.1
116	Lama1	Lama; Lama-1	LAMA1_MOUSE	3084 aa	P19137.1
117	Aspm	Calmbp1; Sha1	ASPM_MOUSE	3122 aa	Q8CJ27.2
118	Alms1	Kiaa0328	ALMS1_MOUSE	3251 aa	Q8K4E0.2
119	Vps13b	Coh1; Kiaa0532	VP13B_MOUSE	4013 aa	Q80TY5.2

Table 13. Haplotype analysis of the *Fpr3* gene in different mouse strains

Strains	Fpr3 Variant	Subspecific Origin of Fpr3	Origin	Inbred Strain Category
Laboratory Mouse Strains				
C57Bl/6NCrl	<i>Fpr3_{wt}</i>	<i>M. m. domesticus</i>	England	Castle's mice
C57Bl/6NJ	<i>Fpr3_{wt}</i>	<i>M. m. domesticus</i>	England	Castle's mice
C57Bl/10J	<i>Fpr3_{wt}</i>	<i>M. m. domesticus</i>	England	Castle's mice
C57BR/cdJ	<i>Fpr3_{wt}</i>	<i>M. m. musculus</i>	England	Castle's mice
C57L/J	<i>Fpr3_{wt}</i>	<i>M. m. musculus</i>	England	Castle's mice
C58/J	<i>Fpr3_{wt}</i>	<i>M. m. musculus</i>	England	Castle's mice
ILnJ	<i>Fpr3_{wt}</i>	<i>M. m. domesticus</i>	England	Castle's mice
NZB/B1NJ	<i>Fpr3_{wt}</i>	<i>M. m. domesticus</i>	England	Castle's mice
NZB/Ola	<i>Fpr3_{wt}</i>	n. e.	England	Castle's mice
NZW/LacJ	<i>Fpr3_{wt}</i>	<i>M. m. domesticus</i>	England	Castle's mice
KK/Hij*	<i>Fpr3_{wt}</i>	<i>M. m. domesticus</i>	Japan	Colonies from China and Japan
NOD/ShiLtJ	<i>Fpr3_{wt}</i>	<i>M. m. domesticus</i>	Switzerland	Swiss mice
ST/bJ	<i>Fpr3_{wt}</i>	<i>M. m. domesticus</i>	unknown	Other inbred strains
129X1/Sv	<i>Fpr3$\Delta_{424-435}$</i>	<i>M. m. domesticus</i>	England	Castle's mice
129P2/OlaHsd	<i>Fpr3$\Delta_{424-435}$</i>	<i>M. m. domesticus</i>	England	Castle's mice
129S1/SvImJ	<i>Fpr3$\Delta_{424-435}$</i>	<i>M. m. domesticus</i>	England	Castle's mice
129S5SvEvBrd	<i>Fpr3$\Delta_{424-435}$</i>	<i>M. m. domesticus</i>	England	Castle's mice
AKR/J	<i>Fpr3$\Delta_{424-435}$</i>	<i>M. m. domesticus</i>	England	Castle's mice
A/J	<i>Fpr3$\Delta_{424-435}$</i>	<i>M. m. domesticus</i>	England	Castle's mice
BALB/cJ	<i>Fpr3$\Delta_{424-435}$</i>	<i>M. m. domesticus</i>	England	Castle's mice
C3H/HeH	<i>Fpr3$\Delta_{424-435}$</i>	<i>M. m. domesticus</i>	England	Castle's mice
C3H/HeJ	<i>Fpr3$\Delta_{424-435}$</i>	<i>M. m. domesticus</i>	England	Castle's mice
CBA/J	<i>Fpr3$\Delta_{424-435}$</i>	<i>M. m. domesticus</i>	England	Castle's mice
DBA/1J	<i>Fpr3$\Delta_{424-435}$</i>	<i>M. m. domesticus</i>	England	Castle's mice
DBA/2J	<i>Fpr3$\Delta_{424-435}$</i>	<i>M. m. domesticus</i>	England	Castle's mice
LP/J	<i>Fpr3$\Delta_{424-435}$</i>	<i>M. m. domesticus</i>	England	Castle's mice
NZO/HILaJ	<i>Fpr3$\Delta_{424-435}$</i>	<i>M. m. domesticus</i>	England	Castle's mice
RF/J	<i>Fpr3$\Delta_{424-435}$</i>	<i>M. m. domesticus</i>	England	Castle's mice
SEA/GnJ	<i>Fpr3$\Delta_{424-435}$</i>	<i>M. m. domesticus</i>	England	Castle's mice
FVB/Ncrl	<i>Fpr3$\Delta_{424-435}$</i>	n. e.	Switzerland	Swiss mice
FVB/NJ	<i>Fpr3$\Delta_{424-435}$</i>	<i>M. m. domesticus</i>	Switzerland	Swiss mice
BUB/BnJ	<i>Fpr3$\Delta_{424-435}$</i>	<i>M. m. domesticus</i>	unknown	Other inbred strains
Wild-Derived Mouse Strains				
SPRET/EiJ	<i>Fpr3_{wt}</i>	<i>M. m. spretus</i>	Spain	Strains derived from wild mice
CZE/DT	<i>Fpr3_{wt}</i>	<i>M. m. musculus</i>	Czech Republic	Strains derived from wild mice
PWK/PhJ	<i>Fpr3_{wt}</i>	<i>M. m. musculus</i>	Czech Republic	Strains derived from wild mice
GER/DT	<i>Fpr3_{wt}</i>	<i>M. m. domesticus</i>	Germany	Strains derived from wild mice
FRA/DT	<i>Fpr3_{wt}</i>	<i>M. m. domesticus</i>	France	Strains derived from wild mice
CAST/EiJ	<i>Fpr3_{wt}</i>	<i>M. m. castaneus</i>	Thailand	Strains derived from wild mice
KAZ/DT	<i>Fpr3_{wt}</i>	<i>M. m. musculus</i>	Kazakhstan	Strains derived from wild mice
ZALENDE/EiJ	<i>Fpr3$\Delta_{424-435}$</i>	<i>M. m. domesticus</i>	Switzerland	Strains derived from wild mice
LEWES/EiJ	<i>Fpr3$\Delta_{424-435}$</i>	<i>M. m. domesticus</i>	United States of America	Strains derived from wild mice
WSB/EiJ	<i>Fpr3$\Delta_{424-435}$</i>	<i>M. m. domesticus</i>	United States of America	Strains derived from wild mice

Subspecific origins were examined on chromosome 17 in the nucleotide range from 17,970,000 to 17,972,000.

n. e. = not examined.

Publications

Journal Articles

Stempel H, Jung M, Pérez-Gómez A, Leinders-Zufall T, Zufall F, Bufe B (2016) Strain-specific loss of formyl peptide receptor 3 in the murine vomeronasal and immune systems. J Biol Chem 291: 9762-9775

Stempel H, Zufall F, Bufe B. Evidence for an Orthologous Function of Mouse and Human Formyl Peptide Receptor 3. In preparation

Abstracts

Stempel H, Schumann T, Bufe B, Zufall F
RNA editing alters the function of vomeronasal formyl peptide receptors.
29.08.2013: 22nd Annual Meeting of the European Chemoreception Research Organization

Bufe B, Schumann T, **Stempel H**, Zufall F
Evolution of formyl peptide receptor function in mammals
05.11.2012: 17th Joint Meeting of the Signal Transduction Society

Schumann T, **Stempel H**, Chamero P, Leinders-Zufall T, Zufall F, Bufe B
Formyl peptide detection by vomeronasal sensory neurons is mediated by functionally distinct cell populations
07.09.2012: Sonderforschungsbereich 894 Symposium on Calcium Signaling

Bufe B, Schumann T, **Stempel H**, Zufall F
Agonist profiling of the mouse formyl peptide receptors reveals a stereoselective tuning of mFpr-rs1
27.06.2012: 16th International Symposium on Olfaction and Taste

Copyright Permission Policy of the American Society for Biochemistry and Molecular Biology

These guidelines apply to the reuse of articles, figures, charts and photos in the *Journal of Biological Chemistry*, *Molecular & Cellular Proteomics* and the *Journal of Lipid Research*.

For authors reusing their own material:

Authors need **NOT** contact the journal to obtain rights to reuse their own material. They are automatically granted permission to do the following:

- Reuse the article in print collections of their own writing.
- Present a work orally in its entirety.
- Use an article in a thesis and/or dissertation.
- Reproduce an article for use in the author's courses. (If the author is employed by an academic institution, that institution also may reproduce the article for teaching purposes.)
- Reuse a figure, photo and/or table in future commercial and noncommercial works.
- Post a copy of the paper in PDF that you submitted via BenchPress.
- Link to the journal site containing the final edited PDFs created by the publisher.
- Authors who published their papers under the "Author's Choice" option may post the final edited PDFs created by the publisher to their own/departamental/university Web sites immediately upon publication. All other authors may do so 12 months after publication.

EXCEPTION: If authors select the Author's Choice publishing option:

- The final version of the manuscript will be covered under the Creative Commons Attribution license (CC BY), the most accommodating of licenses offered.
- The final version of the manuscript will be released immediately on the publisher's website and PubMed Central.

Please note that authors must include the following citation when using material that appeared in an ASBMB journal:

"This research was originally published in Journal Name. Author(s). Title. *Journal Name*. Year; Vol:pp-pp. © the American Society for Biochemistry and Molecular Biology."

Updated May 13, 2016

Citation:

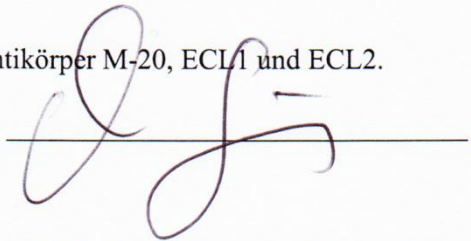
Figures 13 to 23, 25 to 31, and 39, the corresponding figure legends and text passages, tables 10 to 12, and text passages of the experimental procedures and discussion of the work in hand were in part originally published in The Journal of Biological Chemistry. Stempel H, Jung M, Pérez-Gómez A, Leinders-Zufall T, Zufall F, Bufe B. Strain-specific loss of formyl peptide receptor 3 in the murine vomeronasal and immune systems. *J Biol Chem*. 2016; 291: 9762-9775. © the American Society for Biochemistry and Molecular Biology.

Einverständniserklärung

Ich bin damit einverstanden, dass Herr Hendrik Stempel die von ihm angegebenen Daten zur inhaltlichen Darstellung seiner Dissertation verwenden darf. Die Daten wurden unentgeltlich erstellt und freiwillig zur Verwendung genehmigt.

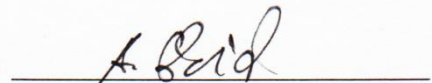
- (1) Bilder der Original Peptid Spot-Arrays der Antikörper M-20, ECL1 und ECL2.

Mit freundlicher Genehmigung: Martin Jung

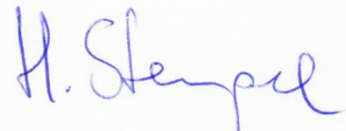


- (2) Messung von Calciumsignalen in sensorischen Köpfen in whole mount Präparationen des Vomeronasalorgans von C57Bl/6NCrl und 129X1/Sv Mäusen ausgelöst durch *Salmonella*-SP24.

Mit freundlicher Genehmigung: Andreas Schmid



Alle Angaben wurden nach bestem Wissen und Gewissen erstellt.



Acknowledgements

First of all, I want to thank **Prof. Dr. Dr. Frank Zufall** for giving me the opportunity to work on a challenging doctoral thesis that combined interesting questions and diverse methodology. Through working on this thesis I gained insight into many facets of science and had the opportunity to develop myself as a scientist as well as a person. Further, I would like to thank him for the support of my project with inspiring discussions, smooth access to expensive working material, and funding my project. I also thank him for enabling me to travel to a scientific meeting and associated with that the opportunity to present and discuss my work with leading international scientists. Finally, I thank him for reviewing this thesis as 1st reviewer.

I am very grateful to **Dr. Bernd Bufe** for his commendable supervision. His always friendly mentoring and advice helped me a lot during the laboratory work as well as the writing of publications and this thesis. Our encouraging and insightful discussions allowed me to continually develop and improve my skills in all requirements of science, be it strategic experimentation, time scheduling, scientific writing, or critical thinking. I appreciate his open-mindedness and his benevolent support for external advanced trainings. Finally, I thank him for thoroughly proofreading this thesis.

I thank **PD. Dr. Martin Jung** for the kind collaboration and, as part of this, for performing the peptide-spot array experiments for antibody characterization. Further, I thank him for supporting me with friendly and valuable scientific advice and for many inspiring conversations. Finally, I appreciate his willingness to review this thesis as 2nd reviewer.

I thank **PD. Dr. Andreas Schmid** for the permission to use *in vivo* calcium imaging data on whole mount preparations of the sensory knob side of VNOs of C57Bl/6NCrl and 129X1/Sv mice with *Salmonella*-SP24 in this thesis. I also thank him for teaching me how to perform a whole mount preparation of the vomeronasal organ and for his support in my attempts to stain single dendritic knobs of Fpr3-expressing cells with my self-generated antibodies.

I am very grateful to **Sabine Plant** for her always friendly and benevolent technical support in many issues. Our very nice and humanly conversations often have shortened the time of experiments. Furthermore, I thank her for sharing her professional expertise in heterologous cell culture and her dedication in solving upcoming problems. Finally, I thank her for the thawing and cultivating cells, collecting of antibody supernatants, and purifying plasmids from time to time.

I thank **Prof. Dr. Trese Leinders-Zufall** for her friendly ear and her commitment for all of her students. Further, I thank her for providing me with C57Bl/6NCrI (MGI:2683688), BALB/cJ (MGI:2159737), and 129X1/Sv (MGI:2164536) mice. I also thank the staff of the animal facility, **Andrea Degreif**, **Angelika Ströer**, **Sarah Boll**, **Monika Vorndran**, **Kerstin Becker**, and **Lisa Knieriemen** for the animal caretaking and their friendly and professional support in all issues regarding mice.

I thank **Prof. Dr. Frank Kirchhoff** for providing me with FVB/NCrI (MGI:2165215) mice. In this context, I would like to thank **Dr. Anja Scheller** and **Daniel Rhode** for their uncomplicated and kind help on organizing mice from the animal facility of Prof. Dr. Frank Kirchhoff.

I thank **Prof. Dr. Dieter Bruns** for providing me with C57Bl/6NCrI (MGI:2683688) mice. I thank **Marina Wirth** und **Judith Arend** for their always kind and reliable help on organizing mice from the animal facility of Prof. Dr. Dieter Bruns.

I thank **Prof. Dr. Diethard Tautz** from the Max-Planck-Institut für Evolutionsbiologie in Plön, Germany for kindly providing me with ear stamps of wild-derived mouse strains. These included *Mus musculus musculus* (Kazakhstan, Czech Republic), *M. m. domesticus* (Germany, France), *M. m. castaneus* (Thailand), and *M. m. spretus* (Spain).

I would like to thank **Dr. Reinhart Kluge** from the Max Rubner Laboratorium at the German Institute of Human Nutrition, Potsdam Rehbrücke, Germany for kindly providing me with NZB/Ola (MGI:2160555) mice.

I would like to thank **Dr. Anabel Pérez-Gómez** for her scientific advice in many issues and for introducing me into the method of performing immunostainings on dissociated vomeronasal cells.

I thank **Dr. Martina Pyrski** for her scientific advice in complicated issues and many nice conversations.

I thank **Dr. Pablo Chamero** for his scientific advice in many issues.

I thank **Marta Podgórska** for helping me with the assessment of the purity of my human neutrophil preparations with FAC sorting.

I thank **Petra Hammes** for providing me with antibodies, technical advice in some issues and many nice conversations.

I thank **Gabriele Mörschbacher** for helping and advising me with all kinds of bureaucracy during the thesis.

I thank **Holger Frisch** for his always kind and competent help with IT-problems and for his very refreshing dry humor.

I also thank my fellow students **Dr. Timo Schumann, Benjamin Stein, Florian Bolz, Eugenia Eckstein, Dennis Bakker, and Henrike Reder** for many lovely conversations and support in all circumstances. I also want to thank **Katherin Bleymehl, Michael Dieli, Dr. Christian Schauer, Yannick Teuchert, Thomas Blum, and Tong Tong** for the always benevolent support among the students. I want to thank **Benjamin Stein** for introducing me to the method of vomeronasal cell dissociation.

Last but not least, I am grateful to my **family** and all my **friends** who supported and motivated me in situations of life over the years spent on this thesis.

Danke.